ELECTROCHEMICAL RECOGNITION AND TRANSPORT OF IONS AT LIQUID/LIQUID INTERFACES AS A PRINCIPLE FOR ENVIRONMENTAL AND BIOMEDICAL ANALYSIS AND BEYOND

by

Patrick J. Rodgers

Bachelor of Science, University of Maryland Eastern Shore, 2004

Submitted to the Graduate Faculty of

Arts and Sciences in partial fulfillment

of the requirements for the degree of

Doctor of Philosophy

University of Pittsburgh

2010

UNIVERSITY OF PITTSBURGH

SCHOOL OF ARTS AND SCIENCES

This dissertation was presented

by

Patrick J. Rodgers

It was defended on

January 22, 2010

and approved by

Adrian C. Michael, Professor, Department of Chemistry

Michael V. Mirkin, Professor, Department of Chemistry and Biochemistry

Stephen G. Weber, Professor, Department of Chemistry

Dissertation Advisor: Shigeru Amemiya, Associate Professor, Department of Chemistry

ELECTROCHEMICAL RECOGNITION AND TRANSPORT OF IONS AT LIQUID/LIQUID INTERFACES AS A PRINCIPLE FOR ENVIRONMENTAL AND BIOMEDICAL ANALYSIS AND BEYOND

Patrick J. Rodgers, PhD

University of Pittsburgh, 2010

Recognition and transport of important species at the membrane of a biological cell are critical for regulation of intracellular communication, metabolic pathways, vital internal conditions, and pharmaceutical drug up-take. Both processes are mediated by membrane-bound proteins functioning as pores, channels, and transporters that recognize and facilitate the transport of ions, nucleic acids and sugars. This whole process can be driven actively by membrane potential against the concentration gradient of transported species. In my PhD work, I fundamentally characterized dynamics of active ion transport, both in the presence and absence of recognition events, at liquid/liquid interfaces to understand electrochemically-controlled interfacial ion recognition and transfer. A deeper understanding of the kinetic and thermodynamic properties is achieved to realize applications in biomedical and environmental science, sensor technology and nanotechnology. The interface between two immiscible solutions served as an artificial model of a cell membrane. By manipulation of the interfacial potential, the active transport of ionic species was mimicked, which was monitored by an ionic current. Micrometer and nanometer sized interfaces were formed experimentally at the orifice of micropipets and nanopipets to probe ion-transfer reactions. Micropipet/nanopipet voltammetry was advanced to accurately obtain quantitative kinetic and thermodynamic parameters through numerical simulations of ion transfer and diffusion. Ion transfer rates for reversible and

nonreversible reactions were determined to demonstrate how the rate controls the current, which affects the sensitivity of ion transfer as a sensing principle. Molecular recognition and transport of biomedical ionic drugs by hydrophobic receptors was examined thermodynamically, demonstrating how the interfacial interactions influence the selectivity of the sensing principle. Kinetic and thermodynamic analysis of the transfer of perfluoroalkyl surfactants, an emerging class of environmental contaminants that accumulate in wildlife, yielded high lipophilic values to suggest a possible origin of their high toxicity. Although, the focus of my research was primarily fundamental in nature, I tested the ion transfer principle practically with an ion selective electrode, developed in our group. Hexafluoroarsenate, an arsenical biocide found recently in wastewater, was detected at sub-nanomolar levels to confirm a thermodynamic mechanism that controls the detection limit.

TABLE OF CONTENTS

LIST OF TABLES

LIST OF FIGURES

LIST OF SCHEMES

LIST OF EQUATIONS

ACKNOWLEDGEMENTS

I would like to express my sincere gratitude to my advisor, Professor Shigeru Amemiya, for the training that he has provided during my graduate program. Professor Amemiya has invested a tremendous amount of time and energy to help me to develop into a professional scientist. I greatly appreciate his contributions to my success.

I want to thank Professor Adrian Michael, Professor Stephen Weber and Professor Michael Mirkin for their willingness to serve on my dissertation committee. I value my interaction with each of them, which has been beneficial for my development and continued success in my scientific career.

I want to acknowledge the former and past members of the Amemiya research group for their support and encouragement. I am thankful for their scientific contributions and friendship.

I also want to acknowledge my family, friends and colleagues. Their consistent support through successful and challenging periods during my graduate program is invaluable.

Finally, I want to give special honor to my wife, Melyssa. She has sacrificed so much of our time together so that I could be successful in this program. Thank you for supporting me through my graduate program, which demanded so much of me. I sincerely appreciate that you stayed on this path with me.

1.0 INTRODUCTION

In my PhD work, I fundamentally characterized dynamics of active ion transport, both in the presence and absence of recognition events, at liquid/liquid interfaces to understand electrochemically-controlled interfacial ion recognition and transfer. In the first chapter, a theoretical model for cyclic voltammetry at micropipet electrodes is established for the kinetic study of ion transfer at liquid/liquid interfaces when the ion is initially present in the external solution. Chapter 3 highlights theoretical simulations that were performed for nanopipet voltammetry to analyze steady-state voltammograms from rapid ion transfer. The theory serves as the basis for a new approach in which the ion of interest is present in both liquid phases initially to accurately determine kinetic and thermodynamic parameters. The developed experimental and theoretical approach is utilized in Chapter 4 for the determination of a standard ion-transfer rate constant for the rapid transfer of tetraethylammonium across a 1,2-dichloroethane/water interface. The determined standard rate constant and transfer coefficient of the TEA^+ transfer are compared with previously reported values to demonstrate limitations of conventional nanopipet voltammetry with a transferrable ion present only in one liquid phase. My contributions in Chapters 3 and 4 include the theoretical analysis of voltammograms, both simulated and experimental. Chapter 5 presents the investigation of molecular recognition of a synthetic heparin mimetic drug, Arixtra, by micropipet voltammetry. From this study, we

achieve a greater understanding of interfacial recognition and sensing of heparin and its analogues. My contributions in this work include the collection and analysis of any voltammetric and chronoamperometric data from the pipets that are filled with the organic phase. In Chapter 6, micropipet voltammetry is utilized to determine remarkably high lipophilicity of a homologous series of perfluoroalkyl carboxylates and perfluorooctyl sulfonate, to suggest reasons for bioaccumulation. This quantitative study is significant because we are able to identify that high lipophilicity originates from the strong electron withdrawing effect of the perfluoroalkyl group on the adjacent oxoanion group. A new model is proposed to assess the effect of high lipophilicity on ion permeation through a thin bilayer lipid membrane. In this project, I contributed to the analysis of voltammograms by the aforementioned numerical simulation method. Although the majority of my PhD research was fundamental in nature, as an additional project, I tested the sensitivity of ion-transfer voltammetry using a more practical electrochemical device created by our group. In Chapter 7, subnanomolar limits of detection are obtained for cationic and anionic species, utilizing stripping voltammetry based on ion transfer at the interface between the aqueous sample and a thin polymeric membrane supported with a solid electrode. Herein, we demonstrate experimentally that a significantly lower LOD are obtained for more lipophilic ionic species. My contribution to this project includes the collection and analysis of all data regarding hexafluoroarsenate.

2.0 CYCLIC VOLTAMMETRY AT MICROPIPET ELECTRODES FOR THE STUDY OF ION-TRANSFER KINETICS AT LIQUID/LIQUID INTERFACES

This work has been published as Patrick J. Rodgers and Shigeru Amemiya, *Anal. Chem.* **2007**, *79*, 9276–9285.

2.1 ABSTRACT

Cyclic voltammetry at micropipet electrodes is applied to the kinetic study of ion transfer at liquid/liquid interfaces. Simple and facilitated transfer of an ion that is initially present outside a tapered pipet was simulated by the finite element method, enabling complete analysis of the resulting transient cyclic voltammogram (CV) with a sigmoidal forward wave followed by a peak-shaped reverse wave. Without serious effects of uncompensated ohmic resistance and capacitive current, more parameters can be determined from a transient CV than from the steady-state counterpart obtained with a smaller pipet or at a slower scan rate. A single transient CV under kinetic limitation gives all parameters in a Butler-Volmer-type model, i.e., the formal potential, the transfer coefficient, the standard ion-transfer rate constant, k^0, and the charge of a transferring ion as well as its diffusion coefficients in both phases. Advantages of the transient approach are demonstrated experimentally for reversible, quasi-reversible, and irreversible cases.

With a multistep transfer mechanism, an irreversible transient CV of facilitated protamine transfer gives an apparent k^0 value of 3.5×10^{-5} cm/s, which is the smallest k^0 value reported so far. With the largest reliable k^0 value of ~1 cm/s reported in literature, an intrinsic rate of the interfacial ion transfer varies by at least 5 orders of magnitude.

2.2 INTRODUCTION

Selective ion transfer at liquid/liquid interfaces is attractive for electrochemical detection of redox inactive ions that are ubiquitous in biological, biomedical, and environmental systems. A phase boundary potential based on equilibrium partitioning of an analyte ion between the two liquid phases results in a Nernstian response of potentiometric ion-selective electrodes (ISEs),[1, 2] which found a variety of practical applications.[3, 4] Alternatively, a current response based on the interfacial ion transfer is measured with voltammetric/amperometric ISEs, which serve as an analytical application of electrochemistry at liquid/liquid interfaces.[5, 6] An important advantage of these current-detection approaches is their sensitivity.[7] The current response varies directly with the concentration and charge of an analyte ion, while the potential change is dependent on the logarithm of the concentration and the inverse of the charge. The current response, however, is more complicated than the equilibrium potentiometric response. Not only a mass-transfer rate but also an ion-transfer rate control interfacial ion flux in voltammetric/amperometric[8-13] and non-equilibrium potentiometric[14-16] modes, where ion transfer is not necessarily Nernstian (or reversible) as assumed in the phase boundary potential model for potentiometric ISEs.[17] Further development of voltammetric/amperometric ISEs requires better understanding of the ion-transfer kinetics.[18, 19]

During the last two decades, voltammetry at glass micropipet electrodes[20] was developed as one of the powerful experimental approaches to study ion-transfer dynamics at liquid/liquid interfaces.[21, 22] With silanization of the inner or outer pipet wall, a stable disk-shaped interface can be formed at the tip.[23] A small current across the microinterface results in a negligibly small ohmic potential drop in the resistive organic phase, which is a prerequisite for reliable kinetic measurement. Moreover, fast mass transfer to a nanoscopic interface enables determination of large ion-transfer rate constants.[24-27] Micropipet electrodes were used also for scanning electrochemical microscopy[28] to probe ion transfer at liquid/liquid interfaces[29, 30] and bilayer lipid membranes.[31]

Unique cyclic voltammograms (CVs) are obtained at pipet-supported interfaces,[32] which are asymmetrically accessible to species in the inner and outer solutions. A conventional steady-state voltammogram can be obtained only for facilitated transfer of an ion in large excess in the inner solution, where mass transfer is controlled by hemispherical diffusion of ionophores and ion–ionophore complexes in the outer solution (Figure 2-1a).[33] The resulting sigmoidal voltammogram can be analyzed quantitatively using a theory well-developed for steady-state voltammetry at solid ultramicroelectrodes (UMEs).[34, 35] A sigmoidal forward wave followed by a peak-shaped reverse wave is obtained for simple transfer of an ion that is initially present in the outer solution (Figure 2-1b) as well as for facilitated transfer of the ion by an ionophore in large excess in the inner solution (Figure 2-1c). The peak-shaped response is due to transient diffusion of transferred ions or their ionophore complexes in the inner solution. For reversible ion transfer at a cylindrical pipet, such a transient CV was reproduced theoretically by the semi-quantitative[36] and boundary element[37] methods. In recent studies, however, steady-state CVs of simple ion transfer were obtained with nanopipets[26, 27] and also with micropipets.[38-41] The lack of a transient

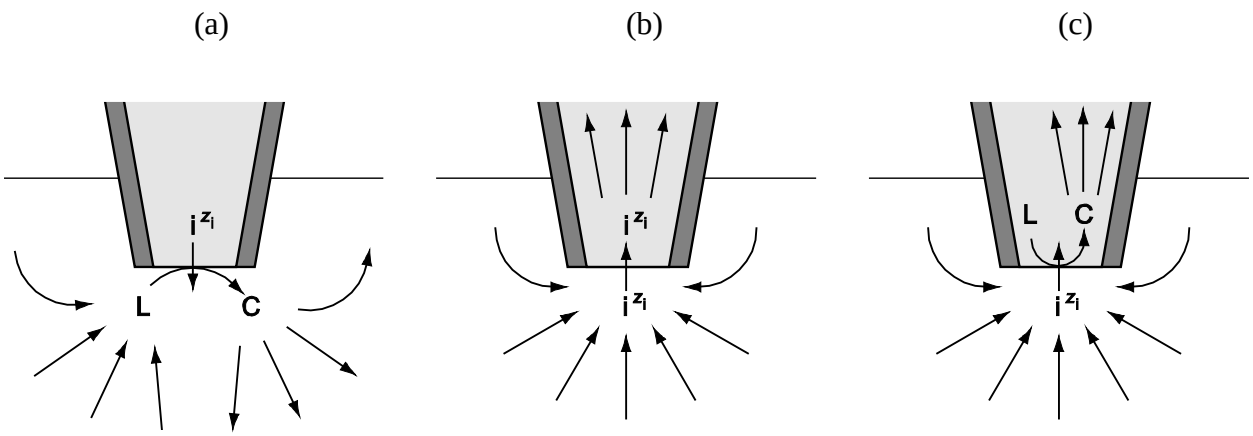

Figure 2-1. Scheme of (a) and (c) facilitated and (b) simple ion transfer. The direction of the arrows corresponds to the direction of forward ion transfer. The arrows in the inner and outer solutions are shown only for species, diffusion of which affects a voltammetric response.

response at nanopipets was ascribed to its unique tip geometry that allows for steady-state non-linear diffusion in the inner solution.[26, 27] More recently, Kakiuchi and co-workers reported that steady-state diffusion is achieved inside a tapered pipet even with a small tip angle.[39]

Here we extend the theory of ion-transfer cyclic voltammetry at micropipet electrodes by a finite element simulation of diffusion processes both in the inner and outer solutions. Simulation conditions are more generalized than those in the previous studies[36, 37] by considering effects of a pipet tip angle and an ion-transfer rate on a voltammetric response. The simulation is applied for analysis of reversible, quasi-reversible, and irreversible CVs obtained under a transient and a steady-state condition to demonstrate that an intrinsic rate of ion transfer at liquid/liquid interfaces varies by at least 5 orders of magnitude.

2.3 THEORY

2.3.1 Model

The geometry of a micropipet electrode is defined in cylindrical coordinates (Figure 2-2), where *r* and *z* are the coordinates in directions parallel and normal to the interface, respectively. The inner and outer solutions are denoted as phase 1 and 2. The pipet size is defined by the inner and outer tip radii, a and r_g. The inner and outer tip angles are given by θ_1 and θ_2. The pipet shaft is long enough for semi-infinite diffusion in the inner solution on a simulation time scale. The space behind the tip in the outer solution is large enough to accurately simulate back diffusion from behind the tip.[29]

An ion with the charge z_i, i^{z_i}, is initially present only in the outer solution so that simple transfer of the ion (Figure 2-1b) is defined by

$$i^{z_i}\ \text{(outer solution)} \rightleftharpoons i^{z_i}\ \text{(inner solution)}$$

Equation 2.1

When an ionophore with the charge z_L, L^{z_L}, forms complexes with the ion in the inner solution (Figure 2-1c), the facilitated transfer is defined by

$$i^{z_i}\ \text{(outer solution)} + sL^{z_L}\ \text{(inner solution)} \rightleftharpoons iL_s^{z_i+sz_L}\ \text{(inner solution)}$$

Equation 2.2

Since the ionophore is assumed to be in large excess, the facilitated transfer may be written simply as a first-order process by

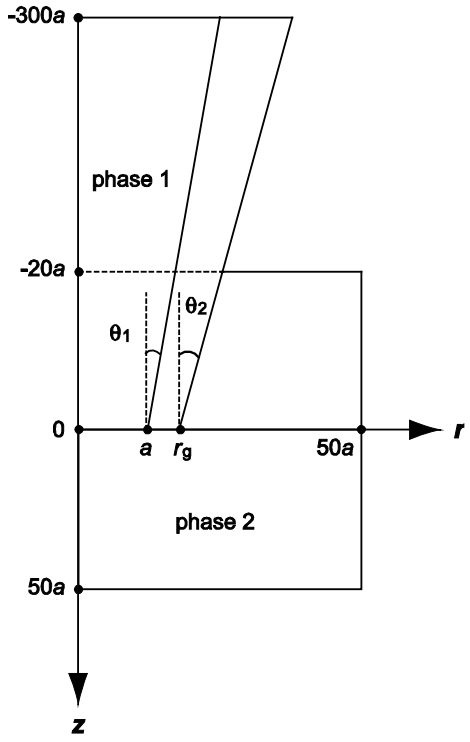

Figure 2-2. Defined space domain for a finite element simulation of ion transfer at a tapered micropipet electrode.

$$i^{z_i} \text{ (outer solution)} \rightleftharpoons i^{z_i} \text{ (inner solution as ionophore complexes)}$$

Equation 2.3

The transfer of an ion that is initially present only in the inner solution is not simulated in this work. Theory is available for a steady-state voltammogram as obtained for facilitated transfer of an ion in large excess in the inner solution (Figure 2-1a).[34, 35] When an ionophore is in large excess or absent, i.e., simple transfer, in the outer solution, the following model is applicable simply by changing the initial conditions (Equations 10 and 11).

Diffusion in the inner solution is expressed as

$$\frac{\partial c_1(r,z,t)}{\partial t} = D_1\left[\frac{\partial^2 c_1(r,z,t)}{\partial r^2} + \frac{1}{r}\frac{\partial c_1(r,z,t)}{\partial r} + \frac{\partial^2 c_1(r,z,t)}{\partial z^2}\right]$$

Equation 2.4

where $c_1(r,z,t)$ and D_1 are the local concentration and diffusion coefficient of the ion in the inner solution, respectively. Diffusion in the outer solution is expressed as

$$\frac{\partial c_2(r,z,t)}{\partial t} = D_2\left[\frac{\partial^2 c_2(r,z,t)}{\partial r^2} + \frac{1}{r}\frac{\partial c_2(r,z,t)}{\partial r} + \frac{\partial^2 c_2(r,z,t)}{\partial z^2}\right]$$

Equation 2.5

where $c_2(r,z,t)$ and D_2 are the local concentration and diffusion coefficient of the transferring ion or its complex in the outer solution, respectively.

The boundary condition at the liquid/liquid interface is given by

$$D_1\left[\frac{\partial c_1(r,z,t)}{\partial z}\right]_{z=0} = D_2\left[\frac{\partial c_2(r,z,t)}{\partial z}\right]_{z=0} = k_f c_2(r,0,t) - k_b c_1(r,0,t)$$

Equation 2.6

where k_f and k_b are the first-order heterogeneous rate constants for forward and reverse transfer, respectively (see Equations 2-1 and 2-3). The rate constants are given by the Butler-Volmer-type relation as[8, 42]

$$k_f = k^0 \exp[-\alpha z_i F(\Delta_2^1\phi - \Delta_2^1\phi_i^{0'})/RT]$$

Equation 2.7

$$k_b = k^0 \exp[(1-\alpha) z_i F(\Delta^1_2\phi - \Delta^1_2\phi_i^{0'})/RT]$$

Equation 2.8

where k^0 is the standard rate constant, α is the transfer coefficient, $\Delta^1_2\phi$ is the Galvani potential difference between the inner and outer solutions, and $\Delta^1_2\phi_i^{0'}$ is the formal ion-transfer potential. In cyclic voltammetry, the potential is swept linearly at the rate of v from the initial potential, $\Delta^1_2\phi_i$, and the sweep direction is reversed at the switching potential, $\Delta^1_2\phi_\lambda$, maintaining the sweep rate. The triangle potential wave is expressed as

$$\Delta^1_2\phi = \Delta^1_2\phi_i + \frac{2(\Delta^1_2\phi_\lambda - \Delta^1_2\phi_i)}{\pi} \sin^{-1}\left\{\sin\left[\frac{\pi v t}{2(\Delta^1_2\phi_\lambda - \Delta^1_2\phi_i)}\right]\right\}$$

Equation 2.9

The other boundary conditions are defined in Supporting Information. The initial conditions are given by

$$c_1(r,z,0) = 0$$

Equation 2.10

$$c_2(r,z,0) = c_0$$

Equation 2.11

where c_0 is the bulk ion concentration. A current, i, is obtained by integrating flux of the transferring ion over the liquid/liquid interface, yielding

$$i = 2\pi z_i F D_2 \int_0^a r\left[\frac{\partial c_2(r,0,t)}{\partial z}\right]dr$$

Equation 2.12

The time-dependent diffusion problem was solved by COMSOL Multiphysics® version 3.2 (COMSOL, Inc., Burlington, MA), which applies the finite element method. Simulation accuracy of this software package for two-phase diffusion processes was demonstrated previously.[43] The diffusion problem defined above was solved in a dimensionless form (Supporting Information) such that a current response is normalized with respect to a limiting current at an inlaid disk-shaped interface, yielding i/i_{ss}, where $i_{ss} = 4z_i F D_2 c_0 a$. The normalized current is plotted with respect to $z_i\Delta\phi$ in cyclic voltammetry, where $\Delta\phi = \Delta_2^1\phi - \Delta_2^1\phi_i^{0'}$, or dimensionless time, τ, in chronoamperometry, where

$$\tau = \frac{4D_2 t}{a^2}$$

Equation 2.13

(13)

Features of the current response depend on the tip geometry and following dimensionless parameters

$$K = \frac{k^0 a}{D_2}$$

Equation 2.14 Dimensionless rate constant

$$\gamma = D_1/D_2$$

Equation 2.15 Diffusion coefficient ratio

$$\sigma = \frac{a^2}{4D_2}\frac{Fv}{RT}$$

Equation 2.16 Dimensionless scan rate

Calculation of each CV or chronoamperogram took 3–5 minutes on a workstation equipped with a Xeon 3.0 GHz processor unit and 5.0 GB RAM with Linux.

In the following theory section, $\tan\theta_1 = \tan\theta_2 = 0.10$ with the angle of 5.7° was assumed unless otherwise mentioned. Preliminary simulations demonstrated that a small change in θ_2 from this typical inner angle does not affect the results. A typical RG (= r_g/a) value of 1.5 was also used. Moreover, $\gamma = 1$ was assumed so that the unique shape of a transient CV with a sigmoidal and a peak-shaped wave is not due to different diffusion coefficients.[44] In practice, however, γ can be significantly different from 1, because of ion–ionophore complexation[33] and different solvent viscosities in the inner and outer solutions.[45] Effects of γ on a simulated transient CV are discussed in Supporting Information.

2.3.2 Chronoamperometry Inside Pipets

Recently, Kakiuchi and co-workers reported that steady-state diffusion is achieved in the inner solution at a tapered pipet even with a small tip angle.[39] In order to understand the tip-angle effect more quantitatively, a chronoamperometric response limited by diffusion in the inner solution was calculated by solving only Equation 2.4 with the boundary condition of $c_1(r,0,t) = c_0$ at the liquid/liquid interface (Figure 2-3). With any tip angle, a normalized chronoamperometric response, $i(\tau)/i_{ss}$, varies inversely with $\sqrt{\tau}$, yielding an approximated equation

$$\frac{i(\tau)}{i_{ss}} \approx f(\theta) + \frac{g(\theta)}{\sqrt{\tau}}$$

Equation 2.17

Table 2-1 lists $f(\theta)$ and $g(\theta)$ for a variety of θ values. The intercept, $f(\theta)$, represents a normalized steady-state current, which increases from 0 to 1 as the tip angle increases from 0 to $\pi/2$.[39] With $\tan\theta < 0.5$, $g(\theta) \approx \sqrt{\pi}/2$ so that $g(\theta)/\sqrt{\tau}$ in Equation 2.17 is equivalent to the Cottrell current normalized against i_{ss}.[46]

A long time is required for steady-state diffusion in the inner solution, resulting in a thick diffusion layer. A steady state is achieved when $f(\theta) >> g(\theta)/\sqrt{\tau}$ in Equation 2.17, yielding

$$\tau >> \frac{g(\theta)^2}{f(\theta)^2}$$

Equation 2.18

With Equations 2.13 and 2.18, the diffusion layer thickness at a steady state, δ_{ss}, is given by

$$\delta_{ss} = \sqrt{4D_1 t} >> a\frac{g(\theta)}{f(\theta)}$$

Equation 2.19

Equation 2.18 indicates that, for typical tip angles with $\tan\theta = 0.05$–0.15, the time required for a steady state is 100–1000 times longer than that at an inlaid disk-shaped interface with $\theta = \pi/2$. Also, Equation 2.19 shows that a δ_{ss} value inside the pipets is 10–25 times larger than that at the disk-shaped interface.

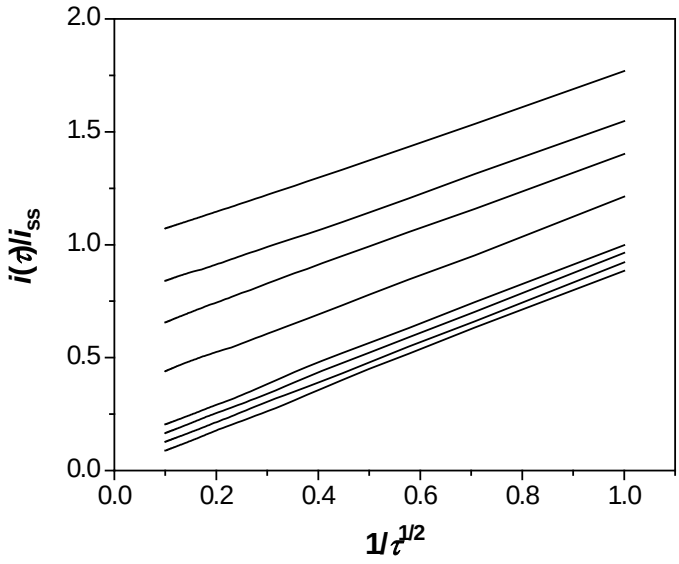

Figure 2-3. Effects of the tip angle, θ, on a simulated chronoamperometric response governed by diffusion in the inner solution, where tan θ = 0, 0.05, 0.1, 0.15, 0.5, 1, and 2 from the bottom. The top line shows a response at an inlaid disk-shaped interface.[10]

Table 2-1. Parameters in Equations 2.17 and 2.22 with different tip angles.

$\tan\theta$	$f(\theta)$	$g(\theta)$	$(RT/F)\ln f(\theta)$ mV[a]
0	0.000	0.891	–
0.05	0.038	0.882	−83.7
0.1	0.077	0.886	−65.8
0.15	0.114	0.893	−55.7
0.5	0.357	0.844	−26.5
1.0	0.576	0.834	−14.1
2.0	0.762	0.771	−6.9
∞	0.995	0.763	0.1

[a] Values at 25 °C.

2.3.3 Reversible Cyclic Voltammetry at Cylindrical and Tapered Pipets

Effects of the pipet geometry on a reversible CV (K = 10) were investigated at different σ. With either a cylindrical or a tapered pipet (Figure 2-4a or b, respectively), sufficiently small σ (< 1) gives a sigmoidal forward wave. Although a reverse peak indicates that a true steady state is not achieved, the shape of a sigmoidal forward wave agrees with the theoretical shape of a reversible steady-state voltammogram given by

$$\Delta_2^1\phi = \Delta_2^1\phi_{1/2} + \frac{RT}{z_i F}\ln\frac{i_{ss}(x) - i}{i}$$

Equation 2.20

with

$$i_{ss}(x) = 4xz_i FD_2c_0a$$

Equation 2.21

where $\Delta_2^1\phi_{1/2}$ is the half-wave potential, $i_{ss}(x)$ is the current limited by diffusion of a transferred ion in the outer solution, and x is a function of RG.[47]

At a cylindrical pipet, a sigmoidal forward wave is followed by a reverse peak (Figure 2-4a), which is due to purely linear diffusion in the inner solution. The peak current is nearly independent of σ and is 110–120 % with respect to the limiting current. These features of a reversible CV at a cylindrical pipet were predicted by the approximated[36] and boundary element[37] methods. Moreover, our simulation results demonstrate that both forward and reverse

(a)

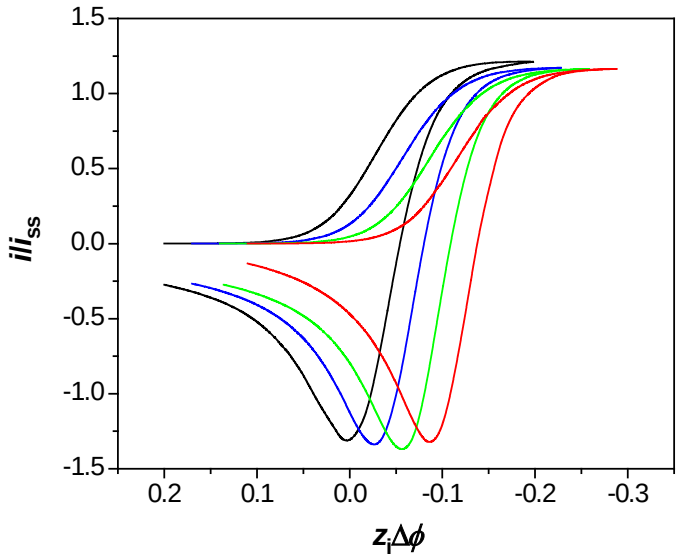

(b)

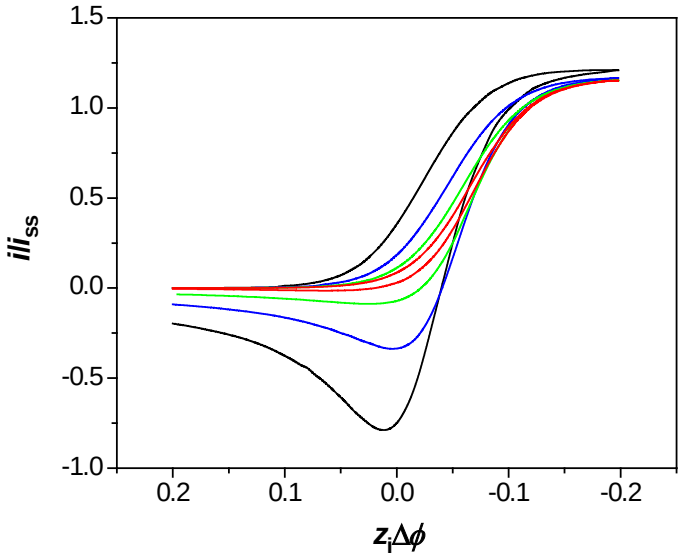

Figure 2-4. Effects of the dimensionless scan rate, σ, on simulated CVs at (a) a cylindrical and (b) a tapered (tan θ = 0.01) pipet, where σ = 0.1 (black), 0.01 (blue), 0.001 (green), and 0.0001 (red). The other dimensionless parameters are K = 10 and γ = 1.

waves shift toward negative potentials by $30/z_i$ mV for every decade decrease in σ, while the separation between the half-wave and peak potentials is maintained at $32/z_i$ mV.

In contrast to the cylindrical case, a reverse wave at a tapered pipet changes from a peak shape to a sigmoidal shape as σ decreases from 0.1 to 0.0001 (Figure 2-4b). The reverse wave at σ = 0.0001 is nearly identical with the forward wave, confirming a steady state. Such a steady-state response was obtained at larger σ with a larger tip angle (data not shown), where a steady state is reached more quickly (Equation 2.18). For the reversible steady-state voltammogram, $\Delta_2^1\phi_{1/2}$ is given by (Supporting Information)

$$\Delta_2^1\phi_{1/2} = \Delta_2^1\phi_i^{0'} + \frac{RT}{z_iF}\ln\gamma + \frac{RT}{z_iF}\ln\frac{f(\theta)}{x}$$

Equation 2.22

With γ = 1, $(RT/z_iF)\ln f(\theta)$ is due to a mass-transfer resistance in the inner solution and is significant for typical tip angles with $\tan\theta$ = 0.05–0.15 (Table 2-1).

2.3.4 Kinetic Effects on Steady-State and Transient CVs

Effects of an intrinsic ion-transfer rate on steady-state and transient CVs at a tapered pipet were investigated in a range of K = 0.01–10 with α = 0.5. With σ = 0.0001 (Figure 2-5a), forward and reverse waves superimpose well in all kinetic regimes, confirming a steady state. Kinetic effects under the steady-state condition are very similar to those in steady-state voltammetry at solid UMEs.[48] As K decreases from 10 to 0.3, the sigmoidal waves become less steep and shift toward negative potentials, corresponding to a change from a reversible wave to a quasi-reversible wave.

(a)

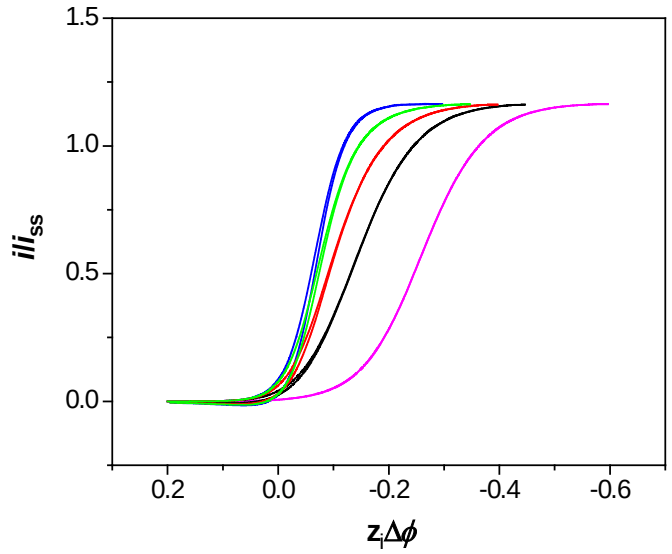

(b)

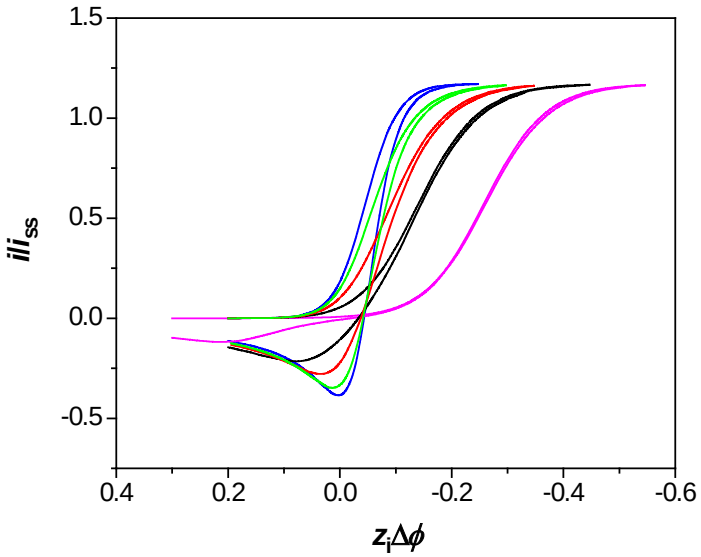

Figure 2-5. Effects of the dimensionless ion-transfer rate constant, *K*, on (a) steady-state and (b) transient CVs at σ = 0.0001 and 0.01, respectively, where *K* = 10 (blue), 1 (green), 0.3 (red), 0.1 (black), and 0.01 (magenta). The other dimensionless parameters are tan θ = 0.10 and γ = 1.

A further decrease in K results in an irreversible kinetic regime, where the sigmoidal waves shift toward negative potentials without a change in the shape.

Under a transient condition (σ = 0.01 in Figure 2-5b), kinetic effects on a sigmoidal forward wave are similar to those under a steady-state condition. On the other hand, a reverse peak becomes smaller and broader as K decreases. At the same time, the peak potential shifts toward positive potentials, increasing the separation between the sigmoidal and peak-shaped waves. In an irreversible kinetic regime at K = 0.01, the voltammetric response on reverse potential sweep traces the sigmoidal forward wave and then becomes peak-shaped. The sigmoidal portions of the forward and reverse waves under a transient condition are identical, because egress ion transfer is negligible at the large negative potentials. In all kinetic regimes, forward and reverse waves under a transient condition are different so that more parameters are obtainable from a transient CV than from the steady-state counterpart with identical forward and reverse waves (see below).

2.3.5 Parameters Obtainable from Steady-State and Transient CVs

With a reverse peak, a transient CV allows for determination of parameters that can not be obtained from the steady-state counterpart. In either case, each of obtainable parameters is qualitatively relevant to the shape, height, or position of a forward or a reverse wave. Knowledge of these relationships is useful for determination of multiple parameters by fitting an experimental CV with a simulated CV (Results and Discussion). A significant deviation between simulated and experimental CVs was found when a parameter was more than 15 % larger or smaller than the value determined from the best fit.

In a reversible case, z_i can be determined from the shape of a forward wave so that D_2 is obtainable from a limiting current using Equation 2.21. Under a transient condition, the height of a reverse peak is sensitive to γ (Supporting Information), yielding D_1 from γ and D_2. With these three parameters, $\Delta_2^1\phi_i^{0'}$ is determined from the position of the forward wave as represented by $\Delta_2^1\phi_{1/2}$. Without a reverse peak under a steady-state condition, an additional measurement of D_1 is required for determination of $\Delta_2^1\phi_i^{0'}$ and vice versa (Equation 2.22). For instance, both D_1 and D_2 can be determined by steady-state voltammetry with a transferred ion in both phases.[33]

A transient CV under kinetic control gives k^0 and α in addition to all parameters that are available from a reversible transient CV. In either a quasi-reversible or an irreversible case, k^0 determines the separation between forward and reverse waves, while z_i and α control the shape of a forward and a reverse wave. On the other hand, k^0, α, and $\Delta_2^1\phi_i^{0'}$ are obtainable from a quasi-reversible steady-state voltammogram by numerical analysis (see below), when z_i, D_2, and D_1 are known. Much less information is obtainable from an irreversible steady-state voltammogram. The wave shape is just an indicator of αz_i so that additional chronoamperometric measurement is required for determination of z_i and D_2 and subsequently α.[10] Knowledge of $\Delta_2^1\phi_i^{0'}$ is still required to obtain k^0 and vice versa. Overall, a transient CV is most useful for a kinetic study of irreversible ion transfer.

It should be noted that a simulation of hindered diffusion in the inner solution is required for analysis of quasi-reversible voltammograms even under a steady-state condition. Biased values of $\Delta_2^1\phi_i^{0'}$ and k^0 are obtained from the steady-state waves using a method developed for simple analysis of quasi-reversible steady-state voltammograms at solid UMEs[35] (Table 2-2). A bias in $\Delta_2^1\phi_i^{0'}$ becomes larger at a sharper tip, corresponding to an error due to a mass-transfer

resistance in the inner solution. A biased k^0 value is larger than a true value by a factor of 2 even for a large tip angle with tanθ = 0.5. The simple method or original theory developed for solid UMEs[49] is not applicable either under a transient[9] or a steady-state[26, 27] condition when quasi-reversible ion transfer is coupled with hindered diffusion in the inner solution.

2.3.6 Conditions for Recording a Transient CV

A transient CV is obtained when σ is sufficiently large (Figure 2-4b). Equation 2.16 indicates that larger σ can be achieved experimentally using a faster scan rate or a larger pipet. The scan rate and pipet size, however, also affect a mass-transfer rate in the inner solution, thereby controlling electrochemical reversibility. A faster scan rate enhances the mass-transfer rate so that a CV becomes less reversible, which is beneficial for a kinetic study of fast ion transfer. On the other hand, slower mass transfer at a larger pipet enhances reversibility. A larger pipet is useful for a study of slow ion transfer, where widely separated sigmoidal and peak-shaped responses must be observed within a relatively small potential window at liquid/liquid interfaces.

2.3.7 EXPERIMENTAL SECTION

2.3.8 Chemicals

Tetradodecylammonium bromide, 1,2-dichloroethane (1,2-DCE, 99.8 % HPLC grade), nitrobenzene (>99 %), and chlorotrimethylsilane (98 %) were obtained from Aldrich (Milwaukee, WI). *N*,*N*,*N*',*N*'-tetracyclohexyl-3-oxapentanediamide (ETH 129) and tetradocecylammonium tetrakis(4-chlorophenyl)borate (TDDATPBCl, ETH 500) were obtained from Fluka (Milwaukee, WI). Protamine sulfate (Grade III, from herring), tetraethylammonium

Table 2-2. Biased parameters obtained from quasi-reversible steady-state voltammograms by the simple method

$\tan\theta$	α (0.5^a)	$\Delta^{in}_{out}\phi^{0'}_i$ mV[b]	K^c
	(0^a)		
0.15	0.55	−57.7	2.2 (1.0)
	0.52	−54.8	1.5 (0.5)
	0.50	−55.6	0.9 (0.3)
0.50	0.52	−24.0	2.8 (2.0)
	0.45	−23.2	2.0 (1.0)
	0.50	−30.6	0.8 (0.5)

[a] Values used for simulations. [b] Values at 25 °C. [c] Simulation values are shown in the parentheses.

hydroxide (TEAOH, 20 wt% in water), and tris(hydroxylmethyl)aminomethane (Tris, 99.9 %) were from Sigma (St. Louis, MO). Calcium dinonylnaphthalenesulfonate (CaDNNS, NACORR® 1351) was a gift from King Industries (Norwalk, CT). Boulder Scientific Company (Mead, CO) provided the potassium tetrakis(pentafluorophenyl)borate (KTFAB). TDDA salts of DNNS and TFAB were prepared as reported elsewhere.[11, 13] All reagents were used as received. All aqueous solutions were prepared with 18.3 MΩ cm^{-1} deionized water (Nanopure, Barnstead, Dubuque, IA).

2.3.9 Fabrication of Micropipet Electrodes

Micropipets were made from borosilicate glass capillaries (o.d./i.d.=1.0 mm/0.58 mm, 10 cm in length) from Sutter Instrument Co. (Novato, CA) using laser-based pipet puller (model P-2000, Sutter Instrument).[10] The inner wall of each pipet was silanized[30] to fill the inside with an organic solution. The micropipet tip geometry was inspected using an optical microscope model BX 41 (×100 to ×500) or IX 71 (×600 with an oil immersion lens) from Olympus America (Melville, NY). The inner tip angle was determined from a digitalized optical image of a micropipet taken from the side of the wall (Figure 2-6), yielding typical inner and outer angles of 6° and 10°, respectively, within an error of ± 1° using a program, Simple PCI 6. The inner and outer tip diameters were determined within an error of ± 0.25 μm from an image taken from the side of the tip.

2.3.10 Electrochemical Measurements

A computer controlled CHI 660B electrochemical workstation equipped with CHI 200 picoamp booster and faraday cage (CH instruments, Austin, TX) was used for all electrochemical measurements. The electrochemical cells employed are as follows

Ag | AgCl | 0.14 mM TEAOH in 10 mM NaH_2PO_4/Na_2HPO_4 pH 7.1 (aq) || 0.1 M TDDATPAB (nitrobenzene) | Ag (cell 1)

Ag | AgCl | 0.05 mM $Ba(OH)_2$ in 10 mM Tris/acetate pH 7.8 (aq) || 50 mM ETH 129 in 100 mM TDDATPBCl (1,2-DCE) | AgTPBCl | Ag (cell 2)

Ag | AgCl | 0.022 mM protamine sulfate in 8 mM Tris/acetate pH 7.8 (aq) || 2.5 mM TDDADNNS in 0.01 M TDDATPBCl (1,2-DCE) | AgTPBCl | Ag (cell 3)

Pipets were filled with the organic solution from the back using a 10 μL syringe. The current carried by a positive charge from the aqueous phase to the organic phase was defined to be positive. All electrochemical experiments were performed at 22 ± 3 ºC. A background CV was obtained using a cell without a target ion in the aqueous phase. Only background-subtracted CVs are reported in Results and Discussion.

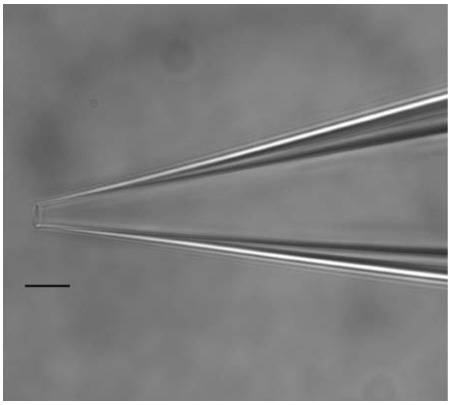

Figure 2-6. An optical microscopic image of a typical micropipet electrode. The scale bar indicates 10 μm.

2.4 RESULTS AND DISCUSSION

2.4.1 Reversible TEA^+ Transfer.

Both transient and steady-state CVs were obtained for reversible TEA^+ transfer using a tapered pipet with the tip radius of 2.1 μm (Figure 2-7). At v = 2–80 mV/s, forward potential sweep resulted in a sigmoidal wave based on simple TEA^+ transfer from the outer aqueous phase into the inner nitrobenzene phase. At v = 2 mV/s, the reverse wave is also sigmoidal and nearly overlaps with the forward wave, confirming the theoretical prediction that steady-state diffusion is achieved in the inner solution at a tapered pipet with a small tip inner angle. As v increases

from 2 mV/s to 80 mV/s, the reverse wave begins to show the peak expected for egress TEA^+ transfer coupled with transient diffusion in the inner solution. Although a steady state was not achieved at v = 20 and 80 mV/s, the shape of a forward wave is independent of v and consistent with the theoretical shape of a reversible steady-state voltammogram given by Equation 2.20, yielding z_i = +1 (red dotted lines in Figure 2-7). With z_i = +1 in Equation 2.21, the v-independent limiting current gives the diffusion coefficient in the outer aqueous phase, D_w, of 9.3 × 10^{-6} cm^2/s, which agrees with a literature value.[45] The forward waves only, however, do not give $\Delta^o_w\phi^{0'}_{TEA^+}$ or the diffusion coefficient in the inner organic phase, D_o, requiring analysis of both forward and reverse waves of a transient CV.

With tip inner and outer angles determined by optical microscopy, the transient CVs at v = 20 and 80 mV/s fit well with simulated CVs (Figure 2-7), yielding values of $\Delta^o_w\phi^{0'}_{TEA^+}$ and D_o in addition to the same values of z_i and D_w as determined from the forward waves. A simulated CV with these parameters also fits with the steady-state CV at v = 2 mV/s. In the simulation of the transient CVs, a peak height with respect to a limiting current is sensitive to γ, yielding a value of 0.5 from the fitting. A combination of the γ and D_w values gives D_o = 4.7 × 10^{-6} cm^2/s, which is close to a literature value of 4.0 × 10^{-6} cm^2/s in the nitrobenzene phase.[45] With the known γ value, a v-independent value of $\Delta^o_w\phi^{0'}_{TEA^+}$ is determined from the wave position, revealing that both $\Delta^o_w\phi_{1/2}$ and the peak potential shift toward negative potentials as v decreases. At v = 2 mV/s, $\Delta^o_w\phi_{1/2}$ is more negative than $\Delta^o_w\phi^{0'}_{TEA^+}$ by 82 mV. The potential difference is consistent with a steady-state value predicted by Equation 2.22, where a negative shift of 18 mV is due to $(RT/F)\ln\gamma$ and the remainder is due to $(RT/F)\ln[f(\theta)/x]$.

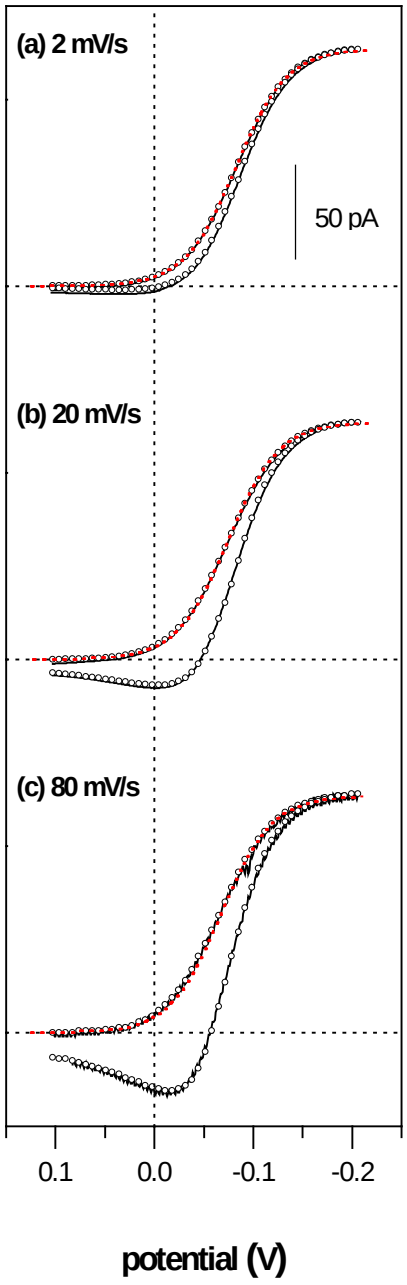

Figure 2-7. Background-subtracted CVs of simple TEA^+ transfer at a 2.1 μm-radius pipet with θ_1 = 6° and θ_2 = 12° (cell 1). The vertical and lateral dotted lines correspond to $\Delta^{o}_{w}\phi^{0'}_{TEA^+}$ and base lines, respectively. The open circles represent simulated CVs of reversible monovalent-cation transfer with parameters described in the text. The red dotted lines in (a) correspond to reversible steady-state voltammograms based on Equation 2.20 with z_i = +1.

2.4.2 Quasi-Reversible Ba^{2+} Transfer Facilitated by ETH 129

Ba^{2+} transfer facilitated by ETH 129[50] was investigated using a 2.5 μm-radius tapered pipet to obtain quasi-reversible CVs both under transient and steady-state conditions (Figure 2-8). At v = 2 mV/s, forward and reverse waves are sigmoidal and nearly superimpose, confirming a steady state. As v increases, the reverse wave becomes peak-shaped, because of transient diffusion of Ba^{2+}–ETH129 complexes in the inner solution. The v-independent shape of a sigmoidal forward wave is broader than expected for reversible transfer of a divalent cation at a steady state (Equation 2.20 with z_i = +2), indicating that the Ba^{2+} transfer is kinetically limited. Since a forward wave is not completely separated from a peak-shaped reverse wave under a transient condition, the transfer process is quasi-reversible rather than irreversible. With z_i = +2 in Equation 2.21, the v-independent limiting current corresponds to $D_w = 1.1 \times 10^{-5}$ cm^2/s, which is consistent with a literature value.[51]

A quasi-reversible transient CV gives kinetic parameters of k^0 and α in a Butler-Volmer-type model (Equations 2.7 and 2.8) as well as all parameters that are obtainable from a reversible transient CV, i.e., z_i, $\Delta^o_w\phi_i^{0'}$, D_w, and D_o. In a quasi-reversible case, the separation between forward and reverse waves is sensitive to k^0. Moreover, the shape of a forward and a reverse wave depends not only on z_i but also on α. The quasi-reversible transient CVs at v = 20 and 100 mV/s fit well with simulated CVs (Figure 2-9), yielding k^0 = 0.012 cm/s, α = 0.45, γ = 0.3, z_i = +2, and a v- independent $\Delta^o_w\phi^{0'}_{Ba^{2+}}$ value of +136 mV with respect to $\Delta^o_w\phi^{0'}_{TEA^+}$. The nearly steady-state CV at v = 2 mV/s also fits with a simulated CV with these parameters. The α value is within the normal range of 0.4–0.6, [54] suggesting that the facilitated Ba^{2+} transfer is a one-step process. As v increases, a forward and a reverse wave shifts toward negative and positive potentials,

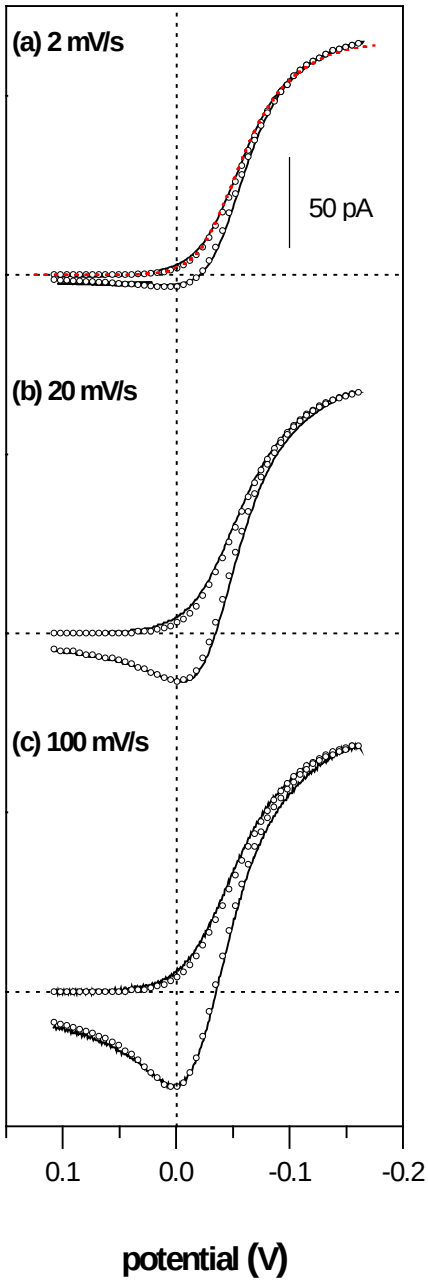

Figure 2-8. Background-subtracted CVs of Ba^{2+} transfer facilitated by ETH 129 at a 2.5 μm-radius pipet with θ_1 = 6° and θ_2 = 12° (cell 2). The vertical and lateral dotted lines correspond to $\Delta^{o}_{w}\phi^{0'}_{Ba^{2+}}$ and base lines, respectively. The open circles represent simulated CVs of quasi-reversible divalent-cation transfer with parameters described in the text. The red dotted line in (a) corresponds to a quasi-reversible steady-state voltammogram based on a theory for disk UMEs (Equation 2.S16 in Supporting Information).

respectively, resulting in wider separation between the waves. The direction of the *v*-dependent shift of a peak potential in a quasi-reversible case is opposite to that in a reversible case. With the D_w value determined from the limiting current, the γ value corresponds to $D_o = 3.3 \times 10^{-6}$ cm^2/s for Ba^{2+}–ETH 129 complexes. A 1:2 stoichiometry of the complexes was determined previously from a voltammetric response limited by ETH 129 diffusion in the presence of an excess amount of Ba^{2+}.[50]

It should be noted that neither a theory[49] nor a simple method[35] for analysis of quasi-reversible steady-state voltammograms at solid UMEs is applicable when a quasi-reversible micropipet voltammogram is coupled with hindered diffusion in the inner solution.[9, 26, 27] In fact, biased k^0 and $\Delta^o_w\phi^{0'}_{Ba^{2+}}$ were obtained by fitting the quasi-reversible steady-state wave at v = 2 mV/s to a theoretical equation derived for disk UMEs (Equation 2.S16 in Supporting Information). Despite a good fit between the experimental wave and Equation 2.S16 with α = 0.45 and γ = 0.3 (red dotted line in Figure 2-8a), the k^0 value of 0.039 cm/s thus determined is ~3 times larger than the value determined by the finite element simulation, while $\Delta^o_w\phi^{0'}_{Ba^{2+}}$ is also biased toward negative potentials by 27 mV. The biases are not due to the transient nature of the voltammogram, because the shape of a forward wave is nearly independent of *v*. The biased parameters indicate that slow mass transfer in the inner solution significantly affects the shape and position of a quasi-reversible wave even under a steady-state condition.

2.4.3 Irreversible Protamine Transfer Facilitated by DNNS

A transient CV is particularly useful for a study of slow ion transfer such as irreversible protamine transfer facilitated by DNNS. Protamine is a naturally occurring polycationic protein

rich in arginine (4.5 kDa and ~+20 charge) and is used as an antidote for heparin.[52] Meyerhoff and co-workers introduced DNNS as an ion exchanger for protamine-sensitive electrodes based on non-equilibrium potentiometric responses.[53] Our previous work demonstrated that protamine transfer facilitated by DNNS results in a transient CV at an organic-filled pipet.[11] The facilitated protamine transfer is so slow that sigmoidal and peak-shaped portions of a transient CV are completely separated at a 2.2 μm-radius tapered pipet (Figure 2-9). This result indicates that the transfer process is totally irreversible.

The irreversible transient CV was analyzed with an assumption of a multistep transfer mechanism.[11] Formation of protamine–DNNS complexes at an interfacial adsorption plane was assumed to be the rate-determining step, yielding

$$k_{\mathrm{f}} = k^{0} \exp[-\alpha(1-\beta) z_{\mathrm{i}} F (\Delta^{\mathrm{o}}_{\mathrm{w}}\phi - \Delta^{\mathrm{o}}_{\mathrm{w}}\phi_{\mathrm{i}}^{0'}) / RT]$$

Equation 2.23

$$k_{\mathrm{b}} = k^{0} \exp[(1-\alpha)(1-\beta) z_{\mathrm{i}} F (\Delta^{\mathrm{o}}_{\mathrm{w}}\phi - \Delta^{\mathrm{o}}_{\mathrm{w}}\phi_{\mathrm{i}}^{0'}) / RT]$$

Equation 2.24

with

$$\beta = \frac{\Delta_{\sigma}{}^{\mathrm{o}}\phi}{\Delta_{\mathrm{w}}{}^{\mathrm{o}}\phi}$$

Equation 2.25

where $\Delta_{\sigma}{}^{\mathrm{o}}\phi$ is the Galvani potential difference between the inner organic phase and the adsorption plane. A good fit between an experimental and a simulated CV was obtained both for

a forward and a reverse wave (Figure 2-9), supporting the multistep mechanism. The analysis gives $\alpha = 0.65$, $(1 - \beta)z_i = 2.9$, $\gamma = 0.5$, $k^0 = 3.5 \times 10^{-5}$ cm/s, and $\Delta^o_w\phi^{0'}_P = +97$ mV with respect to $\Delta^o_w\phi^{0'}_{TEA^+}$. The values of k^0 and $\Delta^o_w\phi^{0'}_P$ were determined for the first time in this work, where the finite element simulation allows for analysis of both sigmoidal and peak-shaped portions of the transient CV. The k^0 value of the facilitated protamine transfer thus determined is the smallest k^0 value reported so far for ion transfer at liquid/liquid interfaces.

It should be noted that β and z_i can not be determined separately from the transient CV based on the multistep mechanism so that $\beta = 0.86$ is obtained with $z_i = +20$, which was determined by chronoamperometry.[11] Also, a transient CV does not give a stoichiometry of DNNS–protamine complexes, which was determined as 20 from a steady-state current limited by DNNS diffusion at a water-filled pipet.[11] We ascribe the slow rate of facilitated protamine transfer to the formation of complexes with the large stoichiometry at the interface.[11]

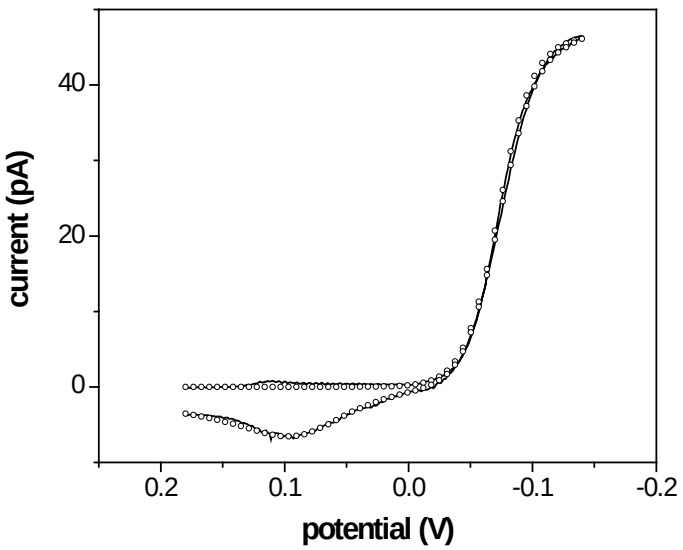

Figure 2-9. A background-subtracted CV of protamine transfer facilitated by DNNS at a 2.2 μm-radius pipet with θ_1 = 6° and θ_2 = 12° (cell 3). The potential is given with respect to $\Delta^{o}_{w}\phi^{0'}_{P}$. The open circles represent a simulated CV of irreversible protamine transfer based on a multistep transfer mechanism (Equations 2.27–29) with parameters described in the text.

2.5 CONCLUSIONS

A transient response in cyclic voltammetry at micropipet electrodes is extremely useful for kinetic studies of simple and facilitated ion transfer at liquid/liquid interfaces. All kinetic and thermodynamic parameters as well as the charge and diffusion coefficients of a transferring ion are obtainable from a kinetically-limited transient CV by the finite element simulation. Because of slow mass transfer in the inner solution, the transient approach is inherently useful for a study of slow ion transfer. In contrast to cyclic voltammetry at macrointerfaces, use of microinterfaces in the transient kinetic measurement at a moderate potential sweep rate avoids serious effects of uncompensated ohmic resistance and capacitive current. An apparent k^0 value of 3.5×10^{-5} cm/s thus determined from a transient CV of irreversible protamine transfer facilitated by DNNS is the smallest k^0 value reported so far for ion transfer at liquid/liquid interfaces.

Numerical treatment of hindered diffusion in the inner solution is required also for accurate analysis of the less informative steady-state CV as obtained at a slower scan rate or with a smaller pipet.[26, 27] A reliable largest k^0 value of ~1 cm/s was reported for quasi-reversible K^+ transfer facilitated by dibenzo-18-crown-6 at nanopipets, where mass transfer is controlled only by hemispherical diffusion in the outer solution.[24-26] Overall, an intrinsic rate of ion transfer at liquid/liquid interfaces varies by at least 5 orders of magnitude. This information will be useful for better understanding of ion transfer at liquid/liquid interfaces and also for further development of voltammetric/amperometric ISEs.

ACKNOWLEDGEMENTS

This work was supported by a CAREER award from the National Science Foundation (CHE-0645623). We thank Professor Stephen G. Weber and Ms. Manyan Wang for help with obtaining optical microscopic images of micropipets.

SUPPORTING INFORMATION

Finite Element Simulation by COMSOL Multiphysics.

The SECM diffusion problem defined in the theory section was solved using dimensionless parameters defined by

$$R = r/a \tag{S1}$$

$$Z = z/a \tag{S2}$$

$$C_1(R,Z,\tau) = c_1(r,z,t)/c_0 \tag{S3}$$

$$C_2(R,Z,\tau) = c_2(r,z,t)/c_0 \tag{S4}$$

$$\theta = \exp\left[\frac{F(\Delta_2^1\phi - \Delta_2^1\phi_1^{0'})}{RT}\right] \tag{S5}$$

The other dimensionless parameters are given by Equations 2.13–16. Diffusion processes (Equations 2.4 and 2.5) are expressed in the respective dimensionless forms as

$$\frac{\partial C_1(R,Z,\tau)}{\partial \tau} = 0.25\gamma\left[\frac{\partial^2 C_1(R,Z,\tau)}{\partial R^2} + \frac{1}{R}\frac{\partial C_1(R,Z,\tau)}{\partial R} + \frac{\partial^2 C_1(R,Z,\tau)}{\partial Z^2}\right] \tag{S6}$$

$$\frac{\partial C_2(R,Z,\tau)}{\partial \tau} = 0.25\left[\frac{\partial^2 C_2(R,Z,\tau)}{\partial R^2} + \frac{1}{R}\frac{\partial C_2(R,Z,\tau)}{\partial R} + \frac{\partial^2 C_2(R,Z,\tau)}{\partial Z^2}\right] \tag{S7}$$

The values of 0.25γ and 0.25 in Equations 2.S6 and 2.S7 were used as dimensionless diffusion coefficients in the corresponding phases. The boundary condition at the liquid/liquid interface (Equation 2.6) is expressed using dimensionless parameters as

$$0.25\gamma\left[\frac{\partial C_1(R,Z,\tau)}{\partial Z}\right]_{z=0} = -\frac{0.25K}{\theta^{\alpha z_i}}[\theta^{z_i}C_2(R,0,\tau) - C_1(R,0,\tau)] \quad \text{(S8)}$$

$$0.25\left[\frac{\partial C_2(R,Z,\tau)}{\partial Z}\right]_{z=0} = 0.25K\theta^{(1-\alpha)z_i}[\frac{C_1(R,0,\tau)}{\theta^{z_i}} - C_2(R,0,\tau)] \quad \text{(S9)}$$

Equations 2.S8 and 2.S9 are equivalent to the expression of a flux boundary condition in COMSOL Multiphysics. The triangle potential wave (Equation 2.9) is given by

$$\theta = \theta_i^{1-(2/\pi)\sin^{-1}\{\sin[\pi\sigma\tau/2\ln(\theta_\lambda/\theta_i)]\}}\theta_\lambda^{(2/\pi)\sin^{-1}\{\sin[\pi\sigma\tau/2\ln(\theta_\lambda/\theta_i)]\}} \quad \text{(S10)}$$

with

$$\theta_i = \exp\left[\frac{F(\Delta_2^1\phi_i - \Delta_2^1\phi_i^{0'})}{RT}\right] \quad \text{(S11)}$$

$$\theta_\lambda = \exp\left[\frac{F(\Delta_2^1\phi_\lambda - \Delta_2^1\phi_i^{0'})}{RT}\right] \quad \text{(S12)}$$

The other boundary conditions and initial condition are also given using dimensionless parameters (see the attached example). The simulation gives a dimensionless current normalized with respect to a limiting current at an inlaid disk-shaped interface.

Effects of Diffusion Coefficient Ratio on Transient CVs

Transient CVs of reversible, quasi-reversible, and irreversible ion transfer were simulated with different diffusion coefficient ratios, γ (Figure 2-S1). In all kinetic regimes, the normalized height of a reverse peak increases as γ decreases, enhancing the transient nature of diffusion in the inner solution. The peak height is useful for determination of a γ value. At the same time, the peak potential shifts toward negative potentials, corresponding to an increase in a mass-transfer resistance in the inner solution. In fact, a reversible forward wave also moves toward positive

potentials as γ decreases. A γ-dependent shift of a quasi-reversible forward wave is much smaller, because the current response on forward potential sweep is affected less by egress ion transfer coupled with transient diffusion in the inner solution. In an irreversible kinetic regime, a forward wave is independent of γ, because the egress ion transfer is negligible at large negative potentials.

Derivation of Equation 2.22

The half-wave potential of a reversible steady-state voltammogram in Equation 2.22 was obtained as follows. In a reversible case at a steady state, the interfacial potential is given by the Nernst equation as

$$\Delta_2^1\phi = \Delta_2^1\phi_i^{0'} + \frac{RT}{z_i F}\ln\frac{c_2(r,0,\infty)}{c_1(r,0,\infty)} \tag{S13}$$

where $c_1(r,0,\infty)$ and $c_2(r,0,\infty)$ are steady-state ion concentrations at the inner and outer solution-sides of the interface, respectively. With Equation 2.18, a steady state current controlled by hindered diffusion in the inner solution is given by

$$i = 4f(\theta)z_i F D_1 a c_1(r,0,\infty) \tag{S14}$$

The same steady-state current is sustained by hemispherical diffusion in the outer solution, yielding from Equation 2.21

$$i = 4xz_i F D_2 a[c_0 - c_2(r,0,\infty)] \tag{S15}$$

Combination of Equations 2.S13–S15 and Equation 2.21 gives Equation 2.22 as well as Equation 2.20.

(a)

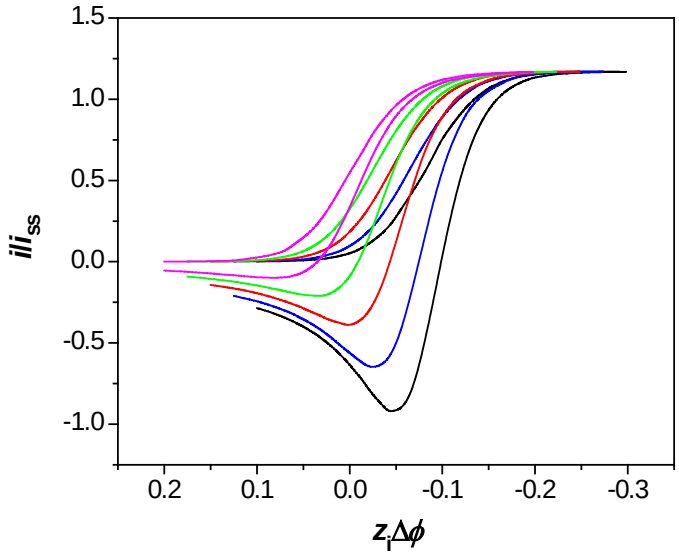
1.5
1.0
0.5
0.0
-0.5
-1.0
0.2
0.1
0.0
-0.1
-0.2
-0.3
iii_ss
z_iΔφ

(b)

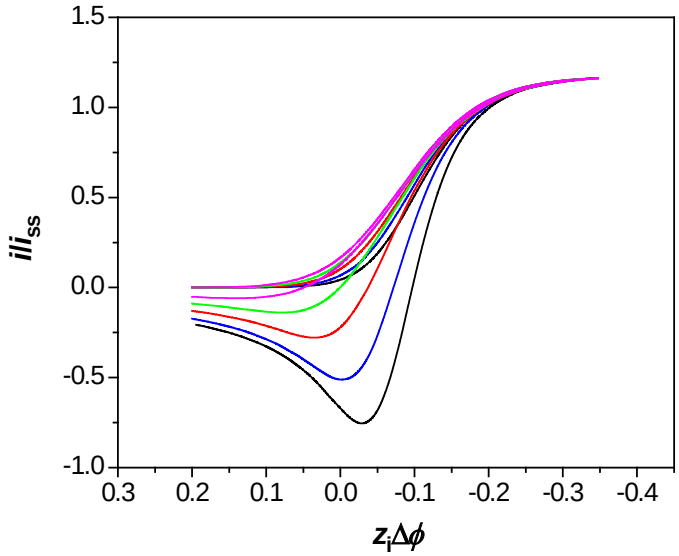
1.5
1.0
0.5
0.0
-0.5
-1.0
0.3
0.2
0.1
0.0
-0.1
-0.2
-0.3
-0.4
iii_ss
z_iΔφ

(c)

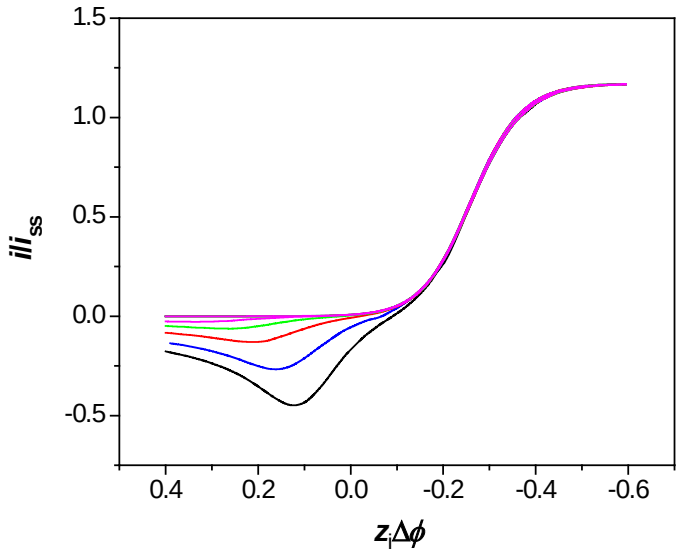

Figure 2-S1. Effects of the diffusion coefficient ratio, γ, on (a) reversible, (b) quasi-reversible, and (c) irreversible CVs (K = 10, 0.3, and 0.001, respectively) simulated under a transient condition (σ = 0.01) at a conical pipet with tan θ = 0.10, where γ = 0.1 (black), 0.3 (blue), 1 (red), 3 (green), and 10 (magenta).

Analysis of Quasi-Reversible Steady-State Voltammograms

A steady-state forward wave of facilitated Ba^{2+} transfer at ν = 2 mV/s was fitted to a theoretical equation originally derived for steady-state voltammetry at disk UMEs (Figure 2-8a).[S1] The equation for ion transfer at liquid/liquid interfaces is given by

$$\frac{i}{i_{ss}} = \frac{1}{\theta'}\left[1 + \frac{\pi}{\kappa\theta'}\left(\frac{2\kappa\theta' + 3\pi}{4\kappa\theta' + 3\pi^2}\right)\right] \tag{S16}$$

with

$$\theta' = 1 + \frac{\exp[z_i F(\Delta^1_2\phi - \Delta^1_2\phi_i^{0'})/RT]}{\gamma} \tag{S17}$$

$$\kappa = \frac{\pi K \exp[-\alpha z_i F(\Delta^1_2\phi - \Delta^1_2\phi_i^{0'})/RT]}{4} \tag{S18}$$

where K and γ are given by Equations 2.14 and 2.15, respectively.

Supporting Info References

(S1) Oldham, K. B.; Zoski, C. G. *J. Electroanal. Chem.* **1988**, *256*, 11–19.

COMSOL Model

A copy of the COMSOL model is available free of charge in the Supporting Information via the Internet at http://pubs.acs.org/doi/suppl/10.1021/ac0711642.

REFERENCES

(1) Bakker, E.; Bühlmann, P.; Pretsch, E. *Chem. Rev.* **1997**, *97*, 3083–3132.
(2) Amemiya, S. In *Handbook of Electrochemistry*; Zoski, C. G., Ed.; Elsevier: New York, 2007, pp 261–294.
(3) Young, C. C. *J. Chem. Edu.* **1997**, *74*, 177–182.
(4) Fry, C. H.; Langley, S. E. M. *Ion-Selective Electrodes for Biological Systems*; Harwood Academic Publishers: Amsterdam, Netherlands, 2001.
(5) Senda, M.; Kakiuchi, T.; Ohsakai, T. *Electrochim. Acta* **1991**, *36*, 253–262.
(6) Samec, Z.; Samcová, E.; Girault, H. H. *Talanta* **2004**, *63*, 21–32.
(7) Henn, D.; Cammann, K. *Electroanalysis* **2000**, *12*, 1263–1271.
(8) Samec, Z.; Homolka, D.; Marecek, V. *J. Electroanal. Chem.* **1982**, *135*, 265–283.
(9) Amemiya, S.; Yang, X.; Wazenegger, T. L. *J. Am. Chem. Soc.* **2003**, *125*, 11832–11833.
(10) Yuan, Y.; Wang, L.; Amemiya, S. *Anal. Chem.* **2004**, *76*, 5570–5578.
(11) Yuan, Y.; Amemiya, S. *Anal. Chem.* **2004**, *76*, 6877–6886.
(12) Guo, J.; Yuan, Y.; Amemiya, S. *Anal. Chem.* **2005**, *77*, 5711–5719.
(13) Guo, J. D.; Amemiya, S. *Anal. Chem.* **2006**, *78*, 6893–6902.
(14) Muslinkina, L.; Pretsch, E. *Chem. Commun.* **2004**, 1218–1219.
(15) Muslinkina, L.; Pretsch, E. *Electroanalysis* **2004**, *16*, 1569–1575.
(16) Langmaier, J.; Samcová, E.; Samec, Z. *Anal. Chem.* **2007**, *79*, 2892–2900.
(17) Bakker, E.; Buhlmann, P.; Pretsch, E. *Talanta* **2004**, *63*, 3–20.
(18) Benjamin, I. *Ann. Rev. Phys. Chem.* **1997**, *48*, 407–451.
(19) Marcus, R. A. *J. Chem. Phys.* **2000**, *113*, 1618–1629.
(20) Taylor, G.; Girault, H. H. *J. Electroanal. Chem.* **1986**, *208*, 179–183.
(21) Liu, B.; Mirkin, M. V. *Anal. Chem.* **2001**, *73*, 670A–677A.
(22) Guo, S. X.; Unwin, P. R.; Whitworth, A. L.; Zhang, J. *Prog. React. Kinet.* **2004**, *29*, 43–166.
(23) Shao, Y.; Mirkin, M. V. *Anal. Chem.* **1998**, *70*, 3155–3161.
(24) Shao, Y.; Mirkin, M. V. *J. Am. Chem. Soc.* **1997**, *119*, 8103–8104.
(25) Yuan, Y.; Shao, Y. H. *J. Phys. Chem. B* **2002**, *106*, 7809–7814.
(26) Cai, C. X.; Tong, Y. H.; Mirkin, M. V. *J. Phys. Chem. B* **2004**, *108*, 17872–17878.
(27) Jing, P.; Zhang, M. Q.; Hu, H.; Xu, X. D.; Liang, Z. W.; Li, B.; Shen, L.; Xie, S. B.; Pereira, C. M.; Shao, Y. H. *Angew. Chem., Int. Ed.* **2006**, *45*, 6861–6864.
(28) Bard, A. J.; Mirkin, M. V., Eds. *Scanning Electrochemical Microscopy*; Marcel Dekker: New York, 2001.
(29) Shao, Y.; Mirkin, M. V. *J. Phys. Chem. B* **1998**, *102*, 9915–9921.
(30) Li, F.; Chen, Y.; Sun, P.; Zhang, M. Q.; Gao, Z.; Zhan, D. P.; Shao, Y. H. *J. Phys. Chem. B* **2004**, *108*, 3295–3302.
(31) Amemiya, S.; Bard, A. J. *Anal. Chem.* **2000**, *72*, 4940–4948.
(32) Caçote, M. H. M.; Pereira, C. M.; Tomaszewski, L.; Girault, H. H.; Silva, F. *Electrochim. Acta* **2004**, *49*, 263–270.

(33) Shao, Y.; Osborne, M. D.; Girault, H. H. *J. Electroanal. Chem.* **1991**, *318*, 101–109.
(34) Bond, A. M.; Oldham, K. B.; Zoski, C. G. *Anal. Chim. Acta* **1989**, *216*, 177–230.
(35) Mirkin, M. V.; Bard, A. J. *Anal. Chem.* **1992**, *64*, 2293–2302.
(36) Stewart, A. A.; Taylor, G.; Girault, H. H.; McAleer, J. *J. Electroanal. Chem.* **1990**, *296*, 491–515.
(37) Qiu, F. L.; Fisher, A. C.; Henley, I. E.; Dryfe, R. A. W. *Electrochem. Commun.* **2003**, *5*, 169–174.
(38) Tong, Y.; Shao, Y.; Wang, E. *Anal. Chem.* (in Chinese) **2001**, *11*, 1241–1245.
(39) Tsujioka, N.; Imakura, S.; Nishi, N.; Kakiuchi, T. *Anal. Sci.* **2006**, *22*, 667–671.
(40) Nishi, N.; Imakura, S.; Kakiuchi, T. *Anal. Chem.* **2006**, *78*, 2726–2731.
(41) Li, F.; Chen, Y.; Zhang, M. Q.; Jing, P.; Gao, Z.; Shao, Y. H. *J. Electroanal. Chem.* **2005**, *579*, 89–102.
(42) Samec, Z. *Pure Appl. Chem.* **2004**, *76*, 2147–2180.
(43) Guo, J.; Amemiya, S. *Anal. Chem.* **2005**, *77*, 2147–2156.
(44) Michael, A. C.; Wightman, R. M.; Amatore, C. A. *J. Electroanal. Chem.* **1989**, *267*, 33–45.
(45) Wandlowski, T.; Marecek, V.; Samec, Z. *Electrochim. Acta* **1990**, *35*, 1173–1175.
(46) Bard, A. J.; Faulkner, L. R. *Electrochemical Methods: Fundamentals and Applications*, 2nd ed.; John Wiley & Sons: New York, 2001, pp 163.
(47) Zoski, C. G.; Mirkin, M. V. *Anal. Chem.* **2002**, *74*, 1986–1992.
(48) Bond, A. M.; Oldham, K. B.; Zoski, C. G. *J. Electroanal. Chem.* **1988**, *245*, 71–104.
(49) Oldham, K. B.; Zoski, C. G. *J. Electroanal. Chem.* **1988**, *256*, 11–19.
(50) Wang, E.; Yu, Z.; Xu, C.; Qi, D. *Anal. Sci.* **1993**, *9*, 405–408.
(51) Harned, H. S.; Polestra, F. M. *J. Am. Chem. Soc.* **1954**, *76*, 2064–2065.
(52) Ando, T.; Yamasaki, M.; Suzuki, K. *Protamines: Isolation, Characterization, Structure and Function*; Springer-Verlag: New York, 1973.
(53) Ramamurthy, N.; Baliga, N.; Wahr, J. A.; Schaller, U.; Yang, V. C.; Meyerhoff, M. E. *Clin. Chem.* **1998**, *44*, 606–613.

3.0 NANOPIPET VOLTAMMETRY OF COMMON ION ACROSS A LIQUID–LIQUID INTERFACE. THEORY AND LIMITATIONS IN KINETIC ANALYSIS OF NANOELECTRODE VOLTAMMOGRAMS

This work has been published as Patrick J. Rodgers, Shigeru Amemiya, Yixian Wang and Michael V. Mirkin. *Anal. Chem*, **2010**, *82*, 84-90**.**

3.1 ABSTRACT

Finite element simulations of ion transfer (IT) reactions at the nanopipet-supported interface between two immiscible electrolyte solutions (ITIES) were carried out, and the numerical results were generalized in the form of an analytical approximation. The developed theory is the basis of a new approach to kinetic analysis of steady-state voltammograms of rapid IT reactions. Unlike the conventional voltammetric protocol, our approach requires the initial addition of a transferable ion to both liquid phases, i.e., to the filling solution inside a nanopipet and the external solution. The resulting steady-state IT voltammogram comprises two waves corresponding to the ingress of the common ion into the pipet and its egress into the external solution. We demonstrate that both ingress and egress waves are required for characterization of pipet geometry and precise determination of thermodynamic and kinetic parameters for rapid IT reactions. In this way, one can eliminate large uncertainties in kinetic parameters, which are

inherent in the previously reported approaches to analysis of nearly reversible steady-state voltammograms of either IT at pipet-supported ITIES or electron transfer at solid electrodes. Numerical simulations also suggest that higher current density at the edge of the nanoscale ITIES increases the significance of electrostatic effects exerted by the charged inner surface of a pipet on IT processes.

3.2 INTRODUCTION

Nanometer-sized solid electrodes with well-defined geometry and size and nanopipet-based voltammetric sensors have emerged as an important tool for studying rapid heterogeneous charge transfer.[1] Kinetics of fast charge-transfer reactions can be measurable at a nanoelectrode because of enhanced mass transfer of species to the nanoscale interface.[2] Similar approaches have been used to extract the formal potential and the heterogeneous charge-transfer kinetic parameters (i.e., the standard rate constant, k^0, and the transfer coefficient, α) from a steady-state quasi-reversible voltammogram of either electron transfer at a solid electrode or ion transfer at the pipet-supported liquid/liquid interface. The simplest of them requires only the values of three characteristic potentials that can be easily found from a sigmoidal voltammogram.[3] According to the theory of steady-state voltammetry, a unique combination of kinetic and thermodynamic parameters corresponds to a specific set of the half-wave potential and two quartile potentials, i.e., potentials at which the current is 1/2, 1/4, and 3/4 of the limiting current.[4, 5] Applications of this simple method to nanoelectrode voltammetry, however, require extra care both

experimentally and theoretically. The precise extraction of quartile potentials is only possible if a voltammogram is very well shaped and unaffected by background current, noise, or other experimental artifacts—a stringent requirement for a nanoelectrode voltammogram with a low-pA or sub-pA diffusion limiting current.[6] The accuracy and precision of the extracted parameters can be somewhat improved by fitting the entire voltammogram to the theory.[7] Another issue is the applicability of the classical electrochemical theory (including the assumptions of electroneutrality or diffusion-controlled transport) to nanoelectrodes with a characteristic dimension of ~10 nm or less, where the electrical double layer at the nanoscale electrode/solution interface affects the mass transfer of species to the interface.[8, 9]

Ion-transfer voltammetry at the micropipet-supported interface between two immiscible electrolyte solutions (ITIES) was pioneered by the Girault group[10] to be followed by more recent development of nanopipets.[11] The negligibly small ohmic potential drop (typically, <1 mV) and low double-layer charging current make pipets very convenient and powerful tools for IT measurements at the ITIES.[12] At the same time, the asymmetry of the diffusion field at a pipet-based ITIES, where the diffusion inside a cylindrical shaft is essentially linear in contrast to the spherical diffusion of ions to the pipet orifice in the external solution, gives rise to complications.[13] A cyclic voltammogram (CV) of simple IT at a micropipet consists of an apparently steady-state, sigmoidal wave that corresponds to ingress of an ion into the pipet and a time-dependent, peak-shaped wave produced by egress of the same ion to the external solution. Depending on experimental conditions, simple IT at a nanopipet may produce either an asymmetrical transient (i.e., time-dependent) CV[14] or a sigmoidal and retraceable steady-state voltammogram whose shape, at first glance, is independent of geometry of the pipet inside.[14-16]

In both cases, the orifice radius, a, can be determined from the limiting current, i_{ing}, controlled by ion diffusion in the external solution (i.e., ingress current in Figure 3-1a) as

$$i_{ing} = 4xz_iFD_2c_2a$$

Equation 3.1

where z_i, D_2 and c_2 are the charge of the transferred ion i, its diffusion coefficient and bulk concentration in the external solution (phase 2), respectively; and x is a function of r_g/a (r_g is the outer wall radius; $r_g/a \cong 1.5$ for typical quartz pipets), which was tabulated[17] and expressed by an analytical approximation.[18] With the knowledge of a, kinetic and thermodynamic parameters of simple IT reactions were determined from nanopipet voltammograms by using methods developed for solid electrodes and ignoring the effects of ion diffusion inside the pipet shaft.[14-16]

Recent simulations of micropipet voltammograms showed that geometry of the pipet inside can significantly affect IT voltammograms.[19-21] The ion diffusion in the narrow inner shaft of a tapered pipet is not strictly linear (Figure 3-1b) so that a steady state is attained for egress transfer of an ion into the external solution. The resulting steady-state limiting current, i_{eg}, is

$$i_{eg} = 4f(\theta)z_iFD_1c_1a$$

Equation 3.2

where D_1 and c_1 are the diffusion coefficient and bulk concentration in the internal solution (phase 1), respectively, and $f(\theta)$ is a tabulated function of the tip taper angle, θ.[21] The half-wave potential, $\Delta\phi_{1/2}$, of the reversible (Nernstian) simple transfer of ion i from the external solution to the pipet under steady state depends on θ as follows[21]

$$\Delta\phi_{1/2} = \Delta\phi_{\mathrm{i}}^{0'} + \frac{RT}{z_{\mathrm{i}}F}\ln\frac{D_2}{D_1} + \frac{RT}{z_{\mathrm{i}}F}\ln\frac{x}{f(\theta)}$$

Equation 3.3

where $\Delta\phi_{\mathrm{i}}^{0'}$ is a formal transfer potential of ion *i*. Equation 3.3 as well as simulations of quasi-reversible IT voltammograms[21] suggest that kinetic and thermodynamic parameters of simple ITs determined without taking into account effects of ion diffusion in the inner space of a nanopipet may not be accurate.

Here we establish the theory for a new voltammetric approach to kinetic study of rapid IT at the nanopipet-supported ITIES. We used it to determine kinetic parameters for the rapid transfer of tetraethylammonium at nanoscopic 1,2-dichloroethane/water interfaces.[22] In contrast to previous nanopipet experiments, in which the transferable ion was initially present only in one phase (Figures 1a and b), our approach requires the initial addition of a common ion to both external and internal solutions (Figure 3-1c). The resulting IT voltammogram comprises two waves corresponding to the ingress of the common ion into the pipet and its egress into the external solution. We will demonstrate that this seemingly minor modification is essential for successful kinetic analysis of nearly reversible IT voltammograms.

Although our treatment is focused on steady-state pipet voltammetry, below we will use COMSOL Multiphysics package to simulate time-dependent CVs, as discussed previously.[21, 23-25] The results of these simulations will allow us to formulate a set of criteria, which can be used to ensure that the IT process reaches a steady state under given experimental conditions. Although modeling double layer effects that may result from the presence of charges on the glass pipet surface is beyond the scope of this work, we will try to evaluate the significance of the "edge effect"[26] on the interfacial IT and ion transport inside the pipet.

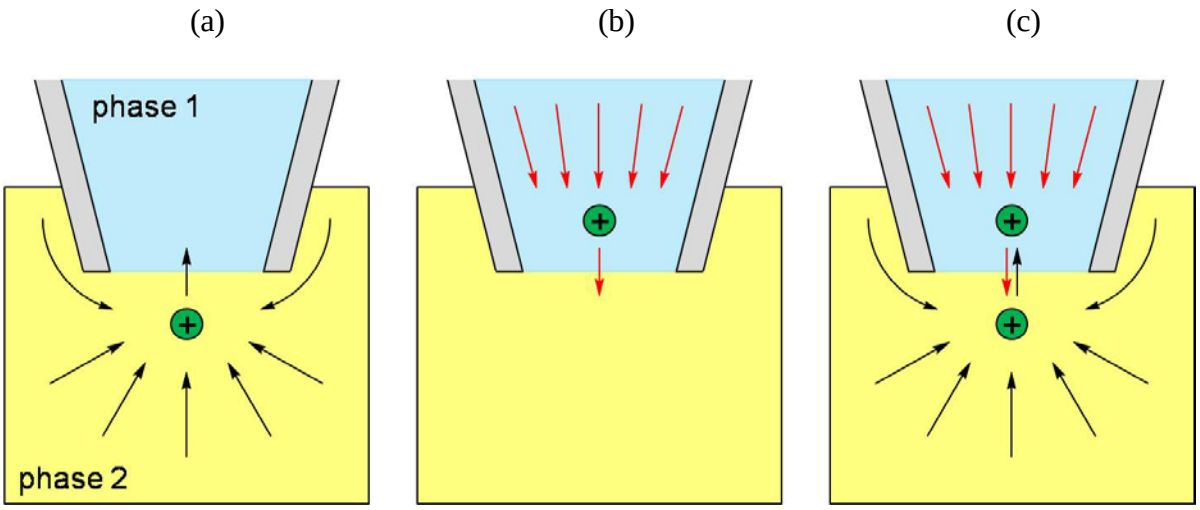

Figure 3-1. Scheme of IT and diffusion at tapered nanopipets when an ion is initially present only in the (a) external or (b) internal solution or (c) in both solutions.

3.3 MODEL

Simple transfer of an ion with a charge of z_i, i^{z_i}, is defined by

$$i^{z_i}\ \text{(external solution)} \underset{k_b}{\overset{k_f}{\rightleftharpoons}} i^{z_i}\ \text{(internal solution)}$$

Equation 3.4

The heterogeneous rate constants, k_f and k_b, are given by the Butler-Volmer-type model[27]

$$k_f = k^0 \exp\left[\frac{-\alpha z_i F(\Delta\phi - \Delta\phi_i^{0'})}{RT}\right]$$

Equation 3.5

$$k_b = k^0 \exp\left[\frac{(1-\alpha) z_i F(\Delta\phi - \Delta\phi_i^{0'})}{RT}\right]$$

Equation 3.6

where k^0 is a standard heterogeneous IT rate constant, F is the Faraday constant, and $\Delta\phi$ is the Galvani potential difference between two liquid phases. The standard rate constant is expressed in a dimensionless form as

$$\lambda = \frac{k^0 a}{D_2}$$

Equation 3.7

where D_2/a represents a mass transfer rate of ions in the outer solution. Equations 3.4, 3.5, 3.6, and 3.7 are also applicable to other first-order charge transfers at ITIES, e.g., facilitated IT with ion[11] or ionophore[21] in excess and electron transfer between aqueous and organic redox species when one of them is in excess.[28]

Low ionic currents across the nanoscale ITIES allow for simplification of our model such that only diffusion is considered as a mode of ion transport in bulk solutions. In nanopipet voltammetry, interfacial transfer of an ion at a few mM bulk concentration produces a pA-range current. The resulting ohmic potential drop in the external and internal solutions is small enough for the effects of migration on ion transport to be negligible. Moreover, the potential gradient inside the pipet is not large enough to drive a significant electroosmotic flow along its charged inner wall.[29] These assumptions have been checked experimentally.[21] In contrast, the effect of the electrical double layer at the charged pipet surface on nearby ion transport can be significant for small pipets as assessed below.

Diffusion problems for IT voltammetry at pipet electrodes were formulated in cylindrical coordinates (Figure 3-2a) and solved using COMSOL Multiphysics version 3.5a (COMSOL, Inc., Burlington, MA), as reported elsewhere[21] (see Supporting Information for an example of Multiphysics simulation). Asymmetric diffusion of ions to the pipet tip in external and internal solutions is characterized by geometric parameters including the outer and inner radii of the tip (r_g and a) as well as its outer and inner taper angles.[21] The ratio r_g/a = 1.5 determined for typical nanopipets by scanning electrochemical microscopy[14] and SEM[21] was assumed in our simulations and yielded x = 1.16 in Equation 3.1.[17, 30, 31] A pipet barrel was assumed to have a single taper with the identical outer and inner angles, θ, along its length. The simulated IT current across the interface, i, was normalized with respect to the limiting current at the inlaid

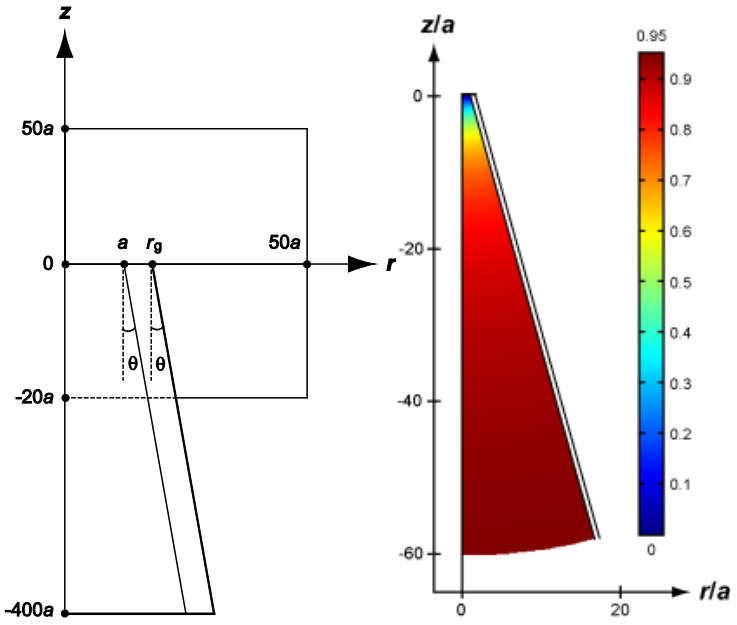

Figure 3-2 (a) Defined space domain for a finite element simulation of ion transfer at a tapered pipet electrode. (b) A steady-state concentration profile of the transferable ion in the internal solution of a nanopipet with θ = 15° simulated with c_1/c_2 = 1 and D_1/D_2 = 1. The ion was completely depleted at the internal-solution side of the interface to simulate the egress limiting current situation. Only the region adjacent to the pipet tip where the ion concentration varies between 0 and 95% of its bulk value is shown.

disk-shaped interface ($i_d = 4z_iFD_2c_2a$). Positive and negative currents in this work correspond to the ingress and egress of a cation, respectively (black and red arrows in Figure 3-1). No capacitive current was considered in the simulations. The normalized current was plotted against $z_i\Delta\phi$ to obtain a CV, where the formal potential was set to 0 V.

3.4 RESULTS AND DISCUSSION

3.4.1 Steady-State Voltammetry at Nanopipets

Previously reported simulations of cyclic voltammetry at pipet-supported ITIES[19-21] suggest that ion diffusion on either side of the nanopipet tip reaches a steady state during a potential cycle at a moderate (mV/s) potential sweep rate, v. The related dimensionless parameter, σ[21]

$$\sigma = \frac{a^2}{4D_2}\frac{z_iFv}{RT}$$

Equation 3.8

compares the radius of the interface, a, to the diffusion distance in the external solution, $\sqrt{D_2RT/z_iFv}$.[32] In general, the IT process attains a steady state if $\sigma << \sim 10^{-4}$.[21] In a typical voltammetric experiment at a nanopipet, v =10 mV/s, a = 50 nm, and $D_2 = 10^{-5}$ cm^2/s correspond to a very small σ value of 2.4×10^{-7}. All CVs in this work were simulated with $\sigma = 10^{-7}$ at tapered pipets with $\theta \geq 7.5°$ to obtain sigmoidal forward and reverse waves that completely

retrace each other, thereby confirming a steady state. The shape of the simulated steady-state voltammograms was independent of the direction of potential sweep, and the initial and final potentials.

Simulation results show that the overall diffusion length at a tapered pipet is mainly determined by steady-state thickness of a diffusion layer in the internal solution. With θ = 15°, ion diffusion in the internal solution reaches a steady state to develop a thick diffusion layer, where the ion concentration reaches ~95 % of the bulk value at ~60a distance from the interface when an ion is completely depleted at the internal-solution side of the interface (Figure 3-2b). Importantly, this thickness corresponds to only 1.5 μm from a 25 nm-radius tip, thereby quickly establishing the steady state. On the other hand, radial diffusion of an ion from the external solution to the tip is much less hindered by the pipet wall to give a much thinner diffusion layer at a steady state, where an ion concentration at the distance of <8a from the interface recovers to 95 % of the bulk concentration (see Figure 3-S2) with complete ion depletion at the external-solution side of the interface. Accordingly, the time required for the IT process to reach a steady state is largely determined by the geometry of the pipet inside. Thus, beside the tip inner radius (which is included in the dimensionless parameter σ), the taper angle, θ can also influence the attainment of a steady state at the nanopipet-based ITIES. In practice, the variations in θ are relatively small, i.e., 9°–22° for quartz nanopipets[22] and 3°–6° for micropipets.[21, 24]

It should be noted that transient cyclic voltammetry is not practical with a nanopipet. A σ value of $>10^{-4}$ is required for obtaining a transient CV of simple IT even at a narrow pipet with the tip angle of ~6° (see Figure 3-4b of ref. 21). This corresponds to v > 4 V/s, assuming z_i = 1, a = 50 nm, and $D_2 = 10^{-5}$ cm^2/s. At such a fast potential sweep, a large capacitive current (mostly due to stray capacitance of a nanopipet) would severely distort a voltammogram.[22] Transient

CVs can be obtained at larger (i.e., μm-sized) pipets. The presence of two—positive and negative—waves in a single transient CV allows one to determine all kinetic and thermodynamic parameters as well as a and θ.[21] A conventional steady-state IT voltammogram, which consists of a single positive or negative wave, is less informative. This limitation can be overcome by dissolving a transferable ion in both liquid phases to obtain a nanopipet voltammogram featuring both positive and negative steady-state waves.

3.4.2 Evaluation of Geometric and Thermodynamic Parameters

Both geometric (a and θ) and thermodynamic ($\Delta\phi_i^{0'}$) parameters are necessary for determination of kinetic parameters (α and k^0) from nanopipet voltammograms. If the D_1 and D_2 values are known, geometric parameters can be directly obtained from the positive and negative limiting currents in the same nanopipet voltammogram produced by ingress and egress transfers of the common ion. Using Equation 3.1, the a value can be found from the ingress limiting current, i_{ing}, which is essentially independent of θ (Figure 3-3a). (Small variations in simulated i_{ing} values are due to simultaneous changes in the external taper angle, which affects ion diffusion from the back of a nanopipet.) With the known tip radius, θ can be determined from the egress limiting current, i_{eg}, using Equation 3.2. $f(\theta)$ increases monotonically from 0 to 1 as θ increases from 0° to 90°[21] (see also Figure 3-3a). This increase reflects gradual transition from linear to hemispherical ion diffusion in the internal solution. The linear dependence of i_{eg} on D_1 predicted by Equation 3.2 was confirmed by numerical simulations for a nanopipet with $\theta = 15°$ (Figure 3-3b).

(a)

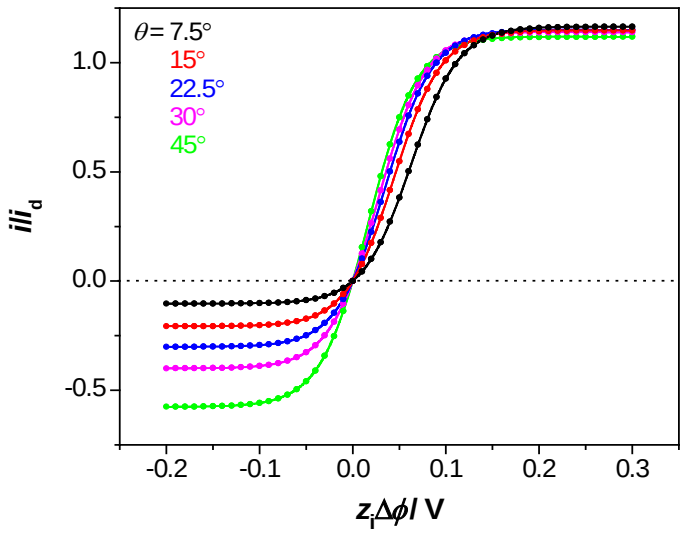

(b)

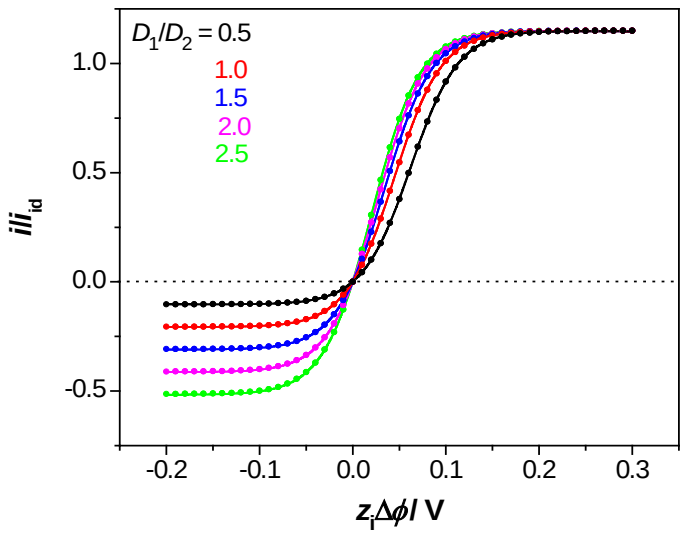

Figure 3-3. Effects of (a) tip angle, θ, and (b) diffusion coefficient ratio, D_1/D_2, on simulated CVs (solid lines) of reversible IT at a nanopipet when an ion is initially present in both phases, and $c_1/c_2 = 1$. (a) $D_1/D_2 = 1$. (b) $\theta = 15^{\circ}$. Closed circles represent Equation 3.10.

The formal potential can be determined directly from the potential value at zero current, $\Delta\phi_{eq}$, in a nanopipet voltammogram of a common ion, as given by

$$\Delta\phi_{eq} = \Delta\phi_i^{0'} + \frac{RT}{z_i F}\ln\frac{c_2}{c_1}$$

Equation 3.9

This equilibrium potential is independent of geometric parameters (Figure 3-3a), diffusion coefficients (Figure 3-3b), and kinetic parameters (Figures S3a and S4a), and therefore the determined $\Delta\phi_i^{0'}$ is unaffected by mass-transfer and charge-transfer effects. The possibility of independent determination of the formal potential is a major advantage of our approach. Previously,[10,13] $\Delta\phi_i^{0'}$ was used as an additional fitting parameter in analysis of quasi-reversible CVs, thus, increasing the uncertainties in the determined k^0 and α values.

3.4.3 Analytical Expression for Nanopipet Voltammograms

To facilitate the extraction of kinetic parameters from experimental steady-state voltammograms, an approximate equation was derived for the case when a common ion is present in both liquid phases:

$$\frac{i}{i_{ing}} = \frac{1}{m_{ing}/m_{eg} + m_{ing}/k_b + k_f/k_b}\left(\frac{k_f}{k_b} - \frac{c_1}{c_2}\right)$$

Equation 3.10

where

$$m_{\text{ing}} = \frac{4xD_2}{\pi a}$$

Equation 3.11

and

$$m_{\text{eg}} = \frac{4f(\theta)D_1}{\pi a}$$

Equation 3.12

Eq. 10 is based on the assumption of the uniform accessibility of the interface; its derivation and accuracy are discussed in Supporting Information.

At $i = 0$, Equation 3.10 gives $k_{\text{f}}/k_{\text{b}} - c_1/c_2 = 0$, which is equivalent to the Nernst equation (Equation 3.9). With either $c_1 = 0$ or $c_2 = 0$, Equation 3.10 is reduced to Equation 3.S4 or Equation 3.S5 (from Supporting Information), which apply to voltammograms with the transferable ion present either in the external or internal solution, respectively. The voltammograms calculated from Equations 3.10, 3.S4, and 3.S5 were compared to simulated curves to find small errors of <1 % for nearly reversible IT (λ >~1), while maximum errors can reach 3% for irreversible reactions. Nevertheless, current density is significantly higher at the edge of the interface as demonstrated below.

It should be noted that electrochemical reversibility of ingress and egress IT processes can be different because of the asymmetry of the diffusion field at a pipet-based ITIES as represented by different expressions of the corresponding mass transfer coefficients (Equations

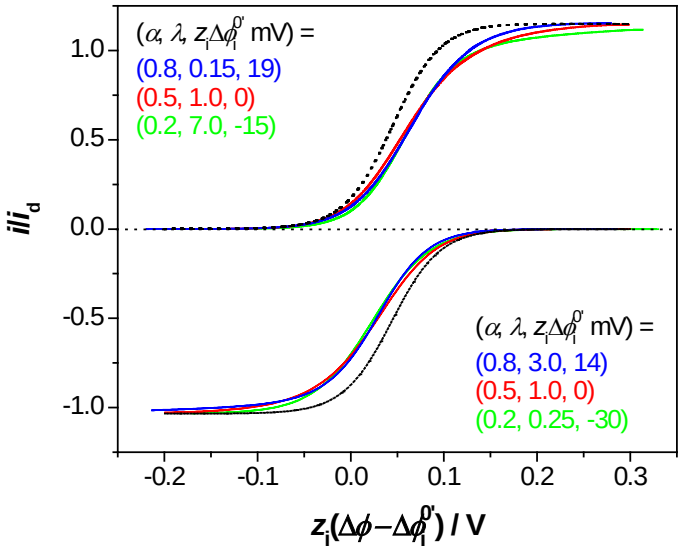

Figure 3-4. Effects of kinetic (α and λ) and thermodynamic ($\Delta\phi_i^{0'}$) parameters on simulated CVs (solid lines) of IT at a nanopipet when an ion is initially present only in the external (top) or internal (bottom) solution. $D_1/D_2 = 1$, $\theta =$ 15°. The c_1 value (bottom graph) is 5 times of the c_2 value (top). The dotted curves are simulated Nernstian voltammograms.

3.11 and 3.12). Thus, different dimensionless kinetic parameters of k^0/m_{ing} ($\sim\lambda$ in Equation 3.7) and k^0/m_{eg} are required for separate assessment of extents of the kinetic/diffusion control of the ingress and egress processes, respectively.[22]

3.4.4 Determination of Kinetic Parameters from Nearly Reversible Steady-State Voltammograms

A problem that was not recognized in the previous nanopipet studies[10,13] is that no unique combination of kinetic and thermodynamic parameters can be determined from a nearly reversible voltammogram of an ion present only in one phase because the shape of such a curve depends weakly on kinetic parameters. The possibility to fit the same experimental curve using different combinations of k^0 and α leads to significant uncertainties in extracted parameter values. For instance, different sets of α and λ can be chosen from wide ranges of 0.20–0.80 and 0.15–7.0, respectively, such that nearly identical positive waves (ingress) are obtained by adjusting $\Delta\phi_i^{0'}$ accordingly (the top of Figure 3-4). This result indicates that an egress IT wave with a "conventional" α value of 0.5 and a relatively large λ value of 1.0 (red line) can be fitted to a voltammogram using an anomalously large (or small) α value of 0.8 (or 0.2) coupled with an underestimated (or overestimated) λ value of 0.15 (or 7.0). Similar trends are also found for egress IT waves (bottom of Figure 3-4). Although positive (or negative) waves in Figure 3-4 are not completely identical, the differences between them are within the range of uncertainties in experimental nanopipet voltammograms caused by capacitive and background currents.[22]

In contrast, the kinetic parameters can be precisely determined from a nearly reversible nanopipet voltammogram of a common ion, which comprises both positive and negative waves.

Separate determination of α and k^0 is straightforward because of different dependences of positive and negative current responses on the respective parameters (see Supporting Information for details). In Figure 3-5a, similar positive current responses are obtained with five different sets of α and λ (0.30 to 0.70 and 0.35 to 3.0, respectively). In these cases, the broadening effect of smaller α on a positive wave is nearly cancelled by larger λ. The corresponding negative responses, however, are readily distinguishable from each other because both smaller α and larger λ cause the negative wave to become narrower. On the other hand, by simultaneously decreasing α and λ, one can obtain similar negative responses (Figure 3-5b). The corresponding positive responses, however, are very different, because decreasing either α or λ results in a broader positive wave. Overall, a unique combination of α, λ, and $\Delta\phi_{\mathrm{i}}^{0'}$ can be obtained from a near-reversible voltammogram of a common ion in contrast to the cases with an ion present only in one liquid phase.

The aforementioned pitfall in kinetic analysis of nearly reversible IT can also hinder the extraction of kinetic parameters from steady-state voltammograms of electron transfer at solid electrodes. If only one (either reduced or oxidized) form of redox species is initially present in solution to give a single anodic or a cathodic wave, a small error in half-wave and quartile potential values can lead to large uncertainties in both kinetic and thermodynamic parameters of rapid electron transfer.[3] For instance, standard deviations of 0.5 to 1.5 mV in the differences between the characteristic potentials produced considerable variations in k^0 (between 0.1 and 1 cm/s) and α (between 0.3 and 0.7) of nearly reversible electroreduction of C60 at a 1 μm-radius disk Pt electrode.[33] Even larger errors in the characteristic potentials are likely to occur in nanoelectrode voltammetry, where low-pA or sub-pA currents have to be measured.

(a)

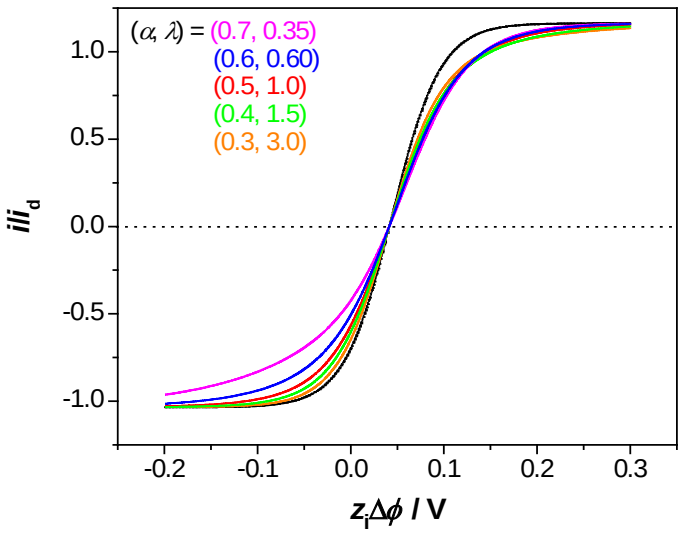

(b)

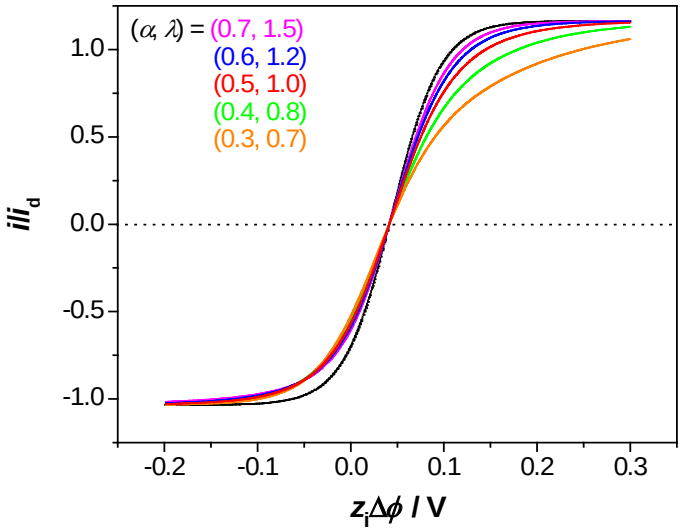

Figure 3-5. Effects of α and λ on simulated CVs (solid lines) of IT at a nanopipet with θ = 15° and the transferable ion initially present in both phases. c_1/c_2 = 5, D_1/D_2 = 1. The dotted curves are Nernstian voltammograms.

3.4.5 Double-Layer and Edge Effects in Nanopipet Voltammetry

Kinetic analysis of nanopipet voltammograms can be complicated by electrostatic effects produced by the negatively charged inner glass wall. The surface charge can influence ion transport along the wall electrostatically (dashed arrows in Figure 3-6a). Additionally, negative charges located very close to the orifice can interact with ions transferred at the edge of the ITIES adjacent to the pipet wall (solid arrows in Figure 3-6a) and, thus, affect the IT rate. The former effect was investigated both experimentally and theoretically using quartz nanopipets[34] and glass nanopore electrodes[35, 36] immersed in an aqueous electrolyte solution. Both electrostatic effects are more significant for smaller nanopipets, especially with $a \approx 10$ nm or less. Also, double layer effects at the nanoscopic ITIES, where the diffusion layer thickness is comparable to that of the diffuse double layer, may result in deviations from the conventional electrochemical theory, as discussed for solid nanoelectrodes.[8, 9] Nanopipets with different tip sizes have to be used to check experimentally whether double layer effects significantly influence kinetic and thermodynamic parameters determined from nanopipet voltammograms.[22]

For both ingress and egress ITs, the diffusion current density is higher at the edge of the disk-shaped ITIES, as revealed by radial distributions of the ion fluxes across the interface simulated for a typical pipet with $\theta = 15°$ (Figure 3-6B and Supporting Information). The integration of the interfacial ion flux from the disk center toward the edge shows that large fractions of i_{ing} and i_{eg} flow through a thin, annulus adjacent to the edge of the interface. For instance, 45 and 25 % of the respective total current passes between $r = 0.9a$ and $r = a$. This range corresponds to <1 nm distance from the charged pipet wall if $a < 10$ nm (red and black

(a)

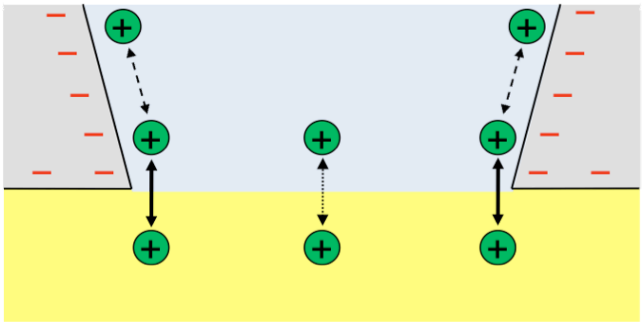

(b)

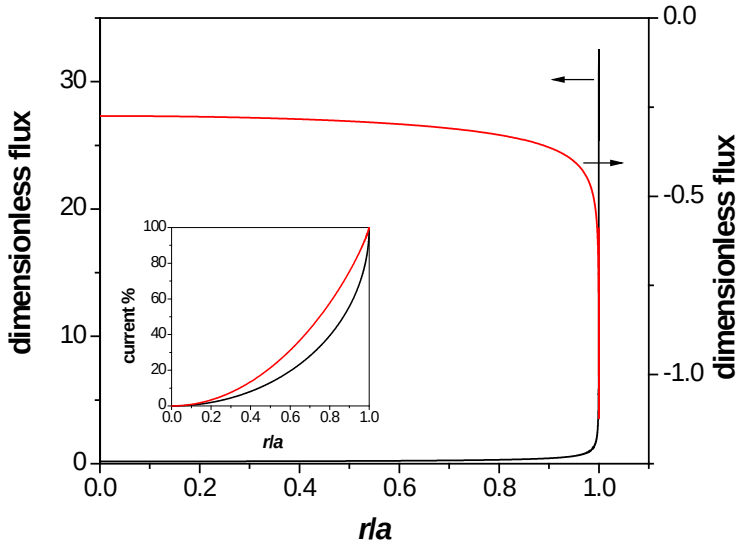

Figure 3-6. (a) Scheme of double layer effects produced by the charged inner pipet wall on IT at the edge of the nanopipet-supported ITIES (solid arrows) and far from it (dotted arrows), and ion transport near the interior wall (dashed arrows). (b) Radial distributions of local flux of a common ion at the disk-shaped interface controlled by diffusion in the internal (red) or external (black) solution. $c_1/c_2 = 5$, $D_1/D_2 = 1$. The inset shows corresponding currents obtained by integrating the ion flux from the disk center toward the edge.

lines in the inset of Figure 3-6b), and therefore a significant electrostatic effect on IT at small nanopipets can be expected whether this process is controlled by diffusion in the internal or external solution (red and black lines, respectively, in Figure 3-6b).

3.5 CONCLUSIONS

The theory developed for IT voltammetry of a common ion at the nanopipet-based ITIES predicts the advantages of this approach over the conventional protocol, in which a transferable ion is initially present only in one liquid phase. These advantages stem from the availability of two waves in a steady-state voltammogram corresponding to the ingress of the common ion into the pipet and its egress to the external solution. From two limiting currents of a single voltammogram, one can assess asymmetric ion diffusion in the internal and external solutions and evaluate the related geometric and transport parameters. Moreover, the analysis of the ingress and egress responses enables accurate and precise evaluation of k^0 and α of rapid (almost reversible) IT reactions. The precision is enhanced by separate determination of the formal potential from the potential of zero current. In contrast, large errors are possible in both kinetic and thermodynamic parameters determined from a nearly reversible steady-state voltammogram (λ > ~1) containing only one (either ingress or egress) IT wave. This problem may also compromise steady-state measurements of rapid electron transfer kinetics at solid electrodes. If only one (either reduced or oxidized) form of redox species is initially present in solution, small experimental errors can lead to large uncertainties in kinetic parameters extracted from a single anodic or cathodic wave.

Another limitation of nanopipet voltammetry is that large current density at the edge of a nanoscopic interface increases the significance of the diffuse layer effect produced by surface charge residing on the adjacent insulating shroud, e.g., charged inner surface of a glass nanopipet. The smaller the electrode radius the stronger the double layer effects; hence the lower limit for the electrode size suitable for heterogeneous kinetic measurements and, subsequently, the upper limit for the measurable rate constant.

ACKNOWLEDGEMENTS

The supports of this work by the National Science Foundation (CHE-0645958; MVM, CHE-0645623; SA) are gratefully acknowledged. In the work presented in Chapter 3, I utilized the numerical model that was described in Chapter 2 to predict the voltammetric responses from ion transfer across nano-liquid/liquid interfaces at nanopipet electrodes and to identify sources of error in kinetic and thermodynamic analyses under steady-state conditions. This work was inspired by erroneous kinetic analysis of steady-state cyclic voltammograms from the transfer of TEA at nanopipets when TEA was initially present only in the outer or inner phases (data not shown). Those experiments were performed by Yixian Wang. As a result, we proposed an experiment, which initially had a common ion in both phases, in order to overcome the limitations of the aforementioned experiment. I predicted the responses with simulated voltammograms utilizing the numerical model. Professor Shigeru Amemiya, my graduate advisor, and Professor Michael V. Mirkin, Yixian Wang's graduate advisor provided intellectual guidance on the analyses and merits of the work presented in Chapter 3.

SUPPORTING INFORMATION

Finite Element Simulation

CVs at nanopipet electrodes were simulated by the finite element method using the COMSOL Multiphysics software package as reported elsewhere.[S1] A simulation report is attached. See ref S1 for definition of normalized parameters.

Steady-State Ion Diffusion in the External Solution

Figure 3-S1 shows a steady-state concentration profile of the common ion in the external solution. This ion is depleted at the phase boundary, and its quasi-spherical diffusion to the pipet orifice in the external solution yields the ingress limiting current (Equation 3.1).

Reversible Nanopipet Voltammograms with a Transferable Ion Present Only in One Phase

CVs were simulated for reversible IT at pipets with various tip angles when the transferable ion is initially present either in the external or internal solution. These two cases are represented in Figure 3-S2a by the top and bottom families of voltammograms, respectively. Effects of the diffusion coefficient ratio, D_1/D_2 (Figure 3-S2b), were simulated for a pipet with $\theta = 15^{o}$ and all other conditions are same as in panel a.

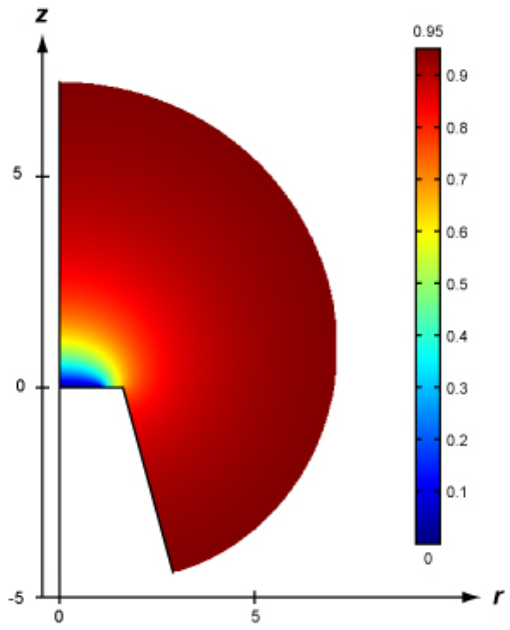

Figure 3-S1. A steady-state concentration profile of the transferable ion in the external solution. The taper angle of the nanopipet is $\theta = 15^{o}$; $c_1/c_2 = 1$, and $D_1/D_2 = 1$. Only the region adjacent to the pipet tip where the ion concentration varies between 0 and 95% of its bulk value is shown.

(a)

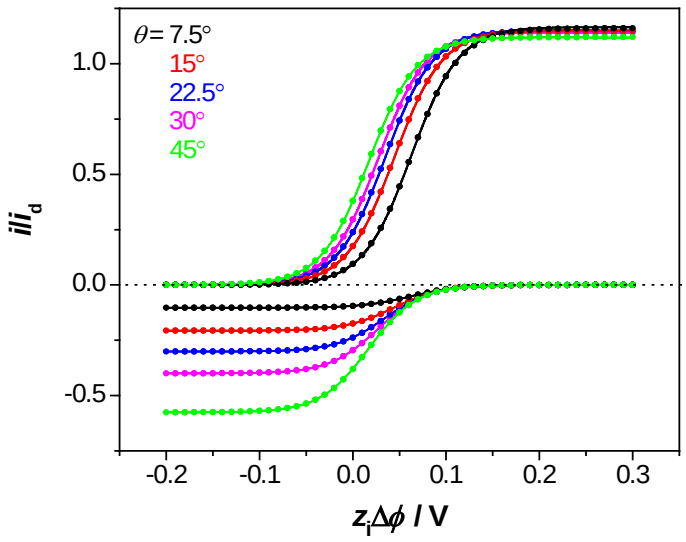

(b)

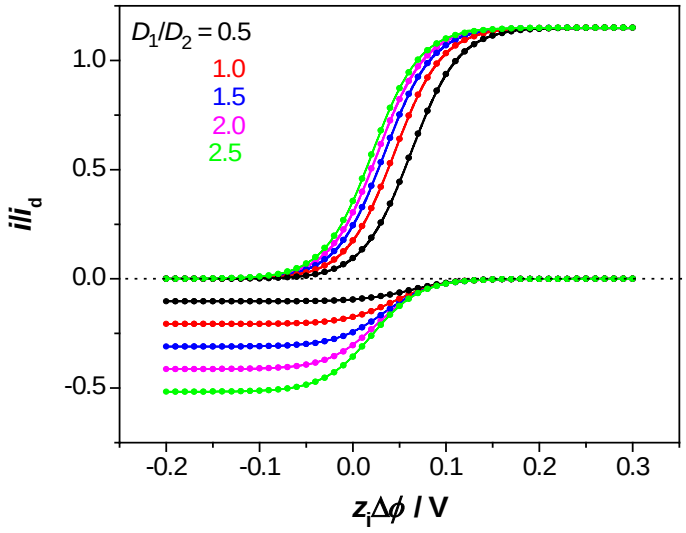

Figure 3-S2. Effects of (a) tip angle, θ, and (b) diffusion coefficient ratio, D_1/D_2, on simulated CVs (solid lines) of reversible IT at a nanopipet when the transferable ion is initially present either in the external or internal solution. The ion concentration in the internal solution for the egress voltammograms (bottom family of curves in each panel) is equal to that in the external solution for the ingress voltammograms (top curves). (a) $D_1/D_2 = 1$. (b) $\theta = 15°$. The closed circles represent Equations 3.S4 and 3.S5 for ingress and egress ITs, respectively.

Effects of IT Kinetics

The effects of kinetic parameters, k^0 and α, on nanopipet voltammograms are assessed independently. Simulation results in Figure 3-S3a demonstrate the effects of λ on ingress and egress waves with a common ion present in both phases. As λ decreases, both ingress and egress responses become broader and shift toward negative and positive potentials, respectively, so that totally irreversible voltammograms are obtained eventually. Similar λ dependences are also found by comparing an ingress and an egress waves produced by an ion present in the external and the internal solution, respectively (Figure 3-S3b). In contrast to k^0, smaller α results in a broader ingress response and a narrower egress response in the quasi-reversible voltammograms of an ion in both phases (Figure 3-S4a with λ = 0.3). The asymmetric α effects on the ingress and egress responses correspond to α dependences of k_f and k_b (see Equations 3.5 and 3.6). This correspondence is noticeable in a nanopipet voltammogram of an ion in both phases, which spans widely to both ingress and egress sides of a formal potential. Asymmetric α dependences are also seen in egress voltammograms of an ion in the internal solution (the bottom of Figure 3-S4b), which are shifted to positive potentials beyond a formal potential because of slow kinetics (λ = 0.3). The α dependence of the egress voltammograms at the positive side, however, is much weaker than that of the ingress responses to an ion in both phases (Figure 3-S4a) or that of ingress responses to an ion only in the external solution (the top of Figure 3-S4b). In the latter case, a smaller α value simply results in a broader ingress response under the otherwise identical conditions, where the whole ingress response is shifted to the positive side of a formal potential because of slow kinetics and asymmetric accessibility of the interface.

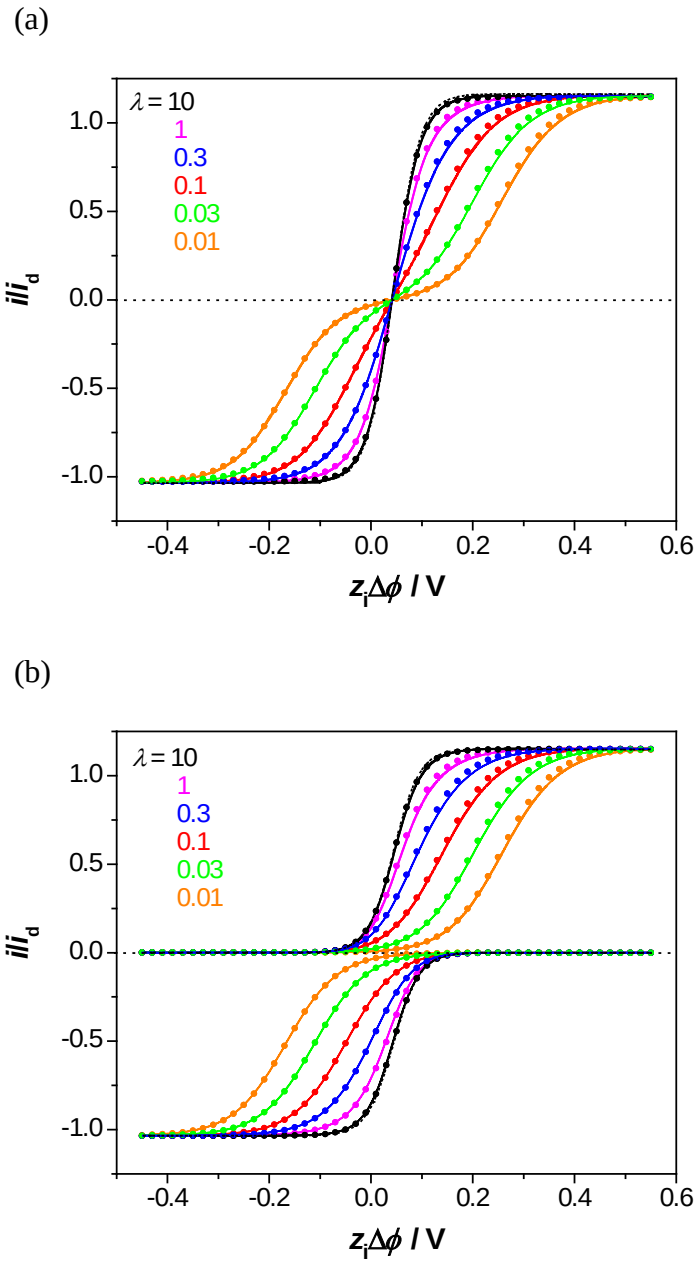

Figure 3-S3. Effects of dimensionless rate constantλ, on simulated CVs (solid lines) of IT with the transferable ion is initially present (a) in both phases and (b) either in the external or internal solution. (a) $c_1/c_2 = 5$, (b) c_1 (bottom family of curves) is five times higher than c_2 (top curves). The closed circles represent (a) Equation 3.10 and (b) Equations 3.S4 and 3.S5 for ingress and egress voltammograms, respectively. $\alpha = 0.5$, $\theta = 15^{o}$, $D_1/D_2 = 1$.

(a)

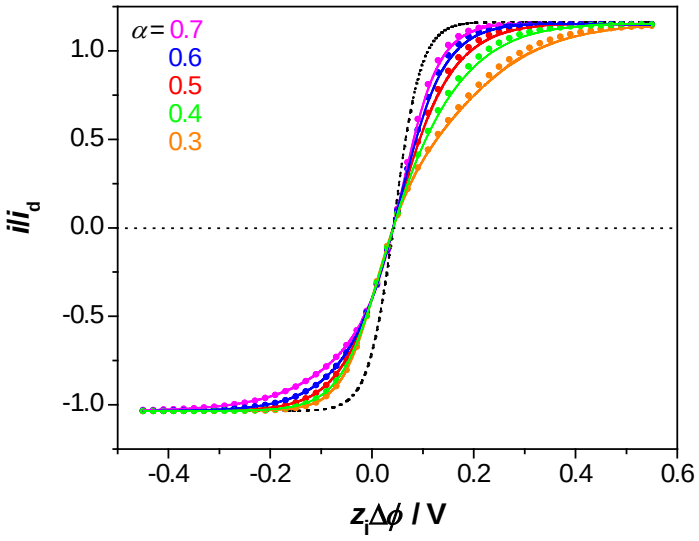

(b)

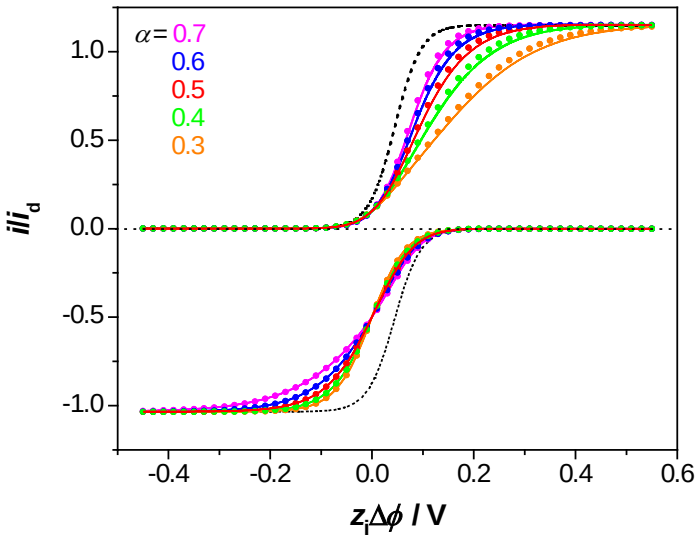

Figure 3-S4. Effects of α on simulated CVs (solid lines) of IT. λ = 0.3. The dotted lines represent reversible CVs. For other conditions and parameters, see Figure 3-S4.

Edge Effects on Ion Transport in the Inner Solution

Simulation results also demonstrate a moderate edge effect on diffusional ion flux in the inner solution when the flux is limited by ion diffusion in the external or internal solution (red and black lines, respectively, in Figure 3-S5). Integration of the respective ion flux (red and black dotted lines, respectively) gives ~28 % and ~ 20 % of the total current within the distance of 0.1*a* from the inner wall.

Derivations of Equation 10 and Relevant Equations

Equation 10 was derived using the assumption that the nanopipet-based liquid/liquid interface is uniformly accessible so that the ion concentrations at both sides of the interface (c_1^0 and c_2^0) are laterally uniform and independent of *r*. With this assumption, the steady-state IT current is

$$\frac{i}{\pi a^2 z_i F} = k_f c_2^0 - k_b c_1^0 \quad \text{(S1)}$$

The same current must flow between the interface and bulk external solution, thereby yielding

$$\frac{i}{\pi a^2 z_i F} = m_{ing}(c_2 - c_2^0) \quad \text{(S2)}$$

Analogously, the current between the interface and internal solution is

$$\frac{i}{\pi a^2 z_i F} = m_{eg}(c_1^0 - c_1) \quad \text{(S3)}$$

By combining Equations 3.S1–S3 to eliminate c_1^0 and c_2^0, one obtains Equation 3.10.

If the transferable ion is initially present only in the external solution, i.e., $c_1 = 0$, Equation 3.10 is reduced to Equation 3.S4:

$$\frac{i}{i_{\text{ing}}} = \frac{1}{m_{\text{ing}}/m_{\text{eg}} + m_{\text{ing}}/k_{\text{b}} + k_{\text{f}}/k_{\text{b}}}\left(\frac{k_{\text{f}}}{k_{\text{b}}}\right) \tag{S4}$$

If the transferable ion is initially present only in the internal solution ($c_2 = 0$), steady-state current has to be normalized by i_{eg}, so that Equation 3.10 gives

$$\frac{i}{i_{\text{eg}}} = \frac{1}{m_{\text{ing}}/m_{\text{eg}} + m_{\text{ing}}/k_{\text{b}} + k_{\text{f}}/k_{\text{b}}}\left(\frac{m_{\text{ing}}}{m_{\text{eg}}}\right) \tag{S5}$$

The accuracy of Equations 3.10, 3.S4, and 3.S5 was checked by comparing them with simulation results in Figures 3 and S2–S4. It is known that the assumption of uniform accessibility at a disk-shaped interface results in larger errors for less reversible reactions.[S2] The approximate equations (closed circles) perfectly fit simulation results (solid lines) when IT is reversible (Figures 3 and S2). A good agreement can be seen for relatively rapid ITs with $\lambda \sim 1$ (Figures S3 and S4). A more significant deviation is seen for less reversible IT with smaller λ (Figures S3). The largest deviations are found in nearly irreversible ingress responses with small α or λ values at highly positive potentials (Figure 3-S3).

Supporting Information References

(S1) Rodgers, P. J.; Amemiya, S. *Anal. Chem.* **2007**, *79*, 9276–9285.
(S2) Oldham, K. B.; Zoski, C. G. *J. Electroanal. Chem.* **1988**, *256*, 11–19.

COMSOL Model

A copy of the COMSOL model is available free of charge in the Supporting Information via the Internet at http://pubs.acs.org/doi/suppl/10.1021/ac9022428.

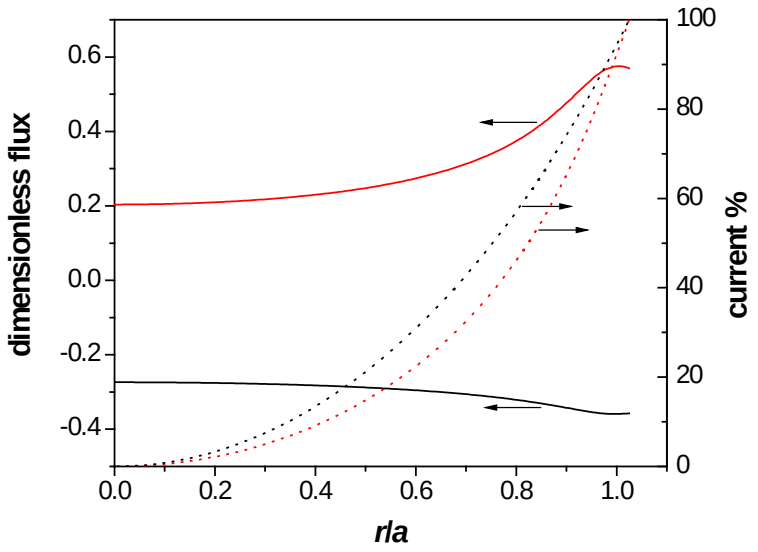

Figure 3-S5. Radial distributions of local flux of a common ion in the inner solution at the distance of 0.1*a* from the disk-shaped interface as controlled by ion diffusion in the external (red line) or internal (black line) solution with $c_1/c_2 = 5$ and $D_1/D_2 = 1$. The dotted curves show the corresponding currents as obtained by integrating the ion flux from the disk center toward the edge.

REFERENCES

(1) Murray, R. W. *Chem. Rev.* **2008**, *108*, 2688–2720.
(2) White, R. J.; White, H. S. *Anal. Chem.* **2005**, *77*, 214A–220A.
(3) Mirkin, M. V.; Bard, A. J. *Anal. Chem.* **1992**, *64*, 2293–2302.
(4) Oldham, K. B.; Zoski, C. G. *J. Electroanal. Chem.* **1988**, *256*, 11–19.
(5) Oldham, K. B.; Myland, J. C.; Zoski, C. G.; Bond, A. M. *J. Electroanal. Chem.* **1989**, *270*, 79–101.
(6) Watkins, J. J.; Chen, J.; White, H. S.; Abruna, H. D.; Maisonhaute, E.; Amatore, C. *Anal. Chem.* **2003**, *75*, 3962–3971.
(7) Sun, P.; Mirkin, M. V. *Anal. Chem.* **2006**, *78*, 6526–6534.
(8) Smith, C. P.; White, H. S. *Anal. Chem.* **1993**, *65*, 3343–3353.
(9) He, R.; Chen, S.; Yang, F.; Wu B. *J. Phys. Chem. B* **2006**, *110*, 3262.
(10) Taylor, G.; Girault, H. H. *J. Electroanal. Chem.* **1986**, *208*, 179–183.
(11) Shao, Y.; Mirkin, M. V. *J. Am. Chem. Soc.* **1997**, *119*, 8103–8104.
(12) Liu, B.; Mirkin, M. V. *Electroanalysis* **2000**, *12*, 1433–1446.
(13) Stewart, A. A.; Taylor, G.; Girault, H. H.; McAleer, J. *J. Electroanal. Chem.* **1990**, *296*, 491–515.
(14) Cai, C. X.; Tong, Y. H.; Mirkin, M. V. *J. Phys. Chem. B* **2004**, *108*, 17872–17878.
(15) Jing, P.; Zhang, M. Q.; Hu, H.; Xu, X. D.; Liang, Z. W.; Li, B.; Shen, L.; Xie, S. B.; Pereira, C. M.; Shao, Y. H. *Angew. Chem. Int. Ed.* **2006**, *45*, 6861–6864.
(16) Li, Q.; Xie, S.; Liang, Z.; Meng, X.; Liu, S.; Girault, H. H.; Shao, Y. *Angew. Chem. Int. Ed.* **2009**, *48*, 8010-8013.
(17) Shoup, D.; Szabo, A. *J. Electroanal. Chem.* **1984**, *160*, 27–31
(18) Zoski, C. G.; Mirkin, M. V. *Anal. Chem.* **2002**, *74*, 1986–1992.
(19) Tsujioka, N.; Imakura, S.; Nishi, N.; Kakiuchi, T. *Anal. Sci.* **2006**, *22*, 667–671.
(20) Nishi, N.; Imakura, S.; Kakiuchi, T. *J. Electroanal. Chem.* **2008**, *621*, 297–303.
(21) Rodgers, P. J.; Amemiya, S. *Anal. Chem.* **2007**, *79*, 9276–9285.
(22) Wang, Y.; Velmurugan, J.; Mirkin, M. V.; Rodgers, P. J.; Kim, J.; Amemiya, S., submitted to *Anal. Chem.*
(23) Rodgers, P. J.; Jing, P.; Kim, Y.; Amemiya, S. *J. Am. Chem. Soc.* **2008**, *130*, 7436–7442.
(24) Jing, P.; Rodgers, P. J.; Amemiya, S. *J. Am. Chem. Soc.* **2009**, *131*, 2290–2296.
(25) Jing, P.; Kim, Y.; Amemiya, S. *Langmuir*, http://dx.doi.org/10.1021/la902336w.
(26) Aoki K. *Electroanalysis* **1993**, *5*, 627–639.
(27) Samec, Z. *Pure Appl. Chem.* **2004**, *76*, 2147–2180.
(28) Cai, C.; Mirkin, M. V. *J. Am. Chem. Soc.* **2006**, *128*, 171–179.
(29) Newman, J.; Thomas-Alyea, K. E. *Electrochemical Systems*; John Wiley & Sons: Hoboken, NJ, 2004.
(30) Shao, Y.; Mirkin, M. V. *J. Phys. Chem. B* **1998**, *102*, 9915–9921.
(31) Amphlett, J. L.; Denuault, G. *J. Phys. Chem. B* **1998**, *102*, 9946–9951.

(32) Bard, A. J.; Faulkner, L. R., *Electrochemical Methods: Fundamentals and Applications*, 2nd ed.; John Wiley & Sons: New York, 2001, p. 232.
(33) Mirkin, M. V.; Bulhões, L. O. S.; Bard, A. J. *J. Am. Chem. Soc*. **1993**, *115*, 201–204.
(34) Wei, C.; Bard, A. J.; Feldberg, S. W. *Anal. Chem.* **1997**, *69*, 4627–4633.
(35) Wang, G.; Zhang, B.; Wayment, J. R.; Harris, J. M.; White, H. S. *J. Am. Chem. Soc.* **2006**, *128*, 7679–7686.
(36) White, H. S.; Bund, A. *Langmuir* **2008**, *24*, 2212–2218.

4.0 KINETIC STUDY OF RAPID TRANSFER OF TETRAETHYLAMMONIUM AT THE 1,2-DICHLOROETHANE/WATER INTERFACE BY NANOPIPET VOLTAMMETRY OF COMMON ION

This work has been published as Yixian Wang, Jeyavel Velmurugan, Michael V. Mirkin, and Patrick J. Rodgers, Jiyeon Kim and Shigeru Amemiya. *Anal. Chem,* **2010**, *82,* 77-83**.**

4.1 ABSTRACT

Steady-state voltammetry at the pipet-supported liquid/liquid interface has previously been used to measure kinetics of simple and facilitated ion transfer (IT) processes. Recently, we showed that the conventional experimental protocol and data analysis produce large uncertainties in kinetic parameters of rapid IT processes extracted from pipet voltammograms. Here, we used a new mode of nanopipet voltammetry, in which a transferable ion is initially present as a common ion in both liquid phases, and improved methodology for silanization of the outer pipet wall to investigate the kinetics of the rapid transfer of tetraethylammonium (TEA^+) at the 1,2-dichloroethane/water interface. This reaction was often employed as a model system to check the IT theory. The determined standard rate constant and transfer coefficient of the TEA^+ transfer

are compared with previously reported values to demonstrate limitations of conventional nanopipet voltammetry with a transferrable ion present only in one liquid phase.

4.2 INTRODUCTION

Ion transfer (IT) at the interface between two immiscible electrolyte solutions (ITIES) has been extensively studied because of its intrinsic interest as well as its relevance to many important chemical and biological systems including sensors, batteries, separations, drug delivery systems, and biomembranes.[1-6] Micropipet-based electrochemical probes pioneered by the Girault group[7] as well as later developed nanopipets[8] have been employed to study these processes. The advantages of small pipet electrodes for studying kinetics of IT reactions include fast mass-transfer rate, negligibly small resistive potential drop, low double-layer charging current, and simple steady-state measurements.[9] Micropipet voltammetry revealed a broad spectrum of standard heterogeneous IT rate constants, k^0 (from ~10^{-1} cm/s to <~10^{-7} cm/s) of simple transfers of alkyl and perfluoroalkyl oxoanions[10] and facilitated transfers of hydrophilic anions,[11] alkali-earth metal cation,[12] polypeptide protamines,[12, 13] and synthetic heparin mimetic.[14, 15] A higher mass-transfer rate at nanopipets allows faster facilitated[8, 16] and simple[17-21] IT reactions (e.g., $k^0 \geq$ 1 cm/s) to be probed by steady-state voltammetry. Pipet-supported ITIES tips were also employed as probes for scanning electrochemical microscopy (SECM) to investigate ITs at a large ITIES under enhanced mass-transfer conditions.[22, 23]

The behaviors of tetraalkylammoniums at the interfaces between water and organic solvents—typically, either 1,2-dichloroethane (DCE) or nitrobenzene—have been studied in detail using various approaches including electrochemical methods,[1-4] synchrotron X-ray

reflectivity measurements,[24-26] and molecular dynamics simulations.[24, 27] Rapid, mechanistically simple transfers of tetraalkylammoniums have been widely used as model experimental systems for IT studies. In particular, Marcus pointed out that a small standard Gibbs free energy of tetraethylammonium (TEA^+) transfer at a DCE/water interface eliminates the need to take into account large effects of the applied field and the supporting electrolyte, thus, simplifying theoretical treatment.[28] The reported experimental values, however, vary dramatically from ~10^{-3} cm/s to ~110 cm/s,[18, 21, 29-37] and there seems to be a strong correlation between the obtained value and the mass-transfer rate of the employed method. In a recent study employing 10–300 nm-radius nanopipets, k^0 = 2.3 cm/s was found from quasi-steady-state voltammetry of the TEA^+ transfer from DCE to the aqueous filling solution, and a very similar value (k^0 = 2.1 cm/s) was obtained by steady-state voltammetry for the reverse reaction.[18] The corresponding transfer coefficients, α = 0.70 and β = 0.60,[18] however, are larger than 0.5, and their sum is larger than the theoretically expected value of 1.[28, 38] More recently, 1.2–3.2 nm-radius pipets were employed to obtain a k^0 value of 110 cm/s,[21] which seems to be overestimated (see below).

At first glance, a nanopipet appears to be an extremely simple device (Figure 4-1). It is created in a flash by pulling a quartz capillary, filling it with an aqueous (or organic) solution and immersing in another liquid immiscible with the filling solution. With one reference electrode inserted into the pipet and the second reference in the external solution, the system is ready for experiments. More detailed studies, however, revealed significant complexity of quantitative nanopipet voltammetry, which requires well-defined nanoscopic ITIES formed at the pipet tip. One issue is the formation of a thin aqueous film on the hydrophilic outer wall of the pipet.[22, 39] Such a film appears when a water-filled pipet is immersed in an organic solution and results in the true area of the liquid/liquid interface being much larger than the geometrical area of the

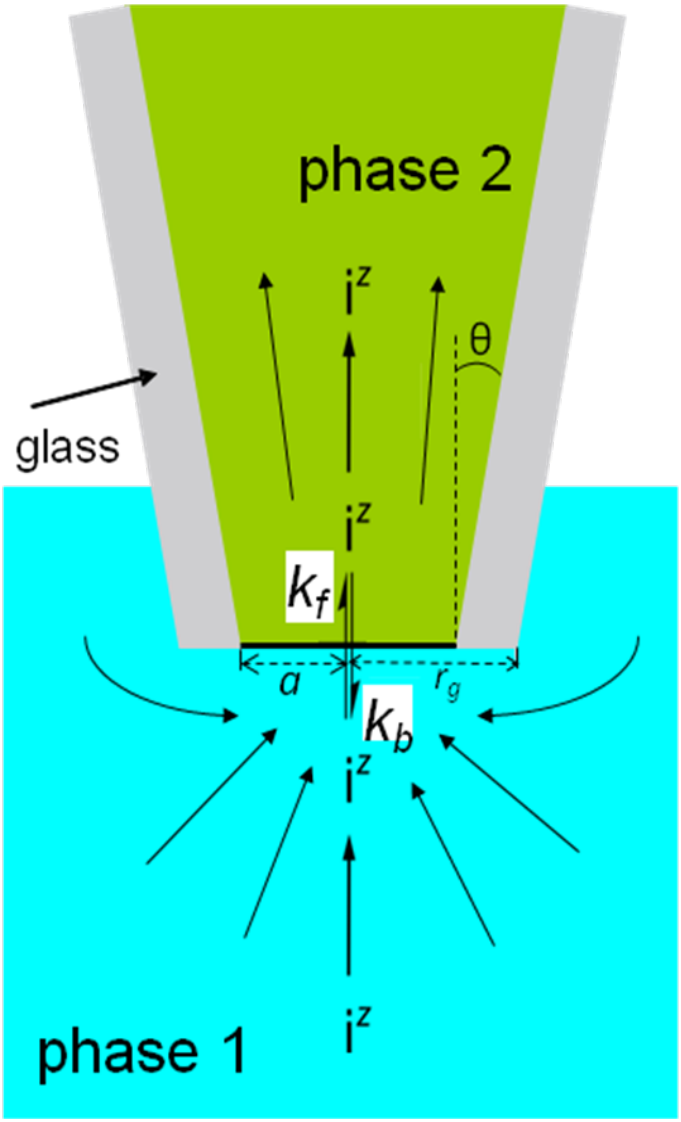

Figure 4-1. Scheme of IT and diffusion at a tapered nanopipet.

pipet orifice. The film formation can be avoided by silanizing the outer pipet wall to render it hydrophobic while keeping the interior wall non-silanized. The formation of a flat ITIES at the orifice of a silanized micropipet[22, 40] and nanopipet[18] was confirmed by SECM.

The pipet geometry and dimensions strongly affect asymmetric diffusion of ions in the inner and outer solutions and, subsequently, IT voltammograms. The steady-state, quasi-spherical diffusion flux of ions from the external solution to the pipet tip (ingress current) depends on two geometric parameters, the orifice radius, a, and the outer wall radius at the tip, r_g. For micrometer-sized pipets, both a and r_g can be determined by optical microscopy. For a nanopipet, both parameters can be evaluated by combination of steady-state voltammetry and SECM.[18] On the other hand, the diffusion flux in the internal solution (egress current) depends on the inner tip angle, θ, in addition to the orifice radius. Recent simulations[12, 41, 42] and experiments at micropipets[12] and nanopipets[21] showed that θ can be determined from the egress current. However, the results of nanopipet studies of simple ITs are inconsistent: sigmoidal and retraceable steady-state cyclic voltammograms (CVs) were obtained with non-silanized[17, 21] and silanized nanopipets,[18] while the latter also gave peak-shaped, transient voltammograms of egress TEA^+ transfer.[18] Improved methodology for silanization of nanopipets discussed below can help to eliminate such artifacts and attain better reliability of nanopipet voltammetry.

In this paper, we employ a new mode of nanopipet voltammetry to study kinetics of rapid TEA^+ transfer at the DCE/water interface. Our recent simulations[43] showed that steady-state pipet voltammograms of a common ion present in both inner and outer solutions comprise positive and negative waves due to ingress and egress ITs. The presence of these two waves enables precise determination of kinetic and thermodynamic parameters along with θ and a values from a single IT voltammogram. Kinetic parameters of the TEA^+ transfer thus

determined are compared with the values obtained previously from conventional nanopipet voltammetry (with TEA^+ initially present only in one liquid phase),[18, 21] and origins of the discrepancies are investigated.

4.3 EXPERIMENTAL SECTION

4.3.1 Chemicals

The following chemicals were used as received: LiCl and chlorotrimethylsilane from Aldrich; tetraethylammonium chloride (TEACl) from Sigma; potassium tetrakis(4-chlorophenyl)borate (KTPBCl), and tetrahexylammonium chloride (THACl) from Fluka. 1,2-dichloroethane (DCE) from Sigma was distilled before use. Tetraethylammonium tetrakis(4-chlorophenyl)borate (TEATPBCl) and tetrahexylammonium tetrakis(4-chlorophenyl)borate (THATPBCl) were prepared by metathesis of KTPBCl with TEACl and THACl, respectively, as described previously.[44] All aqueous solutions were prepared from deionized water (Milli-Q, Millipore Corp.).

4.3.2 Nanopipet Preparation and Characterization by SEM

Nanopipets were made from 10 cm long quartz capillaries (outer/inner diameter ratio of 1.0/0.70; Sutter Instrument Co., Novato, CA) using a laser-based pipet puller (P-2000, Sutter Instrument Co.) as described previously.[8, 18-20] Representative pulling parameters used to produce an ~100 nm pipet are: HEAT = 710, FILAMENT = 4, VELOCITY = 28, DELAY = 120, PULL =130.

However, the parameter values may not be the same for different P-2000 pullers. Moreover, even for the same instrument, the parameters have to be adjusted occasionally to produce pipets of the desired size and shape. The outer glass wall of a pipet was silanized to render it hydrophobic. An improved method for nanopipet silanization is described in Results and Discussion. An Olympus BH2 optical microscope was used to inspect all prepared pipets before measurements.

A field-emission SEM—either Philips Electron Optics XL-30 (image in Figure 4-2) or Zeiss Supra 55 VP (images in Figure 4-3) was employed to visualize the tips of silanized nanopipets. Either an ~3 nm-thick Au (Figure 4-3) or a 20 nm-thick Pd (Figure 4-2) layer was coated on the otherwise insulating nanotip to be imaged without significant charging. An ~1 cm-long tip was cut from the nanopipet and coated with a Au or Pd layer by sputtering while the tapered end was directed vertically toward the target.

4.3.3 Voltammetric Measurements

Voltammetric experiments were carried out at room temperature (23 ± 2 ºC) in a two-electrode cell:

$$\underset{\text{outer DCE solution}}{\text{Ag/AgTPBCl/}c_{\text{DCE}}\text{ mM TEATPBCl + 9.4 mM THATPBCl//}c_{\text{w}}\text{ mM TEACl + 0.1 M LiCl/AgCl/Ag}}_{\text{pipet}} \quad \text{(cell 1)}$$

The pipets were filled with aqueous solution from the rear using a 10 μL syringe. CVs were obtained with a BAS 100B/W electrochemical workstation (Bioanalytical Systems, West Lafayette, IN). The voltage was applied between two 0.25-mm-diameter Ag wires coated with

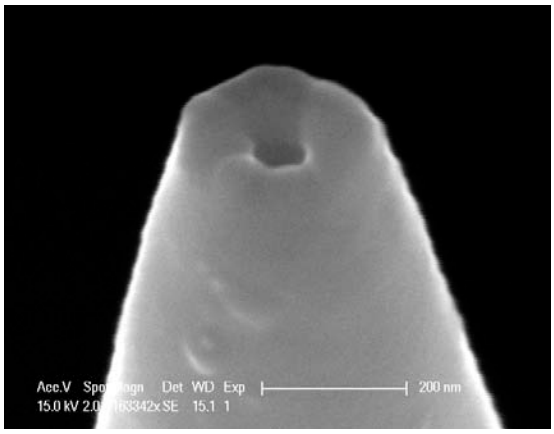

Figure 4-4-2. An SEM image of an “oversilanized” nanopipet.

(a)

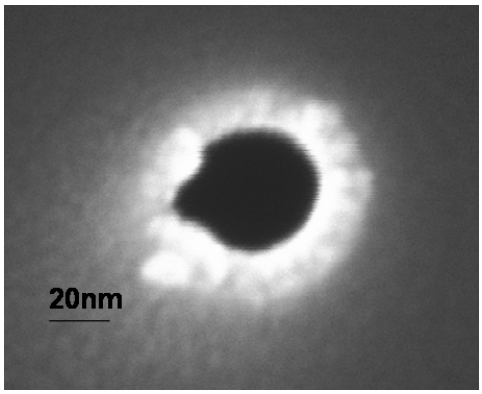

(b)

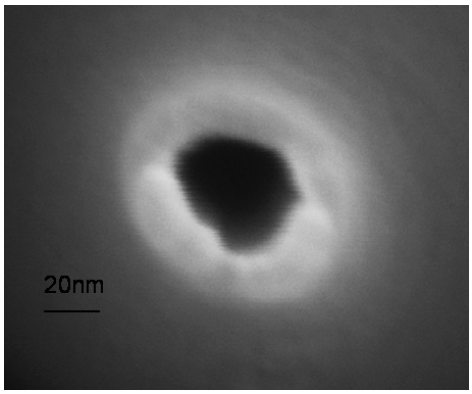

Figure 4-3. Top view SEM images of (a) silanized and (b) non-silanized nanopipets pulled from the same quartz capillary.

either AgCl (aqueous reference inside a pipet) or AgTPBCl (external organic reference). The current produced by the cation transfer from the outer DCE phase to the inner aqueous phase was designated as positive.

4.4 RESULTS AND DISCUSSION

4.4.1 Silanization and SEM of Nanopipets

In previous publications, [8, 18-20, 22, 39] the silanization of the outer wall was done by dipping the pipet tip into a silanizing agent (chlorotrimethylsilane) while passing a flow of argon through the pipet. We found that for nanopipets this method yields less consistent results than for micrometer-sized pipets and often gives "oversilanized" pipets, as revealed by SEM. The wall of an "oversilanized" pipet is very thick (Figure 4-2), and $r_g/a \cong 3.9$ is exceedingly large for a pipet pulled from a thin-wall quartz capillary. Consequently, not only the inner tip radius is decreased but also the pipet shaft can be narrowed, which complicates ion diffusion in the internal solution and may impair the data analysis.

To avoid oversilanization, we silanized nanopipets in the vapor of chlorotrimethylsilane. This was done by holding a pipet 1–2 cm above the surface of liquid chlorotrimethylsilane for ~1 min, while the flow of argon was passed through the pipet from the back to avoid silanization of the inner pipet wall. The required silanization time depends on the distance between the chlorotrimethylsilane surface and the pipet, its radius, and room temperature. An SEM image of a typical, correctly silanized nanopipet is shown in Figure 4-3a, where no orifice blocking occurred. The orifice size and shape of the silanized nanopipet are very similar to those of a non-

silanized nanopipet (Figure 4-3b), which was pulled from the same quartz capillary as the silanized pipet. This result indicates that the thickness of the hydrophobic surface layer produced by silanization is much smaller than the pipet wall thickness. From a series of SEM images, a typical thickness of this layer is a few nm. This number is negligible for a large (e.g., a > 100 nm) pipet, but it may be significant for smaller (a ~ 20 nm) pipets, which require very careful silanization; silanizing very small pipet (e.g., a < 5 nm[21]) may be difficult, if at all possible. Additionally, side-view images of a correctly silanized nanopipet (data not shown) demonstrate that the pipet barrel has a single taper with an outer angle of ~18° along the length of >3 μm from the tip, which supports an assumption in our theoretical model.[43] SEM determination of the inner angle, however, was hampered by the pipet wall.

4.4.2 Voltammetric Characterization of Silanized and Non-Silanized Nanopipets.

Voltammetry of TEA^+ as a common ion was used to characterize silanized and non-silanized nanopipets. A pair of pipets with the same radius was pulled from the same quartz capillary to compare the responses of silanized and non-silanized nanopipets. Both pipets were filled with aqueous TEA^+ solution and immersed in a DCE containing TEA^+ to obtain CVs of TEA^+ egress and ingress (Figure 4-4). Both ingress and egress waves are sigmoidal, thereby confirming steady-state diffusion of TEA^+ on both sides of the nanoscale interface, in agreement with our simulation results.[43] These steady-state voltammograms are not perfectly retraceable, because of capacitive current.

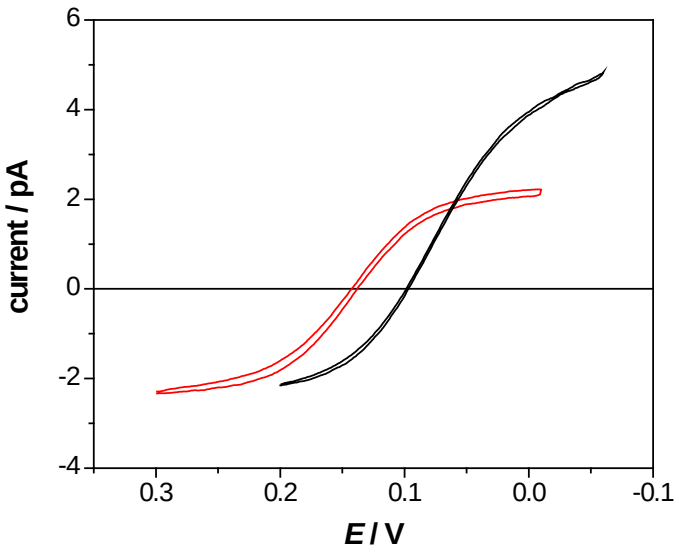

Figure 4-4. CVs of TEA^+ transfer across the DCE/water interfaces obtained with a pair of silanized (red) and non-silanized (black) pipets. The CVs were obtained in cell 1 with c_w = 0.3 mM and c_{DCE} = 2.7 mM. The CV at the silanized pipet corresponds to entry 2 in Table 1. Scan rate was 10 mV/s.

Noticeably, the positive limiting current produced by the ingress of TEA^+ at the non-silanized pipet is ~2.2 times larger than that at the silanized nanopipet. A steady-state diffusion limiting current based on ingress IT is given by

$$i_{ing} = 4xz_iFD_{DCE}c_{DCE}a$$

Equation 4.1

where z_i, D_{DCE} and c_{DCE} are the charge of the transferred ion i, its diffusion coefficient and bulk concentration in the external DCE solution, respectively; and x is a function of r_g/a, which was tabulated[22, 45] and expressed by an analytical approximation for disk-shaped interfaces.[46] Assuming a disk-shaped interface formed at the tip of the silanized pipet with $r_g/a = 1.5$ for $x = 1.16$,[22, 45] $a = 16$ nm was found from the ingress limiting current using Equation 4.1 with $D_{DCE} = 1.0 \times 10^{-5}$ cm^2/s.[14, 39] This radius is very similar to the radius determined from the positive limiting current at the non-silanized pipet, where the formation of a thin water layer on the outer wall results in a larger x value of $3.35\pi/4$.[18] The nearly identical radii of the silanized and non-silanized pipets are consistent with their originating from the same capillary.

In contrast, similar negative limiting currents were obtained with the pair of the silanized and non-silanized nanopipets. With a disk-shaped interface formed at the tip of a silanized nanopipet, the corresponding egress limiting current is given by

$$i_{eg} = 4f(\theta)z_iFD_wc_wa$$

Equation 4.2

where D_w and c_w are the diffusion coefficient and bulk concentration in the internal aqueous solution, respectively, and $f(\theta)$ is a tabulated function of the tip inner angle, θ.[12] An analytical approximation for this function

$$f(\theta) = 0.0023113912 + 0.013191803\theta + 0.000317385960\theta^{1.5} - 5.8554625\times10^{-5}\theta^{2}$$

Equation 4.3

fits the simulated values over the entire range of θ from 1º to 89º within <1%. With the tip radius determined from the ingress limiting current, the corresponding egress limiting current at the silanized nanopipet yields $f(\theta) = 0.16$ with $D_w = 1.0 \times 10^{-5}$ cm^2/s.[14, 39] According to Equation 4.3, $f(\theta) = 0.16$ corresponds to $\theta = 10°$. The very similar egress currents at the silanized and non-silanized nanopipets suggest that inner angles of the pair of the nanopipets pulled from the same capillary are also similar. The geometric quantities, a and θ, are necessary for the determination of kinetic parameters from a nanopipet voltammogram (see below). These parameters control the mass transfer coefficients for the ingress and egress ion transfers, respectively, as given by[43]

$$m_{\text{ing}} = \frac{4xD_{\text{DCE}}}{\pi a}$$

Equation 4.4

$$m_{\text{eg}} = \frac{4f(\theta)D_{\text{w}}}{\pi a}$$

Equation 4.5

For a = 16 nm and $\theta = 10°$, Equations 4.4a and 4.4b yield m_{ing} = 9.0 cm/s and m_{eg} = 1.1 cm/s. The m_{eg} value is smaller than m_{ing}, because the diffusion geometry in the pipet shaft is closer to linear than to hemispherical due to the relatively small taper angle ($f(\theta) << 1$). Importantly, a conventional nanopipet voltammogram obtained with TEA^+ present only in one phase contains either an ingress or an egress wave, so that it is impossible to extract both geometric parameters

(and subsequently both m_{ing} and m_{eg}) from such a voltammogram. Therefore, kinetic parameters can not be precisely determined from a single conventional voltammogram if it is affected by ion diffusion in both phases.[43]

It should be noted that CVs of a common ion contain a zero current point, at which the potential (equilibrium potential, $\Delta^{w}_{DCE}\phi_{eq}$) is given by the Nernst equation

$$\Delta^{w}_{DCE}\phi_{eq} = \Delta^{w}_{DCE}\phi^{0'}_{TEA^+} + \frac{RT}{z_i F}\ln\frac{c_{DCE}}{c_w}$$

Equation 4.6

where $\Delta^{w}_{DCE}\phi^{0'}_{TEA^+}$ is the formal potential of the TEA^+ transfer. (The difference between $\Delta^{w}_{DCE}\phi_{eq}$ values in CVs obtained with silanized and non-silanized nanopipets in Figure 4-4 is due to the use of different organic reference electrodes.) Importantly, $\Delta^{w}_{DCE}\phi^{0'}_{TEA^+}$ can be found directly from $\Delta^{w}_{DCE}\phi_{eq}$ using Equation 4.5. In contrast, no $\Delta^{w}_{DCE}\phi_{eq}$ value can be found from a conventional steady-state IT voltammogram, and $\Delta^{w}_{DCE}\phi^{0'}_{TEA^+}$ has to be determined as an additional fitting parameter; this increases the uncertainties in the extracted k^0 and α values.

4.4.3 Kinetic Analysis of Nanopipet Voltammograms of Tetraethylammonium as a Common Ion.

After the a and θ values are evaluated from the limiting currents, the kinetic parameters (k^0 and α) for rapid TEA^+ transfer can be determined from the same quasi-reversible nanopipet voltammogram of TEA^+. Both parameters are obtained by fitting a whole voltammogram to the theory (Equation 4.6)[43]

$$\frac{i}{i_{ing}} = \frac{1}{m_{ing}/m_{eg} + m_{ing}/k_b + k_f/k_b}\left(\frac{k_f}{k_b} - \frac{c_w}{c_{DCE}}\right)$$

Equation 4.7

The heterogeneous rate constants, k_f and k_b, are given by the Butler-Volmer-type model as

$$k_f = k^0 \exp\left[\frac{-\alpha z_i F(\Delta^w_{DCE}\phi - \Delta^w_{DCE}\phi^{0'}_{TEA^+})}{RT}\right]$$

Equation 4.8

and

$$k_b = k^0 \exp\left[\frac{(1-\alpha) z_i F(\Delta^w_{DCE}\phi - \Delta^w_{DCE}\phi^{0'}_{TEA^+})}{RT}\right]$$

Equation 4.9

where $\Delta^w_{DCE}\phi$ is the Galvani potential difference between the aqueous and DCE phases.

In practice, the precision of kinetic analysis is largely determined by the quality of the experimental voltammogram and particularly by the magnitude of the background current. In previous studies,[8,18] the quality of steady-state voltammograms was improved by background subtraction. In voltammetry of a common ion, the background subtraction is not straightforward because it is difficult to fill the pipet with a blank solution for background measurements and then to refill it with a solution containing the common ion. Without the background subtraction, the aforementioned CV of TEA^+ in both phases of the silanized nanopipet shows significant capacitive current (Figure 4-5a). Nevertheless, it fits well the theoretical curve calculated from Equation 4.6, and the unique combination of the kinetic parameters, α = 0.67 and k^0 = 6.4 cm/s

can be extracted from the best fit. As discussed in ref. 43, the unique fit of the experimental steady-state voltammogram to the theory can be obtained only when both ingress and egress IT waves are quasi-reversible. Different extents of reversibility (i.e., kinetic vs. diffusion control) of the ion ingress and egress processes can be assessed using two dimensionless parameters, $\lambda_{ing} = k^0/m_{ing} = 0.71$ and $\lambda_{eg} = k^0/m_{eg} = 5.8$.[42] Both λ_{ing} and λ_{eg} are smaller than 10, confirming that both ingress and egress ITs are quasi-reversible.

Similar kinetic parameters were determined with various pipets at different TEA^+ concentrations (Table 1). Higher quality CVs with less interference from background currents allow for more accurate and precise determination of kinetic parameters. The measured charging current was always much higher than expected for nm-sized liquid/liquid interfaces, and its value did not decrease significantly with decreasing a (data not shown). These observations suggest that the charging current is mostly due to the stray capacitance of a nanopipet. The background current can be diminished by decreasing the scan rate (e.g., v = 2 mV/s in Figure 4-5b and entries 5 and 6 in Table 1). Also, larger egress current with respect to charging current was obtained at a nanopipet with a larger tip angle (θ = 22º in Figure 4-5c; entry 7 in Table 1), where ingress current was also enhanced by employing a higher concentration of TEA^+ in the outer solution.

In Table 1, $k^0 = 6.1 \pm 0.9$ cm/s and $\alpha = 0.49 \pm 0.09$ were obtained using seven nanopipets with different radii. This α value is expected for a simple one-step IT process[28] not complicated by double-layer effects produced either by ITIES or by the negatively charged orifice and wall of a quartz pipet.[43] The independence of kinetic parameters from pipet size indicates that these tips are large enough to avoid significant double-layer effects. The small voltage required to drive the TEA^+ transfer due to its near-zero standard Gibbs energy is another important factor diminishing the interfacial double layer effects.[28]

The kinetic parameters determined here with TEA^+ as a common ion are significantly different from values previously determined from conventional nanopipet voltammograms with TEA^+ present only in one phase. In the latter case, the analysis of a nearly reversible voltammogram with λ_{ing} (or λ_{eg}) > 1 does not give a unique combination of kinetic and thermodynamic parameters for rapid IT,[43] which is a major source of errors in k^0 and α values previously reported for the TEA^+ transfer.[18] In this way, the underestimated standard rate constants ($k^0 \sim 2$ cm/s) and overestimated transfer coefficients ($\alpha, \beta > 0.5$) were obtained from CVs of ingress and egress TEA^+ transfer recorded at different nanopipets.[18] The errors in the β and k^0 values reported for the egress of TEA^+ from water-filled pipets were somewhat larger because of the neglected effect of ion diffusion in the internal solution.

Several factors discussed above may account for striking differences between the k^o values reported here and the rate constants of the TEA^+ transfer from extremely small ($a \geq 1$ nm) water-filled pipets to DCE measured in ref. 21. The most important factor seems to be slow diffusion inside the pipet. In ref. 21, the mass transfer coefficient for TEA^+ egress was expressed as D_w/a. In this way, m_{eg} for $a = 1$ nm was found to be $\geq$100 cm/s. In contrast, eq. 4b yields m_{eg} = 12.4 cm/s for $a = 1$ nm and $\theta = 7^o$ assumed in ref. 21. With this correction, the rate constants found in ref. 21 would be ~10 times smaller. Another likely reason for significant overestimation of k^0 was the lack of pipet silanization, which may result in the true ITIES area much larger than that evaluated from the diffusion limiting current.[39] Finally, the double layer effects and possible deviations from the conventional theory may complicate the IT kinetic measurements at ultra-small pipets. The last two factors, which are very difficult to control or describe quantitatively, may be assessed experimentally by using common ion voltammetry to

minimize the errors associated with the diffusion inside the pipet and varying *a* within a broad range to explore possible deviations of voltammetric response from the classical theory.

4.5 CONCLUSIONS

A new approach to IT kinetic measurements based on nanopipet voltammetry of a common ion was employed to determine kinetic parameters of the rapid TEA^+ transfer at the DCE/water interface, k^0 = 6.1 ± 0.9 cm/s and α = 0.49 ± 0.09. Both α and k^0 were found to be essentially independent of the pipet radius. The determined α value agrees with the theoretical predictions, and the k^0 value may be representative for IT reactions with a near zero standard Gibbs energy of transfer.[28] The availability of two current waves in the steady-state voltammogram corresponding to the ingress and egress of the common ion improves the reliability of our kinetic analysis and ensures the unique fit of an experimental voltammogram to the theory.

To carry out successful kinetic experiments at the nano-ITIES, one has to correctly silanize the outer nanopipet wall. The developed new protocol helps to avoid the oversilanization problem that was likely undetected in previous nanopipet studies. High-resolution SEM images showed that proper silanization does not significantly affect *a* and causes only a minor increase in r_g even when the pipet radius is as small as ~20 nm. Carefully silanized nanopipets with different tip radii are needed for assessment of double layer effects, which are expected to depend on *a*.[43] Silanized nanopipets can also be employed as SECM probes for high-resolution, chemically selective imaging of topography and ionic conductivity of membranes and various interfaces.[47]

(a)

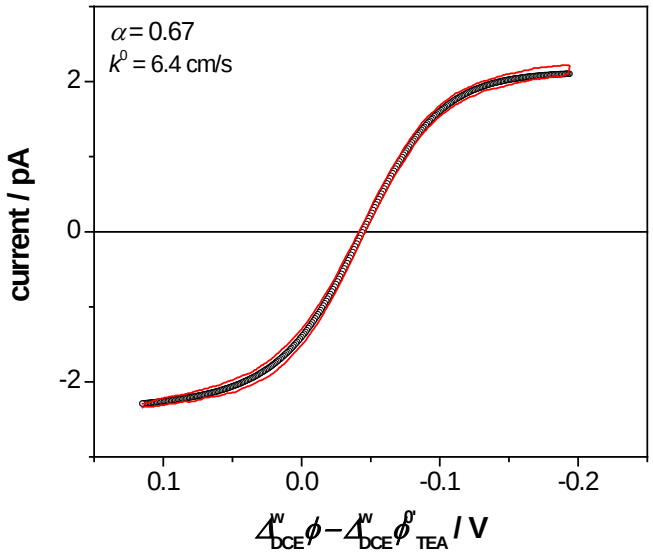
α = 0.67
k⁰ = 6.4 cm/s
current / pA
2
0
-2
0.1
0.0
-0.1
-0.2
Δ^w_DCE φ − Δ^w_DCE φ°_TEA / V

(b)

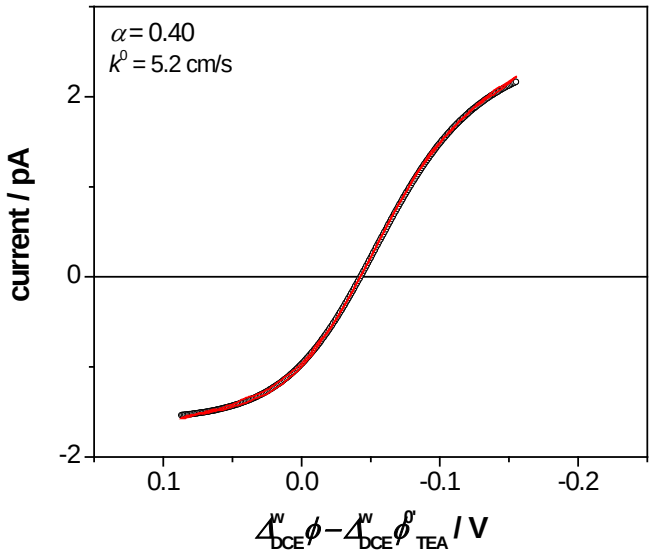
α = 0.40
k⁰ = 5.2 cm/s
current / pA
2
0
-2
0.1
0.0
-0.1
-0.2
Δ^w_DCE φ − Δ^w_DCE φ°_TEA / V

(c)

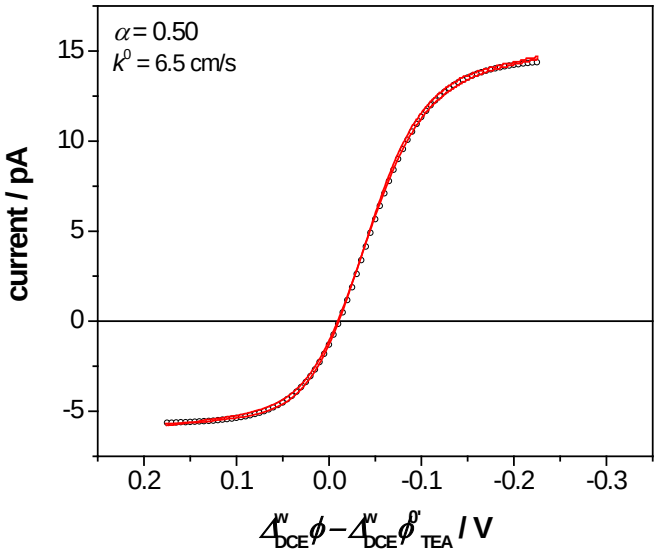

Figure 4-5. Steady-state CVs of TEA^+ transfer across the DCE/water interface obtained with nanopipets in cell 1. The best theoretical fits (closed circles) to the experimental curves (red line) were calculated from Equation 4.6 with parameters in entries (a) 2, (b) 5, and (c) 7 of Table 1. Scan rates are 10, 2, and 10 mV/s, respectively.

Table 4-1. Geometric, Transport, and Kinetic Parameters Determined from Nanopipet Voltammograms of TEA^+ at DCE/Water Interfaces.

		geometric parameters			transport parameters		kinetic parameters	
No.	c_{DCE}:c_w	a nm	$f(\theta)$	θ^p	m_{ing} cm/s	m_{eg} cm/s	k^0 cm/s	α
1	0.3:2.7	20	0.16	12	7.1	1.0	6.5	0.44
2	0.3:2.7	16	0.14	10	9.0	1.1	6.4	0.67
3	0.2:2.1	9.7	0.15	11	15	1.9	4.8	0.51
4	0.4:2.1	11	0.15	11	14	1.8	7.6	0.48
5	0.4:2.1	15	0.13	9.5	9.7	1.1	5.2	0.40
6	0.4:2.1	16	0.12	9.0	9.1	0.97	5.4	0.40
7	1.7:2.6	19	0.29	22	7.8	2.1	6.5	0.50
8	0.56:2.6	33	0.23	17	4.5	0.97	6.5	0.50
9	0.21:2.1	215	0.24	17	0.67	0.14	Nernstian	

ACKNOWLEDGEMENTS

The supports of this work by the National Science Foundation (CHE-0645958; MVM, CHE-0645623; SA) are gratefully acknowledged. In this work, I utilized the numerical simulation and the analytical approximation (Equation 4-6) that were introduced in Chapters 2 and 3, respectively, to kinetically and thermodynamically analyze the data presented here in Chapter 4. The nanopipets were fabricated by Yixian Wang and Jeyavel Velmurugan. Yixian Wang and Jeyavel Velmurugan also optimized the experimental conditions, developed the new approach for silanization (to avoid oversilanization) of the nanopipets, and collected the ion transfer data for TEA. Jieyon Kim captured SEM images of nanopipets. Professor Shigeru Amemiya, my and Jieyon Kim's graduate advisor, and Professor Michael V. Mirkin, Yixian Wang and Jeyavel Velmurugan's graduate advisor provided intellectual guidance on the analyses and merits of the work presented in Chapter 4. We thank Dr. Jorge Morales (CCNY electron microscopy facility) for his help with SEM imaging.

REFERENCES

(1) Girault, H. H. In *Modern Aspects of Electrochemistry*; White, R. E., Conway, B. E., Brockris, J. O. M., Eds.; Plenum Press: New York, 1993; Vol. 25, pp 1–62.
(2) Samec, Z.; Kakiuchi, T. In *Advances in Electrochemical Science and Electrochemical Engineering*; Gerischer, H., Tobias, C. W., Eds.; VCH: New York, 1995; Vol. 4, pp 297.
(3) Benjamin, I. *Ann. Rev. Phys. Chem.* **1997**, *48*, 407–451.
(4) Scholz, F. *Annual Reports on the Progress of Chemistry*; Royal Society of Chemistry: London, 2006.
(5) Reymond, F.; Fermin, D.; Lee, H. J.; Girault, H. H. *Electrochimica Acta* **2000**, *45*, 2647–2662.
(6) Vanysek, P. *Trends Anal. Chem.* **1993**, *12*, 357–363.
(7) Taylor, G.; Girault, H. H. *J. Electroanal. Chem.* **1986**, *208*, 179–183.
(8) Shao, Y.; Mirkin, M. V. *J. Am. Chem. Soc.* **1997**, *119*, 8103–8104.
(9) Liu, B.; Mirkin, M. V. *Electroanalysis* **2000**, *12*, 1433–1446.
(10) Jing, P.; Rodgers, P. J.; Amemiya, S. *J. Am. Chem. Soc.* **2009**, *131*, 2290–2296.
(11) Cui, R.; Li, Q.; Gross, D. E.; Meng, X.; Li, B.; Marquez, M.; Yang, R.; Sessler, J. L.; Shao, Y. *J. Am. Chem. Soc.* **2008**, *130*, 14364–14365.
(12) Rodgers, P. J.; Amemiya, S. *Anal. Chem.* **2007**, *79*, 9276–9285.
(13) Amemiya, S.; Yang, X.; Wazenegger, T. L. *J. Am. Chem. Soc.* **2003**, *125*, 11832–11833.
(14) Rodgers, P. J.; Jing, P.; Kim, Y.; Amemiya, S. *J. Am. Chem. Soc.* **2008**, *130*, 7436–7442.
(15) Jing, P.; Kim, Y.; Amemiya, S. *Langmuir*, http://dx.doi.org/10.1021/la902336w.
(16) Yuan, Y.; Shao, Y. H. *J. Phys. Chem. B* **2002**, *106*, 7809–7814.
(17) Jing, P.; Zhang, M. Q.; Hu, H.; Xu, X. D.; Liang, Z. W.; Li, B.; Shen, L.; Xie, S. B.; Pereira, C. M.; Shao, Y. H. *Angew. Chem. Int. Ed.* **2006**, *45*, 6861–6864.
(18) Cai, C. X.; Tong, Y. H.; Mirkin, M. V. *J. Phys. Chem. B* **2004**, *108*, 17872–17878.
(19) Laforge, F. O.; Sun, P.; Mirkin, M. V. *J. Am. Chem. Soc.* **2006**, *128*, 15019–15025.
(20) Sun, P.; Laforge, F. O.; Mirkin, M. V. *J. Am. Chem. Soc.* **2007**, *129*, 12410–12411.
(21) Li, Q.; Xie, S.; Liang, Z.; Meng, X.; Liu, S.; Girault, H. H.; Shao, Y. *Angew. Chem. Int. Ed.* **2009**, *48*, 8010–8013.
(22) Shao, Y.; Mirkin, M. V. *J. Phys. Chem. B* **1998**, *102*, 9915–9921.
(23) Sun, P.; Zhang, Z. Q.; Gao, Z.; Shao, Y. H. *Angew. Chem. Int. Ed.* **2002**, *41*, 3445–3448.
(24) Luo, G. M.; Malkova, S.; Yoon, J.; Schultz, D. G.; Lin, B. H.; Meron, M.; Benjamin, I.; Vanysek, P.; Schlossman, M. L. *Science* **2006**, *311*, 216–218.
(25) Luo, G. M.; Malkova, S.; Yoon, J.; Schultz, D. G.; Lin, B. H.; Meron, M.; Benjamin, I.; Vanysek, P.; Schlossman, M. L. *J. Electroanal. Chem.* **2006**, *593*, 142–158.
(26) Luo, G. M.; Malkova, S.; Pingali, S. V.; Schultz, D. G.; Lin, B. H.; Meron, M.; Benjamin, I.; Vanysek, P.; Schlossman, M. L. *J. Phys. Chem. B* **2006**, *110*, 4527–4530.
(27) Schweighofer, K.; Benjamin, I. *J. Phys. Chem. A* **1999**, *103*, 10274–10279.
(28) Marcus, R. A. *J. Chem. Phys.* **2000**, *113*, 1618–1629.

(29) Samec, Z.; Marecek, V. *J. Electroanal. Chem.* **1986**, *200*, 17–33.
(30) Wandlowski, T.; Marecek, V.; Holub, K.; Samec, Z. *J. Phys. Chem.* **1989**, *93*, 8204-8212.
(31) Wandlowski, T.; Marecek, V.; Samec, Z.; Fuoco, R. *J. Electroanal. Chem.* **1992**, *331*, 765–782.
(32) Marecek, V.; Lhotský, A.; Racinský, S. *Electrochim. Acta* **1995**, *40*, 2905–2908.
(33) Lhotsky, A.; Holub, K.; Neuzil, P.; Marecek, V. *J. Chem. Soc. Faraday Transac.* **1996**, *92*, 3851–3857.
(34) Kakiuchi, T.; Noguchi, J.; Kotani, M.; Senda, M. *J. Electronanal. Chem.* **1990**, *296*, 517–535.
(35) Kakiuchi, T.; Noguchi, J.; Senda, M. *J. Electroanal. Chem.* **1992**, *336*, 137–152.
(36) Kakiuchi, T.; Teranishi, Y. *J. Electroanal. Chem.* **1995**, *396*, 401–406.
(37) Aminur Rahman, M.; Doe, H. *J. Electroanal. Chem.* **1997**, *424*, 159–164.
(38) Samec, Z. *Electrochim. Acta* **1998**, *44*, 85–90.
(39) Shao, Y.; Mirkin, M. V. *Anal. Chem.* **1998**, *70*, 3155–3161.
(40) Amemiya, S.; Bard, A. J. *Anal. Chem.* **2000**, *72*, 4940–4948.
(41) Tsujioka, N.; Imakura, S.; Nishi, N.; Kakiuchi, T. *Anal. Sci.* **2006**, *22*, 667–671.
(42) Nishi, N.; Imakura, S.; Kakiuchi, T. *J. Electroanal. Chem.* **2008**, *621*, 297–303.
(43) Rodgers, P. J.; Amemiya, S.; Wang, Y.; Mirkin, M. V. *Anal. Chem.*, submitted.
(44) Shao, Y.; Girault, H. H. *J. Electroanal. Chem.* **1991**, *282*, 59–72.
(45) Amphlett, J. L.; Denuault, G. *J. Phys. Chem. B* **1998**, *102*, 9946–9951.
(46) Zoski, C. G.; Mirkin, M. V. *Anal. Chem.* **2002**, *74*, 1986–1992.
(47) Laforge, F. O.; Velmurugan, J.; Wang, Y.; Mirkin, M. V. *Anal. Chem.* **2009**, *81*, 3143–3150.

5.0 ELECTROCHEMICAL RECOGNITION OF SYNTHETIC HEPARIN MIMETIC AT LIQUID/LIQUID MICROINTERFACES

This work has been published as Patrick J. Rodgers Ping Jing, Yushin Kim, and Shigeru Amemiya. *J. Am. Chem. Soc.* **2008**, *130*, 7436–7442.

5.1 ABSTRACT

Electrochemically-controlled molecular recognition of a synthetic heparin mimetic, Arixtra, at nitrobenzene/water microinterfaces was investigated to obtain a greater understanding of interfacial recognition and sensing of heparin and its analogues with biomedical importance. In contrast to unfractionated heparin, this synthetic pentasaccharide that mimics the unique Antithrombin III binding domain of heparin possesses well-defined structure and ionic charge to enable quantitative interpretation of cyclic voltammetric/chronoamperometric responses based on the interfacial recognition at micropipet electrodes. Arixtra is electrochemically extracted from the water phase into the bulk nitrobenzene phase containing highly lipophilic ionophores, methyltridodecylammonium or dimethyldioctadecylammonium. Numerical analysis of the kinetically controlled cyclic voltammograms demonstrates for the first time that formal potentials and standard rate constants of polyion transfer at liquid/liquid interfaces are ionophore-dependent. Moreover, octadecylammonium and octadecylguanidinium are introduced

as new, simple ionophores to model recognition sites of heparin-binding proteins at liquid/liquid interfaces. In comparison to octadecyltrimethylammonium, the best ionophore for heparin recognition at liquid/liquid interfaces reported so far, these new ionophores dramatically facilitate Arixtra adsorption at the interfaces. With a saline solution at physiological pH, an Arixtra molecule is selectively and cooperatively bound to 5 molecules of the guanidinium ionophore, suggesting hydrogen-bond-directed interactions of each guanidinium with a few of 10 negatively charged sulfo or carboxyl groups of Arixtra at the interfaces.

5.2 INTRODUCTION

Molecular recognition of heparin and low-molecular-weight heparin (LMWH) is a crucial step in chemical sensing of these polyanionic carbohydrates[1]with broad biomedical importance as an anticoagulant, an antineoplastic, and beyond.[2] Potentiometric heparin-sensitive electrodes were developed by employing a liquid membrane doped with chloride salts of lipophilic quaternary ammonium ions such as ionophore **1** (Scheme 5-1).[3] Heparin and LMWH have been considered to be extracted from an aqueous sample into the liquid membrane to be ion-paired with the positively charged ionophore. Overall anion-exchange extraction of heparin is thermodynamically favorable, resulting in a large change in the phase boundary potential at the liquid membrane/sample solution interface under non-equilibrium conditions.[3b] More sophisticated ionophores with either primary ammonium[4] or guanidinium[5] groups were synthesized for heparin recognition and assays in bulk water or blood serum. These cationic sites strongly and selectively bind to oxoanionic groups not only by ion pairing but also by hydrogen bonding.[6] In fact, heparin-binding proteins utilize arginine- and lysine-enriched peptides as

recognition sites based on guanidinium and primary ammonium ions, respectively.[7] A highly-selective potentiometric sensor for heparin and LMWH was developed by using silicon field-effect transistors modified with heparin-binding proteins such as protamine and Antithrombin III.[8]

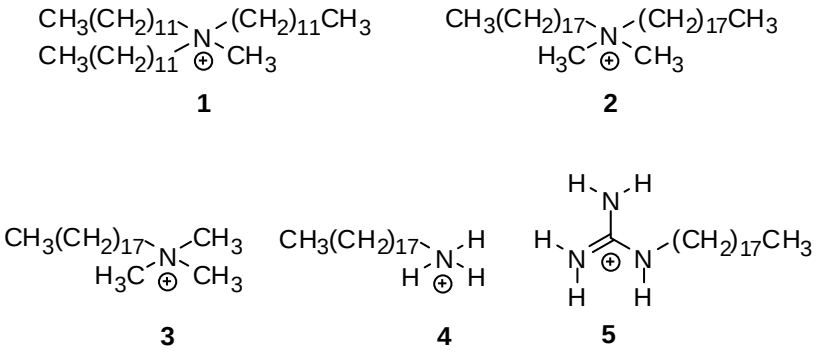

Scheme 5-1

Recently, we[9] and others[10] have successfully developed novel heparin sensors by employing amperometry/voltammetry at interfaces between a heparin-containing aqueous phase and an ionophore-containing organic phase. With this electrochemical approach at liquid/liquid interfaces,[11] the phase boundary potential is controlled externally to selectively and reversibly drive interfacial complexation of heparin with positively charged ionophores such as **1**–**3**, which can be monitored as an ionic current response to heparin. Lowest detection limits of heparin reported so far (0.13 unit/mL in sheep blood plasma[9a] and 0.005 unit/mL in a saline solution[9b]) were obtained by stripping voltammetry based on adsorption of heparin as ionophore **3**

complexes. The detection limits are lower than high-dose heparin (2.3–4.2 unit/mL) during cardiopulmonary bypass, vascular surgery, and angiographic/catheterization procedures[12] and are comparable to low-dose heparin (0.4–0.7 unit/mL) for thromboembolic disease.[13]

The recent amperometric/voltammetric studies also revealed that heparin recognition at liquid/liquid interfaces is poorly understood, thereby limiting further development of this promising sensor technology. The amperometric/voltammetric responses rise from heparin adsorption rather than from complete extraction of heparin into the organic phase.[9,10]The extraction process, however, has been considered as an origin of the non-equilibrium potentiometric heparin responses,[3b,c] which can be also affected by simultaneous interfacial adsorption.[14] Heparin adsorption is facilitated more by an ionophore with a less bulky ammonium group in the order of **3** > **2** > **1** as expected for the strength of the ion pairing.[9a] In contrast, a much larger potentiometric response was obtained with ionophore **1** than with ionophore **2** or hexadecyltrimethylammonium, an analogue of ionophore **3**.[3d] Moreover, facilitated heparin adsorption is so slow that a resulting voltammogram is electrochemically irreversible either at micro-[9a] or macro-interfaces,[9b] while, a nernstian process has been assumed to explain voltammetric[10] and non-equilibrium potentiometric[3b,15] heparin responses at macrointerfaces. A major obstacle to a better understanding of heparin recognition at liquid/liquid interfaces is polydispersity of unfractionated heparin with molecular weight in the range of 5,000–40,000,[7] which hinders quantitative interpretation of the electrochemical responses.

Here we report on electrochemically-controlled molecular recognition of a synthetic heparin mimetic, Arixtra[16] (also known as fondaparinux sodium; Scheme 5-2), at nitrobenzene/water microinterfaces to obtain a greater understanding of interfacial heparin

recognition. This synthetic LMWH mimics a pentasaccharide that serves as the unique Antithrombin III binding domain of heparin to inhibit blood coagulation. Despite its wide use as a FDA-approved anticoagulant drug for prophylaxis of deep vein thrombosis, there have been only a few studies of monitoring Arixtra in a saline solution[8] and human blood samples.[17] Importantly, structurally well-defined Arixtra enables quantitative assessment of its electrochemical recognition by employing cyclic voltammetry/amperometry at the micrometer-sized interface formed at the tip of a glass micropipet electrode (scheme 5-3).[18,19] In addition to quaternary ammonium ionophores **1**–**3**, octadecylammonium **4** and octadecylguanidinium **5** are characterized as new, simple ionophores that model recognition sites of heparin-binding proteins at the interfaces. In fact, Arixtra–Antithrombin III binding is mediated by ammonium and guanidinium groups of lysine and arginine residues of the protein.[20] Also, interfacial interactions of proteins with heparin-like linear, highly charged polysaccharides, glycosaminoglycans, linked to cell membranes regulate intracellular communication.[7b]

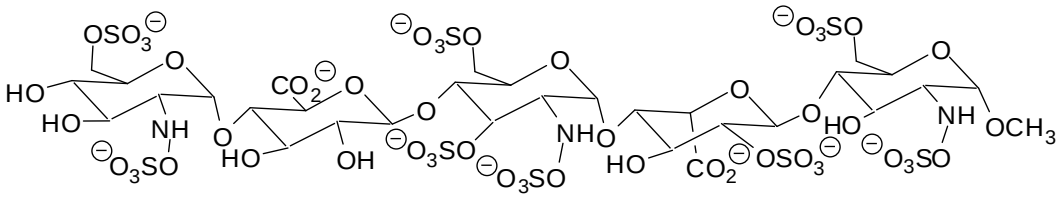

Scheme 5-2

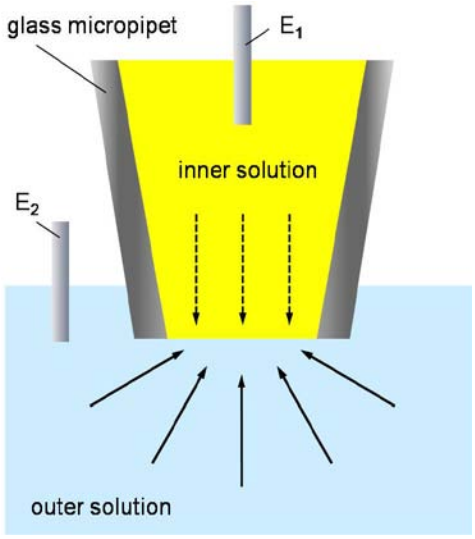

Scheme 5-3

5.3 EXPERIMENTAL

5.3.1 Chemicals

Tetradodecylammonium (TDDA) bromide, methyltridodecylammonium iodide, octadecyltrimethylammonium bromide, nitrobenzene (>99%), chlorotrimethylsilane (99%), and tetraethylammonium (TEA) hydroxide (20 wt % in water) were obtained from Aldrich (Milwaukee, WI). Dimethyldioctadecylammonium chloride was from Tokyo Kasei Kogyo (Tokyo, Japan). Octadecylamine hydrochloride was from Alfa Aesar (Ward Hill, MA). Tris(hydroxylmethyl) aminomethane (Tris Base, 99.9%), and *p*-toluenesulfonate monohydrate (98.5%) were from Sigma (St. Louis, MO). Arixtra (2.5mg/0.5mL and 7.5mg/0.6mL) was purchased from GlaxoSmithKline (Research Triangle Park, NC) as a saline solution for intravenous injection. Potassium tetrakis(pentafluorophenyl)borate (KTFAB) was from Boulder Scientific Co. (Mead, CO). All reagents, except Arixtra, were used as received. All aqueous solutions were prepared with 18.3 MΩ cm^{-1} deionized water (Nanopure, Barnstead, Dubuque, IA).

5.3.2 Dialysis of Arixtra Solutions

Original Arixtra solutions were dialyzed against deionized water using a membrane with 500 molecular weight cutoff to remove sodium chloride because of serious chloride interference in some electrochemical experiments. Ready-to-use devices (DispoDialyzer, Spectrum

Laboratories, Inc., Rancho Dominguez, CA) were used for the dialysis. An Arixtra concentration in the dialyzed solution was determined using a pipet electrode filled with a nitrobenzene solution of ionophore **2** after calibration with standard solutions obtained by diluting an original Arixtra solution.

5.3.3 Preparation of Ionophore–TFAB Salts

TFAB salts of quaternary ammonium ionophores **1**–**3** and a supporting electrolyte TDDA were prepared as reported previously.[9] TFAB salts of octadecylammonium **4** or octadecylguanidinium **5** were prepared by metathesis of KTFAB and octadecylguanidinium *p*-toluenesulfonate or octadecylamine hydrochloride in methanol. A dichloromethane solution of the mixture was washed several times with deionized water. The solvent was removed by rotary evaporator and the product was dried further under vacuum. Octadecylguanidinium *p*-toluenesulfonate was synthesized and characterized as described elsewhere.[21]

5.3.4 Fabrication of Micropipet Electrodes

Micropipet electrodes were made from borosilicate glass capillaries (o.d./i.d. = 1.0 mm/0.58mm, 10 cm in length) from Sutter Instrument Co. (Novato, CA) using laser-based pipet puller (model P-2000, Sutter Instrument).[9a,19] The inner and outer tip radii, a and r_g, and the inner and outer tip angles, θ_1 and θ_2, were determined as reported elsewhere.[19d] The inner or outer wall of each pipet was silanized with chlorotrimethylsilane so that either an organic or an aqueous solution, respectively, was injected into the pipet from the back using a 10-μL syringe.

5.3.5 Electrochemical Measurements

A computer-controlled CHI 660B electrochemical workstation equipped with CHI 200 picoampere booster and Faraday cage (CH instruments, Austin, TX) was used for all electrochemical measurements. The electrochemical cells employed are as follows:

Ag | AgCl | *x* μM Arixtra (aqueous buffer) || *y* mM ionophore–TFAB salt in 0.1 M TDDA–TFAB (nitrobenzene) | Ag

Concentrations of Arixtra and ionophore salt as well as buffer compositions are given in corresponding figures and legends.

The potential of a nitrobenzene phase was given with respect to a formal potential of TEA^+ transfer[19d] in Figures 1–4 and S5. A current carried by a negative charge from the aqueous phase to the organic phase was defined to be negative. Background-subtracted data are reported except in Figure 5-S2. A background current response was obtained using a cell without Arixtra in the aqueous phase. All electrochemical experiments were performed at 22 (±3 °C).

5.4 RESULTS AND DISCUSSION

5.4.1 Electrochemical Characterization of Arixtra Recognition at Microinterfaces: Methodology

In this study, stability of Arixtra–ionophore complexes and potential-dependent dynamics of their formation are elucidated for various ionophores by cyclic voltammetry/amperometry at micropipet electrodes. Recently, we developed this unique electrochemical methodology into a

powerful approach to study complicated transfers of polyions such as unfractionated heparin[9a] and protamine.[19] In addition to the complexation stability and dynamics, it is directly determined from a cyclic voltammogram (CV) whether Arixtra–ionophore complexes formed at the interface are extracted into the organic phase[19a] as defined by

$$A^z \text{ (aqueous phase)} + sLH^+ \text{ (organic phase)} \rightleftharpoons A(LH)_s^{(z+s)} \text{ (interface)} \rightleftharpoons A(LH)_s^{(z+s)} \text{ (organic phase)} \quad (1)$$

where A^z, LH^+, and $A(LH)_s^{(z+s)}$ represent Arixtra, ionophore, and their complexes, respectively. Multiple charges transferred by each Arixtra molecule, *z*, and corresponding large stoichiometry of the complexes, *s*, are determined from limiting currents controlled by diffusion of Arixtra and ionophore to the microinterface, respectively.[19b,c] When the complexes are completely extracted into the bulk organic phase, all thermodynamic and kinetic parameters, i.e., the formal ion-transfer potential, $\Delta_w^o\phi^{0'}$, the standard ion-transfer rate constant, k^0, and the transfer coefficient, α, can be determined from a single CV obtained under kinetic limitation.[19d] Numerical and analytical treatments of voltammetric/amperometric data are detailed in Supporting Information so that only the outcomes are discussed in the following.

5.4.2 Quaternary Ammonium Ionophores 1–3

In contrast to unfractionated heparin,[9,10]Arixtra can be extracted into an organic phase containing highly lipophilic quaternary ammonium **1** or **2** as demonstrated by cyclic voltammetry at organic-filled pipets (Figures 1a and b, respectively). Arixtra extraction is confirmed by a peak current on the reverse potential sweep, which is smaller than a limiting current of a sigmoidal forward wave. The smaller peak current corresponds to linear diffusion of extracted Arixtra–

ionophore complexes in the inner nitrobenzene phase. Arixtra extraction is thermodynamically more favorable with ionophore **2** than with ionophore **1**. Both a half-wave potential, $\Delta^{o}_{w}\phi_{1/2}$, and a peak potential, $\Delta^{o}_{w}\phi_{p}$, are more negative with ionophore **2** (Table 5-1). This result indicates that Arixtra is more stabilized in the nitrobenzene phase by ionophore **2** with more methyl groups attached to the nitrogen's positive charge, which is more accessible for ion pairing with Arixtra's negative charges. On the other hand, Arixtra extraction is faster with ionophore **1** than with ionophore **2**. The separation between $\Delta^{o}_{w}\phi_{1/2}$ and $\Delta^{o}_{w}\phi_{p}$ is much narrower with ionophore **1** than with ionophore **2.** Correspondingly, a peak current is much larger with ionophore **1** than with ionophore **2**.

Structurally well-defined Arixtra enables us to quantitatively assess the apparent thermodynamic and kinetic effects of ionophore structure on Arixtra extraction. The transient CVs based on kinetically limited Arixtra extraction fit well with simulated CVs (Figure 5-1a and b; see Supporting Information for details of the simulation), where the facilitated Arixtra transfer in the presence of excess ionophore was simplified to a first-order process

$$A^{z} \text{ (outer aqueous phase)} \rightleftharpoons A^{z} \text{ (inner organic phase as ionophore complexes)} \quad (2)$$

The numerical analysis gives all parameters (Table 5-1) in the heterogeneous ion-transfer rate constants given by the Butler-Volmer-type relation as[11c,19c,d,22]

$$k_{f} = k^{0} \exp[-\alpha z_{eff} F(\Delta^{o}_{w}\phi - \Delta^{o}_{w}\phi^{0'})/RT]$$

Equation 5.1

$$k_{b} = k^{0} \exp[(1-\alpha) z_{eff} F(\Delta^{o}_{w}\phi - \Delta^{o}_{w}\phi^{0'})/RT]$$

Equation 5.2

where k_f and k_b are heterogeneous rate constants of the forward and backward ion transfer, respectively, in Equation 5.2, z_{eff} is an Arixtra's charge that effectively contributes to transfer kinetics, and $\Delta^o_w\phi$ is the Galvani potential difference between the organic and aqueous phases.

A ~50 mV difference between $\Delta^o_w\phi^{0'}$ values for ionophores **1** and **2** corresponds to a significantly large difference of 48 kJ/mol in a Gibbs free energy of ion transfer given by $-zF\Delta^o_w\phi^{0'}$,[11c] because of a large actual charge of ~−10 transferred by each Arixtra molecule (see below). The k^0 values demonstrate that Arixtra extraction is intrinsically faster with ionophore **1** than with ionophore **2** by an order of magnitude, corresponding to quasi-reversible and irreversible Arixtra transfer with the respective ionophores. Since the α and z_{eff} values are similar, the kinetic effect is not due to different transfer mechanisms. Interestingly, the z_{eff} value of −7 confirms that multiple charges of an Arixtra molecule are transferred simultaneously across the interface. In fact, large potential dependence of Arixtra-transfer rates as governed by z_{eff} and α (Equations 5.2 and 5.3) results in the sigmoidal forward wave (Figures 5-1a and b) that is much steeper than that observed with conventional systems based on nernstian transfer of a monovalent ion at micropipet electrodes.[18] This simultaneous transfer of multiple charges across the interface is a unique electrochemical property of polyion transfer at liquid/liquid interfaces[9,19] and is not observed in redox reactions of multiple, independent redox centers with identical formal potentials at metal/liquid interfaces.[23]Arixtra extraction facilitated by ionophore **1** or **2** is not based on a simple mechanism. The α values of 0.64 and 0.78 obtained with the respective ionophores are larger than normal values in the range of 0.4–0.6. [24] Moreover, the z_{eff} value of −7 is smaller than a total charge number of an Arixtra molecule expected from its 8 sulfo and 2 carboxyl groups (Scheme 1). In fact, actual charges carried by each Arixtra molecule across the interface were determined from

Table 5-1. Ionophore-dependent parameters of Arixtra extraction or adsorption at nitrobenzene/water microinterfaces

ionophore	$\Delta^{o}_{w}\phi_{1/2}$ V [a]	$\Delta^{o}_{w}\phi_{p}$ V [a]	$\Delta^{o}_{w}\phi^{0'}$ V [a]	k^0 cm/s	α	z_{eff}	z [b]
1	0.33	0.30	0.31	1.4×10^{-3}	0.64	−7	−12
2	0.28	0.22	0.26	1.2×10^{-4}	0.78	−7	−10
3	0.24	0.21	–	–	–	–	−11
4	0.00	−0.07	–	–	–	–	−7
4 [c]	0.00	−0.09	–	–	–	–	(−1.06)
5	0.04	−0.04	–	–	–	–	−4.8
5 [c]	0.06	−0.06	–	–	–	–	(−1.02)

[a] Defined with respect to $\Delta^{o}_{w}\phi^{0'}$ of TEA^{+} transfer. [b] A value in the parentheses is *z*/*s*. [c] Studied using water-filled pipets. Parameters in the other rows were obtained using organic-filled pipets.

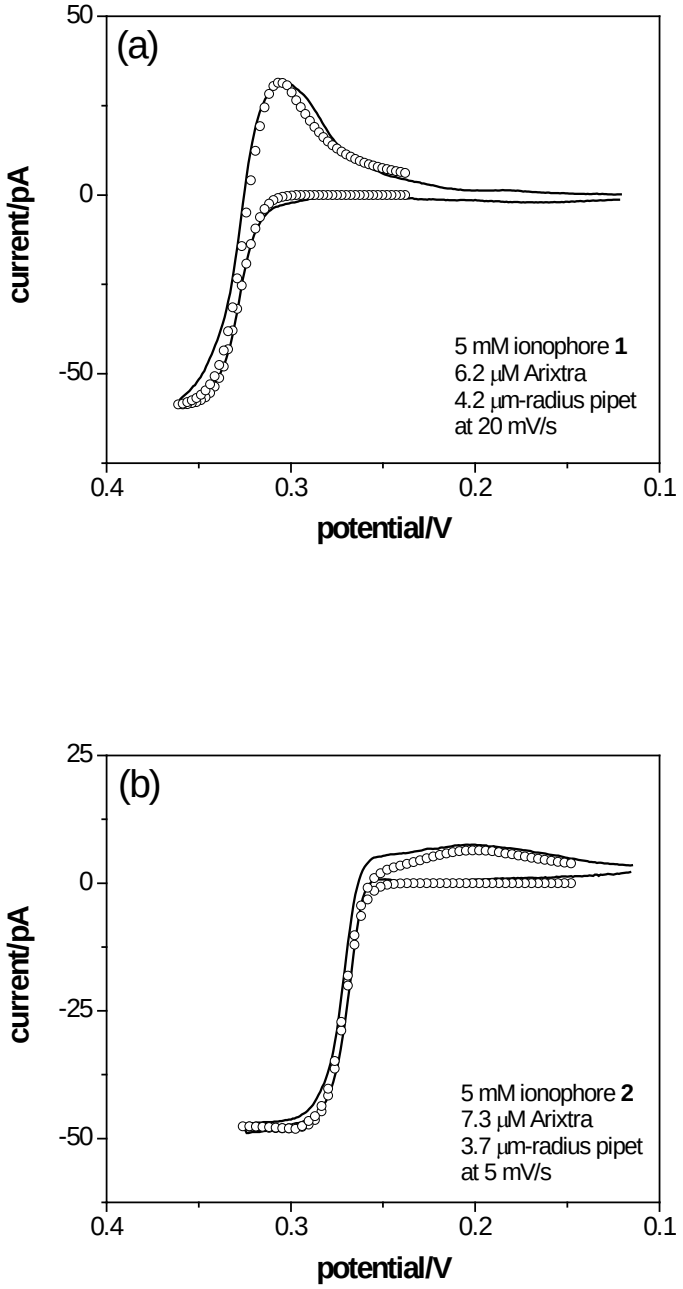

Figure 5-1. Background-subtracted CVs (solid lines) of Arixtra extraction facilitated by ionophores (a) 1 and (b) 2 at organic-filled pipets in contact with dialyzed Arixtra samples diluted with 0.1 M NaH_2PO_4/Na_2HPO_4 at pH 7.1. The open circles represent simulated CVs with parameters listed in Tables 1 and S1.

steady-state (Figure 5-1) and chronoamperometric (Figure 5-S1) diffusion-limited currents, thereby yielding $z = -12 \pm 1$ and -10 ± 1 for ionophores **1** and **2**, respectively (see Supporting Information). These z values, which are close to the number of negatively charged groups of an Arixtra molecule, are larger than the z_{eff} values. The different z and z_{eff} values indicate a multi-step transfer mechanism as previously discussed for protamine transfer,[19c,d] although a z_{eff} value of Arixtra extraction is much closer to the corresponding z value in comparison to the case of facilitated protamine transfer with $z_{eff} = +2.9$ and $z = +20$.[19d] The deviation of α values from 0.5 suggest a double layer effect[25] on a potential-dependent step such as adsorption of charged Arixtra and ionophore molecules involved in the multi-step mechanism.

In contrast to ionophores **1** and **2**, Arixtra–ionophore **3** complexes are adsorbed at nitrobenzene/water interfaces (Figure 5-2). A peak current on the reverse potential sweep, which is larger than a limiting current of a sigmoidal forward wave, corresponds to Arixtra desorption from the interface. This result indicates that a highly lipophilic ionophore is required for extraction of hydrophilic Arixtra into the nitrobenzene phase. On the other hand, Arixtra is more stabilized with ionophore **3** at the interface than with ionophore **1** or **2** in the bulk nitrobenzene phase as indicated by more negative $\Delta^{o}_{w}\phi_{1/2}$ and $\Delta^{o}_{w}\phi_{p}$ values with ionophore **3** (Table 5-1), which possesses a less bulky ammonium group to be ion–paired with Arixtra more strongly. A limiting current obtained with ionophore **3** is equivalent to a charge of -11 ± 1 carried by each Arixtra molecule (see Supporting Information) although the limiting current regime is narrowed by transfer of ionophore **3** from the nitrobenzene phase at more positive potentials than the switching potential. Despite the different interfacial behaviors of Arixtra, the charge transferred by each Arixtra molecule at pH 7.1 is nearly identical among quaternary-ammonium-based ionophores **1**–**3** and is consistent with the number of negatively charged groups of Arixtra.

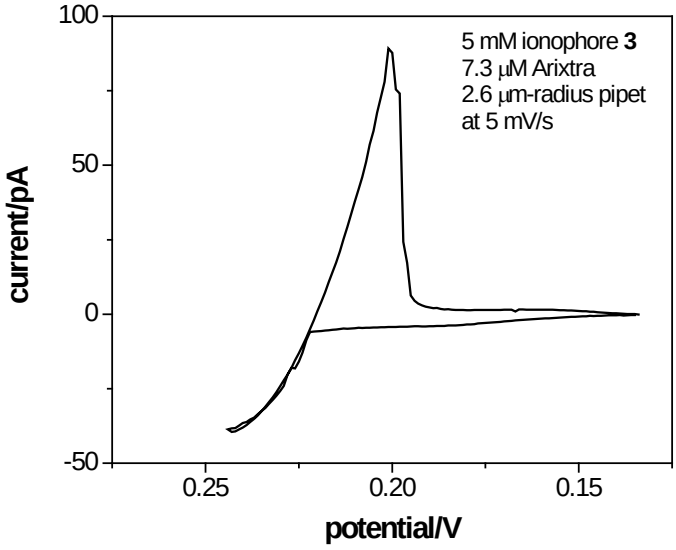

Figure 5-2. A background-subtracted CV of Arixtra adsorption facilitated by ionophore 3 at an organic-filled pipet with r_g/a = 1.1 in contact with a dialyzed Arixtra sample diluted with 0.1 M NaH_2PO_4/Na_2HPO_4 at pH 7.1.

5.4.3 Primary Ammonium Ionophore 4

Octadecylammonium **4** was employed as a new, simple ionophore to assess Arixtra-binding capability of a primary ammonium group at liquid/liquid interfaces. In comparison to quaternary ammonium ionophores **1**–**3**, ionophore **4** with a less bulky ammonium group is expected to bind more strongly to oxoanionic groups. In fact, a primary ammonium group serves as a major recognition site of not only proteins[7] but also several ionophores[4] to bind to heparin in bulk water at physiological pH. At liquid/liquid interfaces, however, deprotonation of a primary-

ammonium-based ionophore, LH^+, is readily driven by the interfacial potential[26] to generate a neutral ionophore, L, with much weaker oxoanion-binding capability

$$LH^+(\text{organic phase}) \rightleftharpoons L\ (\text{organic phase}) + H^+\ (\text{aqueous phase})$$

Equation 5.3

In fact, preliminary experiments demonstrate that deprotonation of ionophore **4** is so favorable with an aqueous phase buffered at pH 7.1 that a large current response based on proton transfer (Equation 5.5) overlaps with a current response to Arixtra (Figure 5-S2).

Arixtra adsorption facilitated by ionophore **4** was clearly observed by using an aqueous solution at pH 5 (Figure 5-4a), where ionophore deprotonation is suppressed.[26] Arixtra adsorption was dramatically facilitated by ionophore **4**, resulting in $\Delta^{o}_{w}\phi_{1/2}$ and $\Delta^{o}_{w}\phi_{p}$ values that are ~250 mV more negative than those with ionophore **3** (Table 5-1). Although ionophore **3** is the best ionophore for heparin recognition at liquid/liquid interfaces reported so far,[9] $\Delta^{o}_{w}\phi_{1/2}$ and $\Delta^{o}_{w}\phi_{p}$ values with ionophore **3** are only <100 mV more negative in comparison to those with ionophore **1** or **2**. These results confirm the expectation that a primary ammonium group is a much stronger binding site for Arixtra than a quaternary ammonium group. On the other hand, large separation between $\Delta^{o}_{w}\phi_{1/2}$ and $\Delta^{o}_{w}\phi_{p}$ with ionophore **4** indicates sluggish Arixtra adsorption and desorption, resulting in the electrochemically irreversible CV. Also, a narrow anodic limit of the potential window is set by transfer of ionophore **4** from the nitrobenzene phase.

A current response to Arixtra with ionophore **4** was found to be rather small as represented by a small limiting current, which corresponds to $z = -7 \pm 1$ (see Supporting Information). This z value is significantly smaller than the z values of ~10 determined with

ionophores **1**–**3** at pH 7.1. The smaller charge may be due to lower pH used for the characterization of ionophore **4**, where Arixtra may be partially protonated to carry the smaller charge across the interface. Alternatively, the charge may be carried by ionophore **4** rather than by Arixtra, indicating that ~7 ionophore molecules are transferred across the interface to cooperatively bind to an Arixtra molecule at the aqueous side of the interface. Such a mechanism was proposed in voltammetric studies of DNA adsorption facilitated by cationic intercalators[27] and also by ionophore **2**.[28] This mechanism is highly likely with ionophore **5** (see below).

Overall stability of Arixtra–ionophore complexes depends not only on strength of interactions between each ionophore molecule and Arixtra, but also on stoichiometry, *s*, defined by Equation 5.1. The complexation stoichiometry was determined for ionophore **4** using a water-filled pipet (Figure 5-3b),[19b,c] where limiting currents controlled by diffusion of ionophore **4** in the outer organic phase correspond to a *z*/*s* value of -1.06 ± 0.08 (see Supporting Information). With a *z* value of −7 determined using an organi c-filled pipet, this *z*/*s* value indicates that 7 ionophore molecules are involved in interfacial complexation with each Arixtra molecule at either nitrobenzene or aqueous side of the interface. In fact, the large complexation stoichiometry results in the sigmoidal forward wave that is not point symmetric with respect to the half-wave potential (Figure 5-3b).[9a] Importantly, these 1:7 Arixtra–ionophore **4** complexes are formed selectively in the presence of ~40 mM Cl^-, which is a major interfering anion in blood samples.[9a]

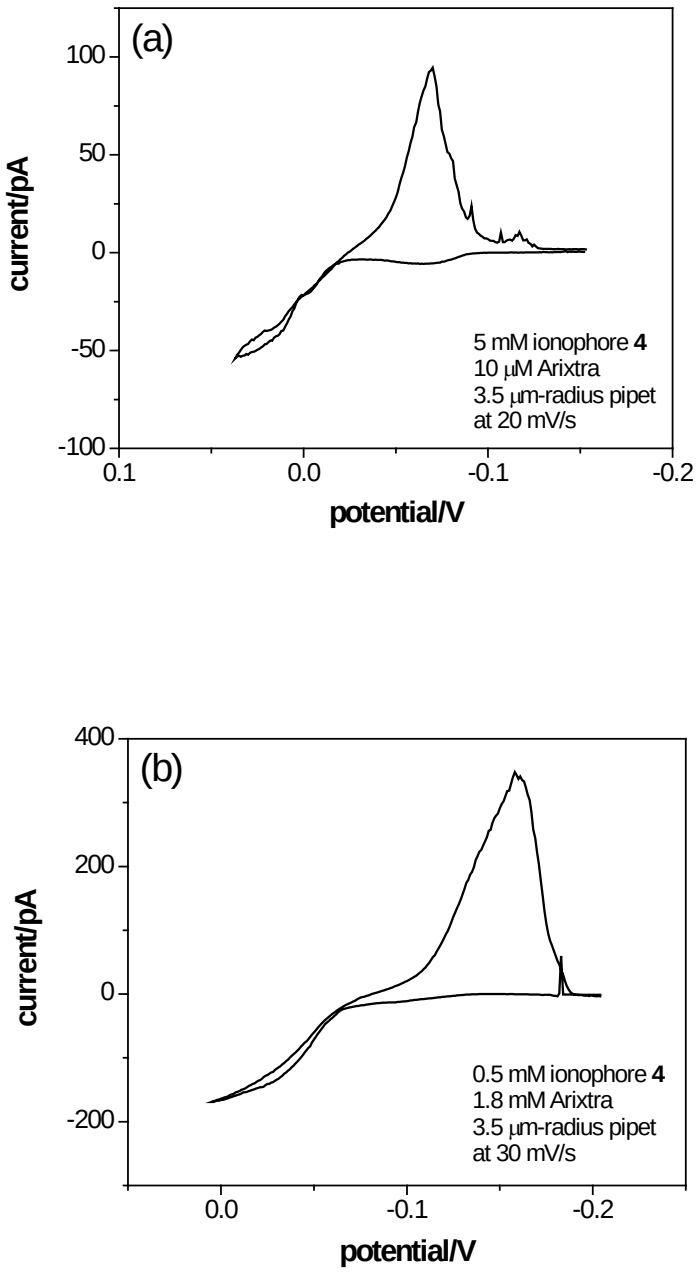

Figure 5-3. Background-subtracted CVs of Arixtra adsorption facilitated by ionophore 4 at (a) an organic- and (b) a water-filled pipet with r_g/a = 1.3. The aqueous solutions were prepared by diluting (a) a dialyzed and (b) an original Arixtra sample with 0.1 M acetic acid/sodium acetate at pH 5.0. The aqueous solution in (b) also contains ~40 mM NaCl.

5.4.4 Guanidinium Ionophore 5

Octadecylguanidinium **5** was synthesized and characterized as a new heparin ionophore to model arginine-enriched recognition sites of heparin-binding proteins[7] at liquid/liquid interfaces. In contrast to ionophore **4**, ionophore **5** with a less acidic guanidinium group facilitates Arixtra adsorption even at pH 7.1 without ionophore deprotonation (Figure 5-4a). In comparison to ionophore **3**, $\Delta^{o}_{w}\phi_{1/2}$ and $\Delta^{o}_{w}\phi_{p}$ values with ionophore **5** are at least 200 mV more negative (Table 5-1), confirming much stronger binding of a guanidinium group to Arixtra. At the same time, slower Arixtra adsorption facilitated by ionophore **5** is electrochemically irreversible as indicated by large separation between $\Delta^{o}_{w}\phi_{1/2}$ and $\Delta^{o}_{w}\phi_{p}$. Importantly, the CV with ionophore **5** is well-defined despite the presence of 0.12 M NaCl in the aqueous phase. An increased current response around the switching potential is not due to Cl^{-} transfer but due to transfer of ionophore **5** from the nitrobenzene phase. These results indicate that the guanidinium unit is more selective to Arixtra against Cl^{-} than quaternary-ammonium-based ionophores.[9a]

The high selectivity of ionophore **5** for hydrophilic Arixtra is remarkable because potentiometric anion selectivity of liquid membranes based on simple alkylguanidinium ionophores follow Hofmeister series for small monovalent and divalent anions,[29] which is solely based on analyte lipophilicity as a measure of a free energy required for analyte extraction from the water phase into the membrane phase.[30] The high Arixtra selectivity is likely due to the requirement of less dehydration of Arixtra for complexation at the interface than for extraction into the bulk nitrobenzene phase. Also, complexation stoichiometry discussed in the

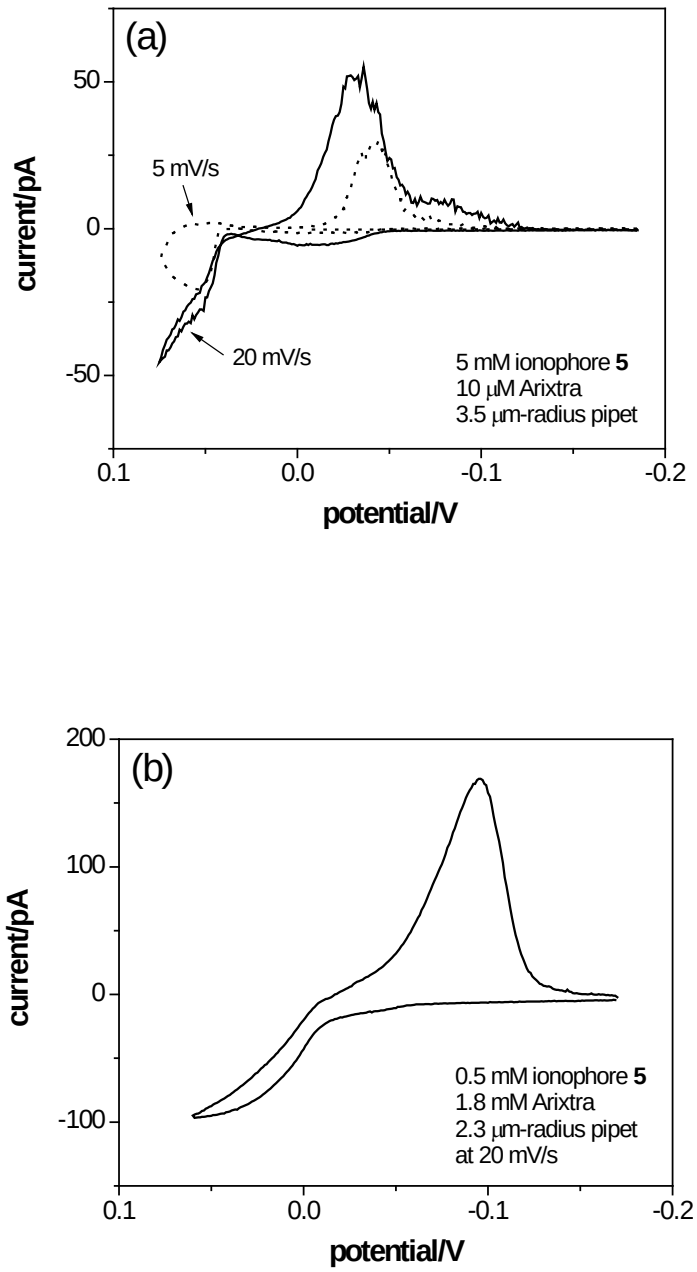

Figure 5-4. Background-subtracted CVs of Arixtra adsorption facilitated by ionophore 5 at (a) an organic- and (b) a water-filled pipet with r_g/a = 1.3. The aqueous solutions were prepared by diluting (a) a dialyzed Arixtra sample with 0.12 M NaCl and 0.01 M Tris/HCl at pH 7.1 and (b) an original Arixtra sample with 0.1 M Tris/acetate acid at pH 7.1. The aqueous solution in (b) also contains ~40 mM NaCl.

following suggests that a guanidinium group of ionophore **5** is attracted electrostatically to multiple negative charges of a polyanionic Arixtra molecule, thereby forming more stable complexes with Arixtra than with such a small anion as Cl^-. On the other hand, Arixtra–ionophore **5** complexes are less stable than Arixtra–ionophore **4** complexes as indicated by more negative $\Delta^o_w\phi_{1/2}$ and $\Delta^o_w\phi_p$ values with ionophore **4**. The lesser degree of stability of ionophore **5** complexes is at least partially due to smaller complexation stoichiometry (see below).

Stoichiometry of Arixtra–ionophore **5** complexes was found to be smaller than the corresponding value of ~7 for ionophore **4** complexes. A charge involved in adsorption of each Arixtra molecule with ionophore **5** is only -4.8 ± 0.8 as determined from limiting currents at organic-filled pipets (Figure 5-4a; see Supporting Information). Since an Arixtra molecule carries a charge of ~10 across the interface at pH 7.1, this smaller charge indicates that ~5 molecules of ionophore **5** are transferred across the interface to form a complex with an Arixtra molecule at the aqueous side of the interface. This complexation stoichiometry was further confirmed using a water-filled pipet (Figure 5-4b), where a z/s value of -1.02 ± 0.07 was obtained from the limiting current (see Supporting Information). The z and z/s values confirm the formation of 1:5 Arixtra–ionophore **5** complexes at the interfaces. Participation of multiple ionophore molecules in the complexation process is supported by the shape of the sigmoidal forward wave without point symmetry with respect to a half-wave potential (Figure 5-4b).[9a]

The formation of 1:5 Arixtra–ionophore **5** complexes is likely due to a multiple-hydrogen-bonding capability of a guanidinium group to simultaneously interact with two or three oxoanionic groups.[31] Figure 5-5 shows a possible mode of 2:1 oxoanion–ionophore **5** binding in the interfacial Arixtra complexes, where overall 10 oxoanionic groups of a Arixtra molecule

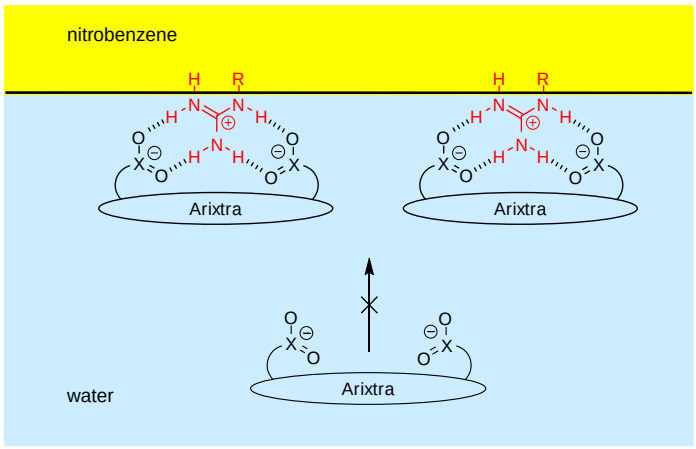

Figure 5-5. A scheme of 2:1 oxoanion–guanidinium binding in 1:5 Arixtra–ionophore 5 complexes and a resulting blocking effect on access of free Arixtra to the interface. XO_2^- represents a negatively charged carboxyl or sulfo group of Arixtra.

are available for binding to 5 molecules of ionophore **5**. Such a binding mode was also found in a crystal structure of Arixtra–Antithrombin III complexes, where a guanidinium unit of an arginine residue of Antithrombin III interacts with a *N*-sulfo and a carboxyl group of adjacent saccharide units of Arixtra.[20] Notably, the 1:5 Arixtra–ionophore **5** complexes possess an overall charge of −5 (Equation 5.8). The formation of highly negatively charged complexes is supported by a "blocking effect[32]" observed as a decay of a limiting current in the potential region of >0.05 V using an organic-filled pipet at slow scan rates (dotted line in Figure 5-4a). At a slower scan rate, more Arixtra–ionophore complexes with negative charges are adsorbed at the interface to block the access of polyanionic Arixtra molecules to the interface (Figure 5-5), thereby resulting in the decay of a current response. Such a blocking double-layer effect was not observed at a water-

filled pipet, where aqueous Arixtra concentration is much higher and is not depleted. No blocking effect of Arixtra adsorption with ionophore **3** or **4** suggests that Arixtra complexes of the respective ionophores without or less hydrogen-bond donors are less negatively charged, while stoichiometry and concomitantly charge of Arixtra complexes were not obtainable for ionophores **1**–**3** using a water-filled pipet because of their weak binding to Arixtra (see Supporting Information).

5.5 CONCLUSIONS

This electrochemical study of a synthetic heparin mimetic, Arixtra, with well-defined structure and ionic charge revealed importance of anion-binding capability, lipophilicity, and acidity of ionophores for electrochemical heparin recognition at liquid/liquid interfaces. This work is the first to demonstrate that formal potentials and standard heterogeneous rate constants of polyion transfer depend on ionophores. The k^0 values in the range of ~10^{-3}–10^{-4} cm/s determined for Arixtra extraction by using highly lipophilic ionophores **1** and **2** indicate that the facilitated Arixtra transfer between bulk solutions can be nearly nernstian at the corresponding macrointerfaces because of relatively slow diffusion of Arixtra and its ionophore complexes with diffusion coefficients in the range of 1–4 × 10^{-6} cm^2/s. A comparison of these results with those of our previous studies of unfractionated heparin with molecular weight in the range of 5,000–40,000[9] suggests that only such a small heparin molecule as Arixtra with molecular weight of 1,498 can be extracted rapidly by the simple quaternary ammonium ionophores. Importantly, it can be determined unambiguously by voltammetry not by traditional potentiometry whether

heparin–ionophore complexes are extracted or adsorbed and also how fast this interfacial process occurs.

A comparison of CVs based on Arixtra adsorption facilitated by ionophores **3**–**5** demonstrates for the first time that primary-ammonium and guanidinium groups serve as very strong and selective heparin-binding sites at liquid/liquid interfaces in comparison to quaternary-ammonium groups, which were used exclusively in traditional potentiometric[3,15,33] and more advanced amperometric/voltammetric[9,10] sensing of heparin at the interfaces. A highly stable Arixtra complex involves several molecules of ionophore **4** or **5**, which cooperatively bind to an Arixtra molecule at the interfaces. Despite similar anion-binding capability, a less acidic guanidinium group is required for interfacial heparin recognition at physiological pH. At the same time, ionophores **3**–**5** with an octadecyl group are not hydrophobic enough to extract Arixtra or avoid potential-driven ionophore transfer from the organic phase, thereby narrowing the potential window at the nitrobenzene/water interface.

In comparison to the potentiometric counterpart, our amperometric/voltammetric approach enables more effective characterization and sensing applications of ionophores for electrochemical heparin recognition at liquid/liquid interfaces. In fact, high Arixtra selectivity against chloride is problematic in non-equilibrium potentiometry,[3,15,33] where simultaneous transfer of a polyion and its co-ions is required for a significant potentiometric response to the polyion. Moreover, by unique analogy between ionically-polarized biological membranes and liquid/liquid interfaces,[34] the interfacial heparin recognition is envisioned as a model of protein–glycosaminoglycan interactions on cell membranes, which is important in intercellular communication.[7b]

ACKNOWLEDGMENT

This work in Chapter 5 was supported by a CAREER award from the National Science Foundation (CHE-0645623). I collected and analyzed all of the data for Arixtra transfers that originated from micropipet electrodes that were filled with the organic solvent, nitrobenzene (data shown in Figures 5-1, 5-2, 5-3a and 5-4a also in the Supporting Information section). I analyzed the cyclic voltammograms of the Arixtra transfer facilitated by ionophores **1** and **2** by numerical simulations to determine all of the kinetic and thermodynamic parameters listed in Table 5-1. Dr. Ping Jing collected and analyzed the data for Arixtra transfer when the pipet was filled with the aqueous buffer solution (Figures 5-3b and 5-4b and data in Supporting Information). Yushin Kim synthesized octadecylguanidinium *p*-toluenesulfonate and subsequently prepared the TFAB salt of octadecylguanidinium **5**. Each one of us was responsible for optimizing the conditions of our own experiments to obtain meaningful data. We each were for analyzing that data. Professor Shigeru Amemiya provided guidance and intellectual contributions for the work presented in Chapter 5.

SUPPORTING INFORMATION

Numerical Simulation of Micropipet Cyclic Voltammograms

Transient cyclic voltammograms obtained with ionophore **1** or **2** (Figure 5-1) were compared with CVs simulated as reported recently.[S1] A diffusion problem at a liquid/liquid interface formed at the tip of a micropipet electrode was defined using dimensionless parameters and solved numerically by COMSOL Multiphysics version 3.2 (COMSOL, Inc., Burlington, MA), which applies the finite element method. An example of the simulation results is attached.

In addition to the parameters defined in Equations 5.3 and 5.4, simulation results depend on parameters listed in Table S1. A diffusion coefficient ratio, γ, is given by

$$\gamma = D_C/D_A \qquad \text{(S1)}$$

where D_A and D_C are diffusion coefficients of Arixtra and its ionophore complexes in the aqueous and organic phases, respectively. A γ value obtained from the fitting gives a D_C value from Equation 5.S1 with $D_A = (3.9 \pm 0.3) \times 10^{-6}$ cm^2/s determined by chronoamperometry (see below).

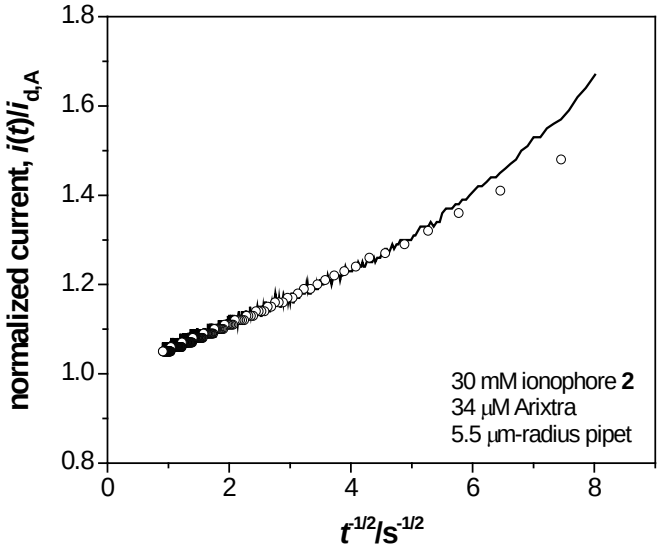

Figure 5-S1. A background-subtracted chronoamperometric response (solid line) to Arixtra as obtained using a pipet (r_g/a = 1.1) filled with a nitrobenzene solution containing 30 mM TFAB salt of ionophore **2** and 0.2 M TDDA–TFAB in contact with a dialyzed Arixtra sample diluted with 0.1 M NaH_2PO_4/Na_2HPO_4 at pH 7.1. The potential was stepped from 0.229 V to 0.279 V (versus the formal potential of TEA^+ transfer) at t = 0 and maintained at the potential for 1.2 s. The circles represent Equation 5.S2.

Table S1. Parameters used in numerical simulations of cyclic voltammograms in Figure 5-1.

ionophore	r_g/a	θ_1°	θ_2°	γ	$D_C \times 10^6$ cm^2/s
1	1.1	4	12	0.33	1.3 ± 0.1
2	1.3	6	12	0.41	1.7 ± 0.2

Determination of Multiple Charges Carried by Arixtra

A charge of z carried by each Arixtra molecule across the interface is determined from a steady-state limiting current, $i_{d,A}$, controlled by Arixtra diffusion in the outer aqueous phase at an organic-filled pipet as given by

$$i_{d,A} = 4xzFD_A c_A a \quad \text{(S1)}$$

where x is a function of r_g/a,[S2] and c_A is an aqueous Arixtra concentration. Numerical simulations described above gave x values of 1.3 and 1.2 for pipets with typical r_g/a values of 1.1 and 1.3, respectively. A D_A value of (3.9 ± 0.3) × 10^{-6} cm^2/s was determined from chronoamperometric responses with ionophore **2** (Figure 5-S1). In the chronomaperometry experiments, an interfacial potential was stepped at t = 0 such that Arixtra extraction was driven to a diffusion limitation. A resulting time-dependent current response, $i_{d,A}(t)$, decays to a steady-state current, $i_{d,A}$, as expressed for a micropipet with r_g/a = 1.1 by[S3]

$$\frac{i_{d,A}(t)}{i_{d,A}} = 0.6533 + 0.3384\frac{a}{\sqrt{D_A t}} + 0.3467\exp\left(-0.4384\frac{a}{\sqrt{D_A t}}\right) \quad \text{(S2)}$$

A chronoamperometric response with ionophore **2** fits well with Equation 5.5 (Figure 5-S1), thereby yielding the D_A value.

Deprotonation of Ionophore 4 at pH 7.1

A large current response based on deprotonation of ionophore **4** was dominant at an organic-filled pipet in contact with an Arixtra solution at pH 7.1 (Figure 5-S2). A peak-shaped forward wave in this CV response corresponds to egress proton transfer, where ionophore **4** diffuses

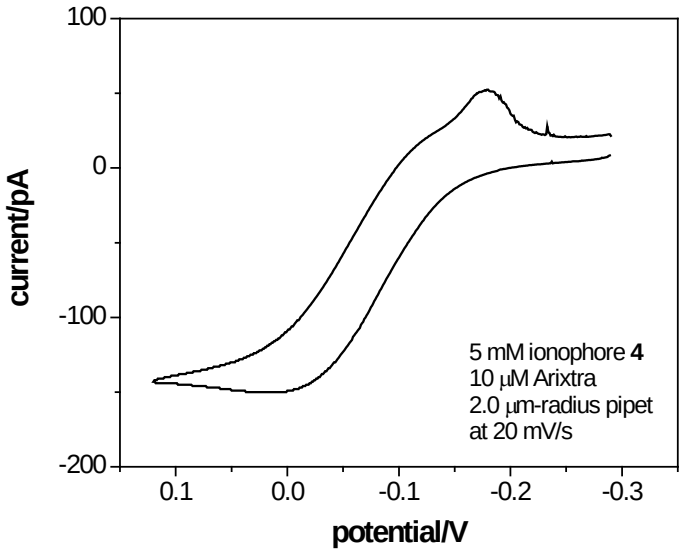

Figure 5-S2. A CV with Arixtra in 0.1 M Tris/acetate acid at pH 7.1 as obtained using a pipet (r_g/a = 1.3) filled with a nitrobenzene solution of ionophore **4**. A dialyzed sample was used to prepare the Arixtra solution. The potential is not defined with respect to the formal potential of TEA^+ transfer.

linearly in the inner nitrobenzene phase to be deprotonated at the interface as represented by the forward process in Equation 5.5. Some of ionophore **4** molecules that diffuse to the interface form Arixtra complexes, which are adsorbed at the interface as indicated by the small peak-shaped wave based on Arixtra desorption on the reverse potential sweep. Such a reverse peak was not observed without Arixtra in the aqueous phase. The major current response is not due to acetate transfer facilitated by ionophore **4**, because no acetate response was observed at pH 5 (Figure 5-3a).

Stoichiometry of Arixtra Complexes with Ionophores 4 and 5

The complexation stoichiometry, *s*, defined by Equation 5.1 was determined from limiting currents at water-filled pipets in contact with a nitrobenzene solution of ionophore **4** or **5** (Figure 5-s 3a or 4a, respectively).[S3,S4] The stoichiometry is related to the limiting current, $i_{d,LH}$, controlled by steady-state diffusion of ionophore in the outer nitrobenzene phase as given by

$$i_{d,LH} = 4x\left(\frac{z}{s}\right)FD_{LH}c_{LH}a \qquad \text{(S3)}$$

where D_{LH} and c_{LH} are a diffusion coefficient and a concentration of a protonated ionophore in the nitrobenzene phase, respectively. A *z* value was determined using an organic-filled pipet as described above. Diffusion coefficients of ionophores **4** and **5** were determined as follows.

Proton transfer facilitated by ionophore **4** was studied using a water-filled pipet to determine a diffusion coefficient of ionophore **4** (Figure 5-S3). Without Arixtra in an aqueous solution at pH 5, ingress proton transfer represented by the forward reaction of Equation 5.5 gave sigmoidal waves on the forward and reverse potential sweeps. The limiting current is controlled by steady-state diffusion of ionophore **4** in the outer nitrobenzene phase, thereby yielding

$$i_{d,LH} = 4xz_{LH}FD_{LH}c_{LH}a \qquad \text{(S4)}$$

where z_{LH} is a charge transferred by each ionophore molecule. The limiting currents correspond to a D_{LH} value of (2.0 ± 0.1) × 10^{-6} cm^2/s in Equation 5.S3 with a z_{LH} value of +1 based on proton transfer.

A micropipet filled with an Arixtra-free aqueous solution was also used to determine a diffusion coefficient of ionophore **5** (Figure 5-S4). The limiting current is controlled by steady-state diffusion of ionophore **5** in the outer nitrobenzene phase. The large peak current on the reverse potential sweep is due to desorption of ionophore **5**, which was transferred across the

interface on the forward potential sweep to be adsorbed at the aqueous side of the interface. The limiting currents correspond to $D_{LH} = (1.8 \pm 0.1) \times 10^{-6}$ cm^2/s in Equation 5.S4 with $z_{LH} = +1$, which represents an ionophore's charge. It should be noted that the CV response in Figure 5-S4 is much more reversible than a CV response based on Arixtra adsorption facilitated by ionophore **5** in Figure 5-4b.

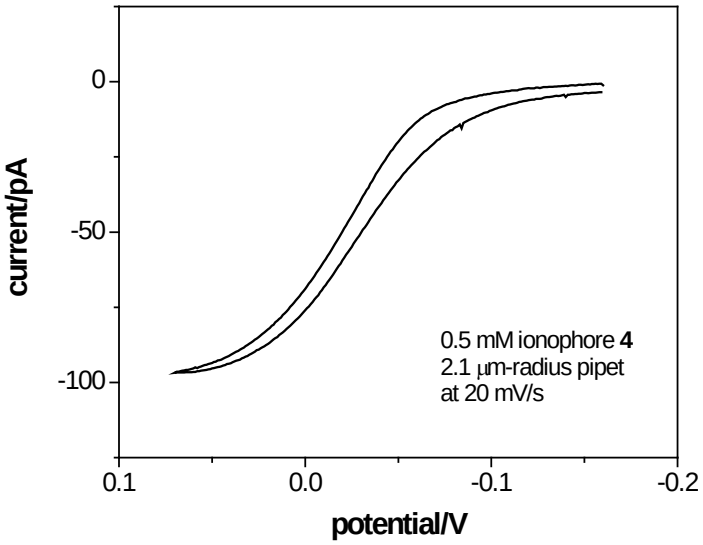

Figure 5-S3. A background-subtracted CV of proton transfer facilitated by ionophore **4** at a pipet ($r_g/a = 1.3$) filled with 0.1 M acetic acid/sodium acetate at pH 5.0. The potential is not defined with respect to the formal potential of TEA^+ transfer.

Failure in Stoichiometry Determination for Ionophores 1–3.

Complexation stoichiometry for ionophores **1**–**3** was not able to be determined using a water-filled pipet, because of weak Arixtra-binding capability of these ionophores. With weakly binding ionophores **1**–**3** in the outer nitrobenzene phase at a water-filled pipet, a current response based on facilitated Arixtra extraction or adsorption overlaps with a much larger current response based on transfer of excess Arixtra molecules, which is facilitated by an organic supporting

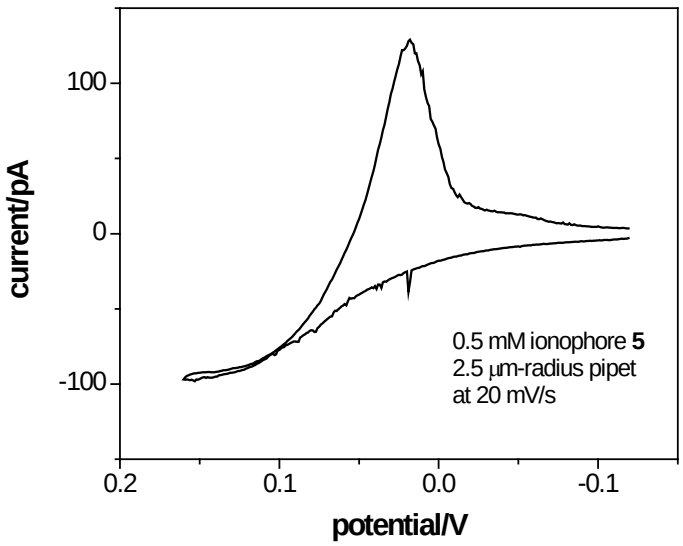

Figure 5-S4. A background-subtracted CV based on adsorption and desorption of ionophore **5** at a pipet filled with 0.1 M Tris/acetic acid at pH 7.1. A r_g/a value of 1.4 gives $4x = 4.7$ in Equation 5.S4. The potential is not defined with respect to the formal potential of TEA^+ transfer.

cation, TDDA. In fact, a CV response to Arixtra is obtained using a pipet filled with an ionophore-free nitrobenzene solution (Figure 5-S5), where $\Delta^{o}_{w}\phi_{1/2}$ and $\Delta^{o}_{w}\phi_{p}$ values are significantly more negative than those with any of the ionophores.

Overall, cyclic voltammetric observation of facilitated ion transfer at a water-filled pipet requires the formation of highly stable ion–ionophore complexes, which is satisfied not with ionophores **1**–**3** but with ionophores **4** and **5**. This requirement is less demanding in cyclic voltammetry with an organic-filled pipet, where Arixtra is depleted by complexation with ionophore in excess so that no free Arixtra is available at the interface for the formation of less stable complexes with TDDA.

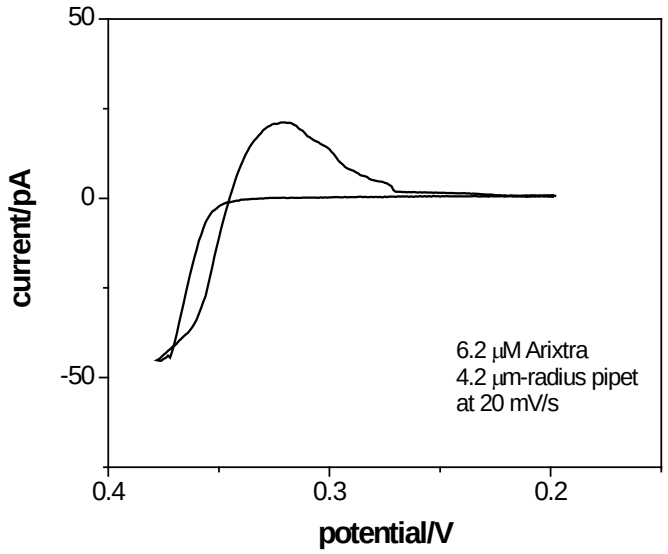

Figure 5-S5. A background-subtracted CV of Arixtra extraction at a pipet (r_g/a = 1.3) filled with an ionophore-free nitrobenzene solution in contact with a dialyzed Arixtra sample diluted with 0.1 M NaH_2PO_4/Na_2HPO_4 at pH 7.1. The potential is defined with respect to the formal potential of TEA^+ transfer.

Supporting Information References

(S1) Rodgers, P. J.; Amemiya, S. *Anal. Chem.* **2007**, *79*, 9276–9285.
(S2) Zoski, C. G.; Mirkin, M. V. *Anal. Chem.* **2002**, *74*, 1986–1992.
(S3) Yuan, Y.; Wang, L.; Amemiya, S. *Anal. Chem.* **2004**, *76*, 5570–5578.
(S4) Yuan, Y.; Amemiya, S. *Anal. Chem.* **2004**, *76*, 6877–6886

COMSOL Model

A copy of the COMSOL model is available free of charge in the Supporting Information via the Internet at http://pubs.acs.org/doi/suppl/10.1021/ja800568q.

REFERENCES

(1) Jelinek, R.; Kolusheva, S. *Chem. Rev.* **2004**, *104*, 5987–6016.

(2) (a) Linhardt, R. J. *J. Med. Chem.* **2003**, *46*, 2551–2564. (b) de Kort, M.; Buijsman, R. C.; van Boeckel, C. A. A. *Drug Disc. Today* **2005**, *10*, 769–779. (c) Day, J. R. S.; Landis, R. C.; Taylor, K. M. *J. Cardiothorac. Vasc. Anesth.* **2004**, *18*, 93–100. (d) Zacharski, L. R.; Ornstein, D. L. *Thromb. Haemostasis* **1998**, *80*, 10–23.

(3) (a) Meyerhoff, M. E.; Fu, B.; Bakker, E.; Yun, J.-H.; Yang, V. C. *Anal. Chem.* **1996**, *68*, 168A–175A. (b) Fu, B.; Bakker, E.; Yun, J. H.; Yang, V. C.; Meyerhoff, M. E. *Anal. Chem.* **1994**, *66*, 2250–2259. (c) Fu, B.; Bakker, E.; Yang, V. C.; Meyerhoff, M. E. *Macromolecules* **1995**, *28*, 5834–5840. (d) Ma, S. C.; Yang, V. C.; Fu, B.; Meyerhoff, M. E. *Anal. Chem.* **1993**, *65*, 2078–2084.

(4) (a) van Arman, S. A.; Czarnik, A. W. *J. Am. Chem. Soc.* **1990**, *112*, 5376–5377. (b) Zhong, Z. L.; Anslyn, E. V. *J. Am. Chem. Soc.* **2002**, *124*, 9014–9015. (c) Wright, A. T.; Zhong, Z. L.; Anslyn, E. V. *Angew. Chem., Int. Ed.* **2005**, *44*, 5679–5682. (d) Sun, W.; Bandmann, H.; Schrader, T. *Chem.—Eur. J.* **2007**, *13*, 7701–7707.

(5) Sauceda, J. C.; Duke, R. M.; Nitz, M. *ChemBioChem* **2007**, *8*, 391–394.

(6) (a) *Anion receptor chemistry* Sessler, J. L.; Gale, P. A.; Cho, W.-S., Eds.; Royal Society of Chemistry: Cambridge 2006. (b) Best, M. D.; Tobey, S. L.; Anslyn, E. V. *Coord. Chem. Rev.* **2003**, *240*, 3–15. (c) Schug, K. A.; Lindner, W. *Chem. Rev.* **2005**, *105*, 67–114.

(7) (a) Capila, I.; Linhardt, R. J. *Angew. Chem., Int. Ed.* **2002**, *41*, 390–412. (b) Linhardt, R. J.; Toida, T. *Acc. Chem. Res.* **2004**, *37*, 431–438.

(8) Milovic, N. M.; Behr, J. R.; Godin, M.; Hou, C. S. J.; Payer, K. R.; Chandrasekaran, A.; Russo, P. R.; Sasisekharan, R.; Manalis, S. R. *Proc. Natl. Acad. Sci. U.S.A.* **2006**, *103*, 13374–13379.

(9) (a) Guo, J.; Yuan, Y.; Amemiya, S. *Anal. Chem.* **2005**, *77*, 5711–5719. (b) Guo, J.; Amemiya, S. *Anal. Chem.* **2006**, *78*, 6893–6902.

(10) (a) Samec, Z.; Trojanek, A.; Langmaier, J.; Samcova, E. *Electrochem. Commun.* **2003**, *5*, 867–870. (b) Langmaier, J.; Olsak, J.; Samcova, E.; Samec, Z.; Trojanek, A. *Electroanalysis* **2006**, *18*, 115–120. (c) Langmaier, J.; Olsak, J.; Samcova, E.; Samec, Z.; Trojanek, A. *Electroanalysis* **2006**, *18*, 1329–1338.

(11) (a) Girault, H. H.; Schiffrin, D. J. In *Electroanalytical Chemistry*; Bard, A. J., Ed.; Marcel Dekker: New York, 1989; Vol. 15, p 1–141. (b) Kakiuchi, T. In *Liquid–Liquid Interfaces: Theory and Methods*; Volkov, A. G., Deamer, D. W., Eds.; CRC press: New York, 1996, p 1–18. (c) Samec, Z. *Pure Appl. Chem.* **2004**, *76*, 2147–2180.

(12) Ireland, I.; Rylance, P. B.; Kesteven, P. In *Heparin: Chemical and Biological Properties, Clinical Applications*; Lane, D. A., Lindahl, U., Eds.; CRC Press: Boca Raton, FL, 1989, p 549–574.

(13) Hirsh, J.; Raschke, R. *Chest* **2004**, *126*, 188S–203S.

(14) (a) Muslinkina, L.; Pretsch, E. *Electroanalysis* **2004**, *16*, 1569–1575.(b) Muslinkina, L.; Pretsch, E. *Chem. Commun.* **2004**, 1218–1219.
(15) Langmaier, J.; Samcová, E.; Samec, Z. *Anal. Chem.* **2007**, *79*, 2892–2900.
(16) (a) Petitou, M.; van Boeckel, C. A. A. *Angew. Chem., Int. Ed.* **2004**, *43*, 3118–3133. (b) van Boeckel, C. A. A.; Petitou, M. *Angew. Chem., Int. Ed.* **1993**, *32*, 1671–1818.
(17) (a) Depasse, F.; Gerotziafas, G. T.; Busson, J.; Van Dreden, P.; Samama, M. M. *J. Thromb. Haemostasis* **2004**, *2*, 346–348. (b) Klaeffling, C.; Piechottka, G.; Brevern, G. D. V.; Mosch, G.; Mani, H.; Luxembourg, B.; Lindhoff-Last, E. *Ther. Drug Monit.* **2006**, *28*, 375–381. (c) Nilsson, C. U.; Engstrom, M. *Blood Coagul. Fibrinolysis* **2007**, *18*, 619–622.
(18) (a) Taylor, G.; Girault, H. H. *J. Electroanal. Chem.* **1986**, *208*, 179–183. (b) Shao, Y.; Mirkin, M. V. *Anal. Chem.* **1998**, *70*, 3155–3161.
(19) (a) Amemiya, S.; Yang, X.; Wazenegger, T. L. *J. Am. Chem. Soc.* **2003**, *125*, 11832–11833. (b) Yuan, Y.; Wang, L.; Amemiya, S. *Anal. Chem.* **2004**, *76*, 5570–5578. (c) Yuan, Y.; Amemiya, S. *Anal. Chem.* **2004**, *76*, 6877–6886. (d) Rodgers, P. J.; Amemiya, S. *Anal. Chem.* **2007**, *79*, 9276–9285.
(20) Johnson, D. J. D.; Li, W.; Adams, T. E.; Huntington, J. A. *EMBO J.* **2006**, *25*, 2029–2037.
(21) Oishi, Y.; Torii, Y.; Kato, T.; Kuramori, M.; Suehiro, K.; Ariga, K.; Taguchi, K.; Kamino, A.; Koyano, H.; Kunitake, T. *Langmuir* **1997**, *13*, 519–524.
(22) Samec, Z.; Homolka, D.; Marecek, V. *J. Electroanal. Chem.* **1982**, *135*, 265–283.
(23) Flanagan, J. B.; Margel, S.; Bard, A. J.; Anson, F. C. *J. Am. Chem. Soc.* **1978**, *100*, 4248–4253.
(24) Samec, Z. *Electrochim. Acta* **1998**, *44*, 85–90.
(25) Marcus, R. A. *J. Chem. Phys.* **2000**, *113*, 1618–1629
(26) Kontturi, A. K.; Kontturi, K.; Murtomaki, L.; Schiffrin, D. J. *Acta Chem. Scand.* **1992**, *46*, 47–53.
(27) Horrocks, B. R.; Mirkin, M. V. *Anal. Chem.* **1998**, *70*, 4653–4660.
(28) Osakai, T.; Komatsu, H.; Goto, M. *J. Phys.: Condens. Matter* **2007**, *19*, 375103.
(29) Hayessen, R.; Mirsky, V. M.; Heckmann, K. D. *Sens. Actuators, B* **1996**, *32*, 215–220.
(30) Wegmann, D.; Weiss, H.; Ammann, D.; Morf, W. E.; Pretsch, E.; Sugahara, K.; Simon, W. *Mikrochim. Acta* **1984**, *3*, 1–16.
(31) (a) Rensing, S.; Arendt, M.; Springer, A.; Grawe, T.; Schrader, T. *J. Org. Chem.* **2001**, *66*, 5814–5821. (b) Zadmard, R.; Schrader, T. *J. Am. Chem. Soc.* **2005**, *127*, 904–915.
(32) Maeda, K.; Yoshida, Y.; Goto, T.; Marecek, V. *J. Electroanal. Chem.* **2004**, *567*, 317–323
(33) Shvarev, A.; Bakker, E. *Anal. Chem.* **2005**, *77*, 5221–5228.
(34) Volkov, A. G. *Liquid Interfaces in Chemistry and Biology*; Wiley: New York, 1998.

6.0 HIGH LIPOPHILICTY OF PERFLUOROALKYL CARBOXYLATE AND SULFONATE: IMPLICATIONS FOR THEIR MEMBRANE PERMEABILITY

This work has been published as Ping Jing, Patrick J. Rodgers, and Shigeru Amemiya. *J. Am. Chem. Soc.* **2009**, *131*, 2290–2296.

6.1 ABSTRACT

Here we report on remarkably high lipophilicity of perfluoroalkyl carboxylate and sulfonate. A lipophilic nature of this emerging class of organic pollutants has been hypothesized as an origin of their bioaccumulation and toxicity. Both carboxylate and sulfonate, however, are considered hydrophilic while perfluroalkyl groups are not only hydrophobic but also oleophobic. Partition coefficients of a homologous series of perfluoroalkyl and alkyl carboxylates between water and *n*-octanol were determined as a measure of their lipophilicity by ion-transfer cyclic voltammetry. Very similar lipophilicity of perfluoroalkyl and alkyl chains with the same length is demonstrated experimentally for the first time by fragment analysis of the partition coefficients. This finding is important for pharmaceutical and biomedical applications of perfluoroalkyl compounds. Interestingly, ~2 orders of magnitude higher lipophilicity of a perfluoroalkyl carboxylate or sulfonate in comparison to its alkyl counterpart is ascribed nearly exclusively to their oxoanion groups. The higher lipophilicity originates from a strong electron-

withdrawing effect of the perfluoroalkyl group on the adjacent oxoanion group, which is weakly hydrated to decrease its hydrophilicity. In fact, the inductive effect is dramatically reduced for a fluorotelomer with an ethylene spacer between perfluorohexyl and carboxylate groups, which is only as lipophilic as its alkyl counterpart, nonanoate, and is 400 times less lipophilic than perfluorononanoate. The high lipophilicity of perfluoroalkyl carboxylate and sulfonate implies that their permeation across such a thin lipophilic membrane as a bilayer lipid membrane is limited by their transfer at a membrane/water interface. The limiting permeability is lower and less dependent on their lipophilicity than the permeability controlled by their diffusion in the membrane interior as assumed in the classical solubility-diffusion model.

6.2 INTRODUCTION

Widespread accumulation of perfluoroalkyl acids such as perfluoroalkyl carboxylic and sulfonic acids in wildlife and humans is an emerging environmental problem worldwide.[1] These synthetic acids with a perfluorinated alkyl group are chemically stable, resistive to biodegradation, and persistent in the environment.[2] More recently, their adverse health effects such as developmental toxicity, immunotoxicity, hepatotoxicity, and carcinogenicity were reported.[3] The bioaccumulation and toxicity of the perfluoroalkyl acids suggest their high lipophilicity. In fact, perfluorooctyl carboxylic and sulfonic acids were detected in umbilical cord blood and brain, indicating that they are lipophilic enough to cross the placental and blood–brain barriers, respectively.[4] Recent in vitro toxicology studies also show that the perfluoroalkyl acids not only interact with cell membranes but also cross the membranes to inhibit intracellular events, cause oxidative stress, and induce apoptosis.[5] Lipophilicity of perfluoroalkyl acids, however, is not

well understood. On one hand, these acids are dissociated under most aqueous environments to carry a net negative charge to enhance their hydrophilicity.[6] This strong acidity is due to an electron-withdrawing effect of the perfluoroalkyl group on the adjacent acid group. On the other hand, a perfluoroalkyl group is considered not only hydrophobic, but also oleophobic.[7] More quantitative understanding of the lipophilicity of perfluoroalkyl groups is significant beyond environmental sciences because perfluoroalkyl compounds have found a wide range of applications as drugs,[8] vehicles for drug and oxygen delivery,[9] and tags for high-throughput synthesis, separation, and identification of biological and organic molecules based on their two-phase partitioning.[7, 10]

Lipophilicity of an organic molecule is a key physicochemical property for assessment of its environmental and human-health risks[11] as well as for its pharmaceutical and biomedical applications.[8, 9, 12] A more lipophilic molecule is more permeable across a biological membrane as governed qualitatively by the so-called Overton rule.[13] Quantitatively, the solubility-diffusion model relates a membrane permeability, P_m, of a molecule to its partition coefficient, P, between the aqueous and membrane phases as a measure of its lipophilicity, thereby yielding[13]

$$P_m = \frac{D_m P}{d}$$

Equation 6.1

where the partition coefficient represents the membrane concentration of the molecule with respect to its aqueous concentration, D_m is the diffusion coefficient of the molecule in the membrane, and d is the membrane thickness. In practice, a partition coefficient of an electrically neutral molecule is measured experimentally by using water and a water-immiscible organic solvent,[14] most typically *n*-octanol,[15] as a model of a bilayer lipid membrane (BLM). So far,

partition coefficients of perfluoroalkyl carboxylic acids between *n*-octanol and water have been estimated empirically and theoretically without experimental assessment.[16] No partition coefficient of a perfluoroalkyl carboxylate or sulfonate has been reported although perfluorooctyl carboxylate and sulfonate partition favorably from water into an organic solvent. The perfluorooctyl oxoanions can be extracted from biological matrices into methyl *tert*-butyl ether as tetrabutylammonium salts for subsequent mass spectrometric detection.[17] Selective partition of the perfluorooctyl species against chloride from water into lipophilic polymer membranes or a fluorous solvent was also demonstrated by potentiometry.[18]

Partition coefficients of nonfluorinated alkyl oxoanions between water and various organic solvents[19] including *n*-octanol[19k] were measured by ion-transfer voltammetry. With this approach, an external potential is applied to a liquid/liquid interface to drive interfacial transfer of an ion, which is monitored as a flow of an ionic current. In contrast to a neutral molecule, a partition coefficient of an ion depends on the Galvani potential difference between the aqueous and organic phases, $\Delta^{o}_{w}\phi$, as given by[20]

$$\log P = -\frac{z_i F(\Delta^{o}_{w}\phi - \Delta^{o}_{w}\phi^{0'})}{2.303RT}$$

Equation 6.2

where z_i is the charge of the ion, and $\Delta^{o}_{w}\phi^{0'}$ is a formal ion-transfer potential as measured voltammetrically. This potential-dependence of ion partition was considered in recent models for ion permeation across a lipophilic liquid membrane sandwiched between two aqueous electrolyte solutions by Kihara and co-workers[21] and others,[22] thereby extending the original solubility-diffusion model. It is assumed in both original and new models that overall ion permeability of a membrane is limited by ion translocation in the interior of the membrane rather than by ion

transfer at the membrane/water interface while Murtomäki and co-workers considered kinetic effects of interfacial ion transfer on membrane permeability.[22d]

Here we report on remarkably higher lipophilicity of perfluoroalkyl carboxylate and sulfonate in comparison to their alkyl counterparts. Partition coefficients of various carboxylates and sulfonates with a fully-, non-, or partially fluorinated alkyl chain (Figure 6-1) between *n*-octanol and water are determined systematically by ion-transfer cyclic voltammetry to identify a main origin of 2 orders of magnitude different lipophilicities of perfluoroalkyl and alkyl oxoanions with the same chain length. Also, this study is the first to experimentally quantify lipophilicity of perfluoroalkyl chains with different lengths, which is required for estimating lipophilicity of perfluoroalkyl compounds with environmental, biomedical, or pharmaceutical importance. In addition, kinetic parameters as obtained from a transient cyclic voltammogram at micrometer-sized interfaces[23] enabled us to model permeability of a lipophilic membrane to the perfluoroalkyl oxoanions without the constraint of rapid partition equilibrium at the membrane/water interface.

6.3 EXPERIMENTAL

6.3.1 Chemicals

All perfluoroalkyl and alkyl carboxylic acids, sodium octyl sulfonate, tetradodecylammonium (TDDA) bromide, sodium tetraphenylborate (TPB), tetraphenylarsonium (TPA) chloride, and *n*-octanol (>99%) were obtained from Aldrich (Milwaukee, WI). Potassium perfluorooctyl sulfonate was obtained from Synquest Laboratories (Alachua, FL). Potassium

tetrakis(pentafluorophenyl)borate (TFAB) was from Boulder Scientific Company (Mead, CO). All reagents were used as received. Preparation of various salts employed for electrochemical measurements is described in Supporting Information. All aqueous solutions were prepared with 18.3 MΩ cm^{-1} deionized water (Nanopure, Barnstead, Dubuque, IA).

6.3.2 Electrochemical Measurements

A computer-controlled CHI 660B electrochemical workstation equipped with CHI 200 picoampere booster and Faraday cage (CH instruments, Austin, TX) was used for CV measurements with the following electrochemical cell

Ag | AgCl | 3 M NaCl | 1 mM $MgSO_4$ in water || 10 μM carboxylate or sulfonate **1**–**5** and 1 mM $MgSO_4$ in water | 40 mM TDDATFAB in *n*-octanol | Ag

An Ohmic potential drop in the *n*-octanol phase was maintained negligibly low in the presence of TDDATFAB as an organic supporting electrolyte, which is highly soluble in *n*-octanol in contrast to other organic supporting electrolyte salts.[19k, 24] A $Mg(OH)_2$ solution was used to adjust the aqueous pH at 6–7 so that the carboxylates and sulfonates are present as monoanions in either *n*-octanol or water phase.[19d]

A micrometer-sized interface was formed at the tip of a glass micropipet filled with a *n*-octanol solution.[25] An inner-wall silanized micropipet was fabricated and characterized as reported elsewhere.[23] The inner diameters of the tips were 3.5–10 μm while the outer diameter was 1.3 times larger than the inner diameter. Estimated tip inner angles were 3–6° while an outer tip angle was 12°. A double junction Ag/AgCl electrode (BASi, West Lafayette, IN) was used as

a reference/counter electrode. The potential of the *n*-octanol phase with respect to the aqueous phase was calibrated by employing tetrabutylammonium as a reference ion and defined on the basis of the nonthermodynamic hypothesis, i.e., TPA-TPB assumption (see Supporting Information).[20, 26] A current carried by a negative charge from the aqueous phase to the organic phase was defined to be negative. Supplemental thermodynamic data were obtained by potentiometry (see Supporting Information), which is less limited by a narrow potential window at the *n*-octanol/water interface and a high resistance of a *n*-octanol solution with a low supporting electrolyte concentration. All electrochemical experiments were performed at 22 ± 3 °C.

1. $CF_3(CF_2)_{n-2}CO_2^-$ (n = 4–10)
2. $CH_3(CH_2)_{n-2}CO_2^-$ (n = 7–12)
3. $CF_3(CF_2)_7SO_3^-$
4. $CH_3(CH_2)_7SO_3^-$
5. $CF_3(CF_2)_5(CH_2)_2COO^-$

Figure 6-1. Molecular formula of oxoanionic surfactants studied in this work.

6.4 RESULTS AND DISCUSSION

6.4.1 Lipophilicity of Perfluoroalkyl and Alkyl Oxoanions

Lipophilicity of oxoanions **1**−**5** with various chains (Figure 6-1) was investigated by employing cyclic voltammetry at *n*-octanol/water microinterfaces formed at the tip of a glass micropipet electrode.[25] During a potential cycle, an oxoanionic surfactant, which was initially present only in the outer aqueous phase, was transferred across the interface between the two bulk liquid phases. The simple transfer of an ion, i^{z}_{i}, is defined as

$$i^{z_i} \text{ (outer aqueous phase)} \rightleftharpoons i^{z_i} \text{ (inner } n\text{-octanol phase)}$$

Equation 6.3

All surfactants **1**−**5** give well-defined CVs without a voltammetric feature of their adsorption or emulsification or instability of the interfaces.[19g, 19i, 27] In a typical CV as obtained with perfluorohexanoate (Figure 6-2A), a sigmoidal anodic wave corresponds to ingress transfer of the carboxylate coupled with its nonlinear diffusion from the outer aqueous phase to the micrometer-sized interface. The transfer of the carboxylate into the bulk *n*-octanol phase was confirmed by the broad cathodic peak, indicating transient diffusion of the carboxylate from the inner *n*-octanol phase to the interface. A CV with a similar feature was also obtained with nonanoate, which requires more positive potentials (Figure 6-2B). This result indicates that nonanoate with a longer chain is less lipophilic than perfluorohexanoate.

Partition coefficients of surfactants **1**−**5** between aqueous and *n*-octanol phases were determined by numerical analysis of their CVs. Figure 6-2A and Figure 6-2B exemplify that experimental CVs fit very well with quasi-reversible CVs simulated for simple, one-step ion

transfer (Equation 3.3; see Supporting Information).[23] A value of $\Delta^{o}_{w}\phi^{0'}$ for an oxoanion thus obtained from a CV corresponds to its formal partition coefficient, $P^{0'}$, as given by[28]

$$\log P^{0'} = \frac{z_i F \Delta^{o}_{w}\phi^{0'}}{2.303RT}$$

Equation 6.4

where $\Delta^{o}_{w}\phi^{0'}$ is standardized on the basis of the nonthermodynamic TPA-TPB assumption (see Supporting Information).[20,26] The values of $\Delta^{o}_{w}\phi^{0'} = -41 \pm 6$ and -4 ± 4 mV for perfluorohexanoate and nonanoate, respectively, in Figure 6-2 correspond to the values of $\log P^{0'} = 0.7 \pm 0.1$ and 0.07 ± 0.07, respectively, in Equation 6.4, indicating that perfluorohexanoate is 4 times more lipophilic than nonanoate. A ~100 mV anodic shift of a half-wave potential with respect to $\Delta^{o}_{w}\phi^{0'}$ (Figure 6-2) is mainly due to asymmetric diffusion in the inner and outer solutions at a micropipet electrode, which contrasts to conventional steady-state voltammetry at a solid ultramicroelectrode.[23] Diffusion of the carboxylates is more efficient in the outer aqueous phase than in the inner *n*-octanol phase, which is not only more viscous (see Supporting Information) but also surrounded by the pipet wall. The anodic shift is partially due to a kinetic limitation in the CVs, which significantly deviate from a nernstian behavior (Figure 6-2).

Higher lipophilicity of perfluoroalkyl carboxylates **1** in comparison to alkyl carboxylates **2** was systematically confirmed by using $\log P^{0'}$ (Figure 6-3). Plots of $\log P^{0'}$ versus the number of carbon atoms, *n*, demonstrate that a perfluoroalkyl carboxylate is ~2 orders of magnitude more lipophilic than the alkyl carboxylate with the same value of *n*. The higher

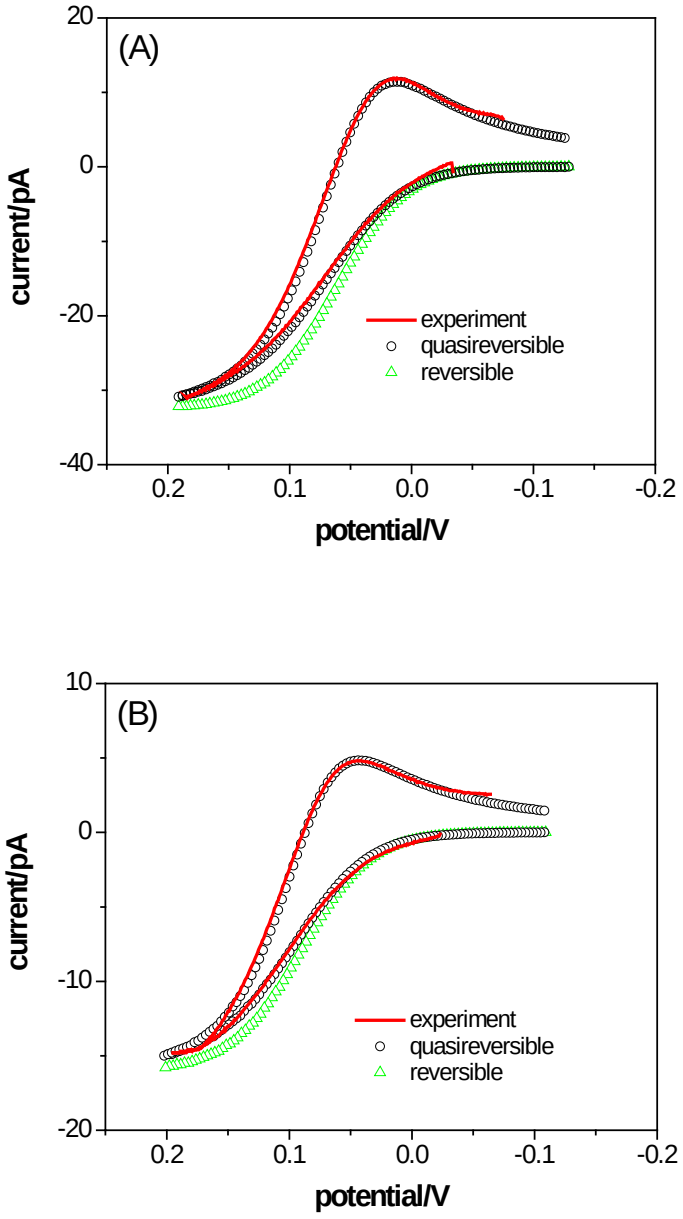

Figure 6-2. Background-subtracted CVs of (A) perfluorohexanoate and (B) nonanoate at *n*-octanol/water microinterfaces formed at the tip of glass micropipets with diameters of 10 and 6.8 µm, respectively.

lipophilicity of perfluoroalkyl carboxylates is remarkable. A perfluoroalkyl carboxylate with a net negative charge is only ~15 times less lipophilic than the electrically neutral, alkyl carboxylic acid with the same carbon number[29] (n = 4–10 in Figure 6-3), which is ~2.5 × 10^3 times more lipophilic than the corresponding alkyl carboxylate (n = 7–12). Moreover, perfluorodecanoate (log $P^{0'}$ = 2.9 ± 0.1) is as lipophilic as TPB (log $P^{0'}$ = 2.89 ± 0.07), where the central ionic entity is effectively shielded by the four phenyl groups. Importantly, the larger $P^{0'}$ for perfluoroalkyl carboxylates in comparison to alkyl carboxylates is not due to stronger ion pairing of the perfluoroalkyl carboxylates with the bulky organic cation, TDDA, in the *n*-octanol phase. A difference in log$P^{0'}$ for perfluoroalkyl and alkyl carboxylates is independent of the concentration of the organic cation as demonstrated by potentiometry (see Supporting Information).

Perfluorooctyl sulfonate **3**, which is another major environmental contaminant, is also ~2 orders of magnitude more lipophilic than octyl sulfonate **4**. CVs of the respective sulfonates with an octyl group give log $P^{0'}$ = 2.45 ± 0.08 and 0.6 ± 0.1. Perfluorooctyl sulfonate is nearly as lipophilic as perfluorononanoate with the same perfluorooctyl group (log $P^{0'}$ = 2.57 ± 0.07) while octyl sulfonate is three times more lipophilic than nonanoate. The latter result is consistent with the previous observation that an alkyl sulfonate with a larger ionic radius is more lipophilic than the carboxylate with the same alkyl group at water/1,2-dichloroethane or nitrobenzene interfaces.[19a]

6.4.2 The Origin of Higher Lipophilicity of Perfluoroalkyl Oxoanions

The higher lipophilicity of perfluoroalkyl carboxylates in comparison to the corresponding alkyl carboxylates was assessed by using a fragment method[15] to identify its origin. A plot of

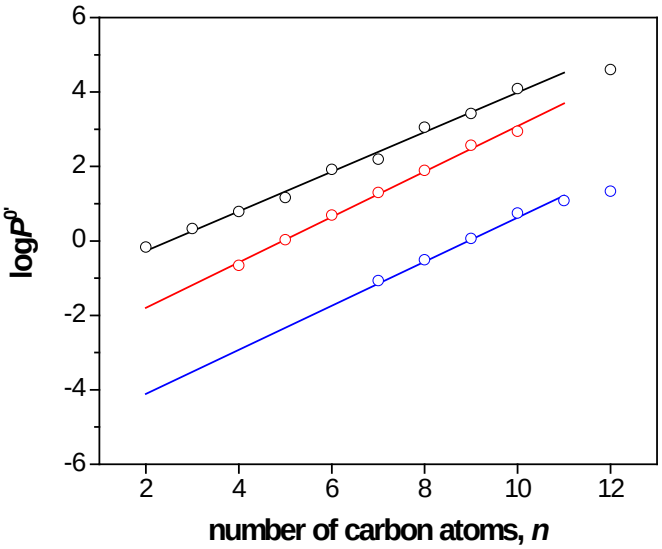

Figure 6-3. Plots of the formal partition coefficient, $P^{0'}$, versus the number of carbon atoms for perfluoroalkyl carboxylates 1 (red circles), alkyl carboxylates 2 (blue circles), and alkyl carboxylic acids (black circles). The value of $P^{0'}$ for perfluorodecanoate was determined by potentiometry (see Supporting Information). The values of $P^{0'}$ for the acids correspond to partition coefficients reported in literatures.[26] The solid lines represent Equation 6.5.

log $P^{0'}$ versus n is linear for perfluoroalkyl or alkyl carboxylates or alkyl carboxylic acids[30] except dodecanoate and dodecanoic acid[19h] (Figure 6-3), thereby yielding

$$\log P^{0'} = (n - 2)f(CX_2) + f(CX_3) + f(COY)$$

Equation 6.5

where f is a fragmental contribution of each unit to the total log $P^{0'}$, X = H or F, and Y = O^- or OH. The slope of the linear plots corresponds to $f(CX_2)$ while the sum of $f(CX_3)$ and f(COY) is equivalent to log $P^{0'}$ extrapolated to n = 2. This analysis clearly demonstrates that the ~2 orders of magnitude higher lipophilicity of perfluoroalkyl carboxylates is ascribed to the difference between $f(CF_3) + f(COO^-)$ and $f(CH_3) + f(COO^-)$, which are equal to −1.9 and −4.1, respectively. On the other hand, a perfluoroalkyl chain is as lipophilic as the alkyl chain with the same length. A value of $f(CF_2)$ = 0.61 is very close to values of $f(CH_2)$ = 0.59 and 0.53 as obtained for alkyl carboxylates and carboxylic acids, respectively. This result suggests that $f(CF_3)$ and $f(CH_3)$ are also very similar, which is confirmed in the following. Overall, the different lipophilicities of perfluoroalkyl and alkyl carboxylates are mainly ascribed to the carboxylate groups.

We hypothesize that the higher lipophilicity of a carboxylate group attached to a perfluoroalkyl group is due to a strong electron-withdrawing effect of the perfluoroalkyl group on the oxoanion group. The oxoanion group with a reduced net negative charge is weakly hydrated to be partitioned favorably into a lipophilic *n*-octanol phase although water-saturated *n*-octanol contains a large mole fraction of water.[15] To test this hypothesis, we examined lipophilicity of fluorotelomer **5**. The ethylene spacer between the perfluorohexyl and carboxylate groups dramatically reduces the electron-withdrawing effect on acidity of perfluorohexanoic acid

to raise pK_a by 2.32 units in 50% aqueous ethanol although a hexyl spacer is required for further increasing pK_a by 1.14 units to eliminate this inductive effect.[30] In fact, our hypothesis was confirmed by much lower lipophilicity of fluorotelomer **5** (log $P^{0'} = -0.05 \pm 0.07$), which is 4.0×10^2 times lower than perfluorononanoate with the same number of carbon atoms. Moreover, the value of log $P^{0'}$ for fluorotelomer **5** is nearly identical to the value for nonanoate. Apparently, the substitution of hydrogen atoms with fluorine atoms in an alkyl group does not affect lipophilicity of the alkyl group. Thus, the different lipophilicities of perfluorooctyl and octyl sulfonates are also ascribed to the sulfonate groups.

6.4.3 Lipophilicity of Perfluoroalkyl Chains

This work is the first to systematically determine an experimental $f(CF_2)$ value between *n*-octanol and water phases. This unique opportunity is given by the carboxylate group, which not only solubilizes relatively long perfluoroalkyl chains in water but also serves as a probe to monitor their partitioning processes by ion-transfer voltammetry.

Our value of $f(CF_2) = 0.61$ is equivalent to a difference in free energy of −0.83 kcal/mol, which is close to the free energy of transfer of a CF_2 group from water to a micelle environment[31] or sediments[32] (−0.95 and −0.75 kcal/mol, respectively). We also compare our value of $f(CF_2)$ with the values that are estimated empirically or theoretically for perfluoroalkyl carboxylic acids between *n*-octanol and water. Figure 6-4 shows logarithmic plots of empirical and theoretical partition coefficients[16] versus *n* together with the corresponding plot for perfluoroalkyl carboxylates as obtained experimentally in this work. Our value is relatively close to a value of $f(CF_2) = 0.50$ as calculated with COSMOtherm C2.1 based on density functional

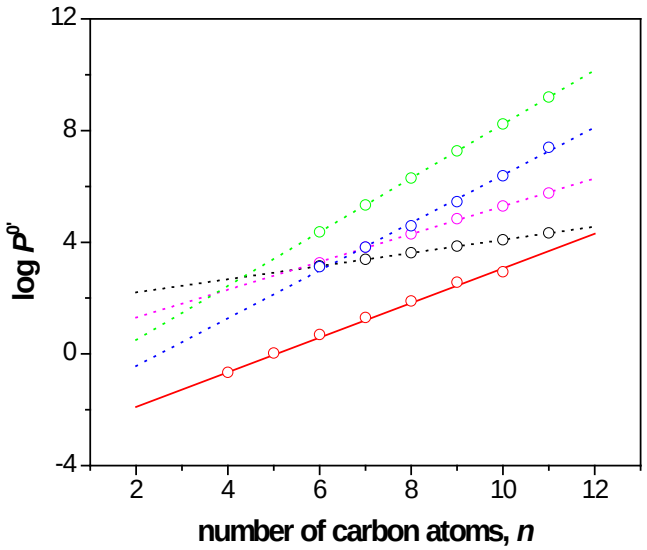

Figure 6-4. Plots of the formal partition coefficient, $P^{0'}$, versus tshe number of carbon atoms for perfluoroalkyl carboxylate 1 (red circles), and perfluoroalkyl carboxylic acids. The values of $P^{0'}$ for the acids correspond to partition coefficients estimated empirically by U.S. EPA's EPI suite and ClogP (green and black circles, respectively) and theoretically by COSMOtherm C2.1 and SPARC (purple and blue circles, respectively).[12] The solid lines represent Equation 6.5.

quantum calculation while a larger value of 0.80 was obtained using the SPARC solvation model. Two common programs based on empirical fragment methods, i.e., the U.S. EPA's EPI suite and ClogP, give much larger or smaller values of 0.90, and 0.20, respectively. This result casts doubt on reliability of the original partition coefficients used in these programs. Moreover, a negative $f(CF_2)$ value −0.097 has been reported for calculation of drug lipophlicity,[12] indicating significance of our experimental assessment of the fragmental partition coefficient.

It should be noted that the similar lipophilicity of perfluoroalkyl and alkyl chains results from the convolution of their different properties. A C−F bond is much more polar than a C−H bond, while a trifluoromethyl group is at least as isosteric as an isopropyl group.[33] Also, a perfluoroalkyl chain is harder and less flexible and changes from a linear to a helical structure as chain length increases.[34]

6.4.4 Permeability of a Thin Lipophilic Membrane to Perfluoroalkyl Oxoanion Species.

A noticeable finding in this work is the very high lipophilicity of oxoanion groups of the perfluoroalkyl surfactants. The high lipophilicity is important in permeation of the perfluoroalkyl oxoanions across a BLM with a lipophilic inner environment. Permeability of such thin lipophilic membranes to the perfluoroalkyl oxoanions was assessed by considering a thin *n*-octanol layer sandwiched between two aqueous phases as a model of a BLM (Figure 6-5).[21, 22] For simplification, identical and constant potentials at both *n*-octanol/water interfaces, $\Delta_w^o\phi$, were assumed, thereby resulting in no potential difference between the two aqueous phases. Heterogeneous rate constants, k_f and k_b, are defined for the forward and backward transfers of an

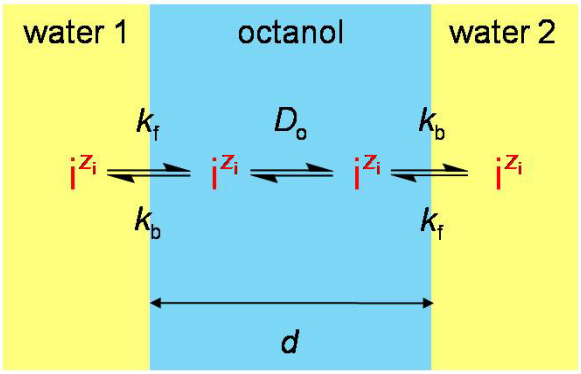

Figure 6-5. Scheme of a thin *n*-octanol layer sandwiched between two aqueous electrolyte solutions.

ion at the *n*-octanol/water interfaces (Equation 6.3) by employing a Butler−Volmer-type model as[20, 23a, 35]

$$k_f = k^0 P^{\alpha}$$

Equation 6.6

$$k_b = k^0 P^{\alpha-1}$$

Equation 6.7

where k^0 is the standard ion-transfer rate constant, and α is the transfer coefficient. These kinetic parameters as well as diffusion coefficients in n-octanol, D_o, were obtained from CVs of perfluoroalkyl and alkyl oxoanions at n-octanol/water microinterfaces (Table 6-S1, Supporting Information).

Permeability of this symmetric membrane is given by (see Supporting Information)

$$P_{\mathrm{m}} = \frac{k_{\mathrm{f}}}{2 + k_{\mathrm{b}} d / D_{\mathrm{o}}}$$

Equation 6.8

Equation 6.8 indicates that as a membrane becomes thinner, its permeability increases toward a limiting value as given by

$$P_{\mathrm{m}}^{\mathrm{lim}} = \frac{k^0 P^{\alpha}}{2}$$

Equation 6.9

This limiting permeability is independent of a membrane thickness and is equivalent to $k_f/2$. This result indicates that permeability of such a thin membrane is limited by interfacial ion transfer rather than by ion diffusion in the interior of the membrane as assumed in the solubility-diffusion model (Equation 6.1). Equation 6.8 is equivalent to Equation 6.1 only when a membrane is thick enough to satisfy $2 << k_b d/D_o$.

Equation 6.8 predicts that membrane permeability to a more lipophilic ion is more amenable to the interfacial transfer control. For instance, the interfacial control is dominant at a thicker membrane for a more lipophilic anion with negative $\Delta_w^o \phi^{0'}$, where smaller k_b results in $k_b d/D_o << 2$ in Equation 6.8 even at positive potentials. In other words, a more lipophilic ion, which is more favorably transferred into a lipophilic membrane, prefers staying in the membrane to being transferred from the membrane phase to the aqueous phase, thereby reaching the interfacial transfer control. This prediction was quantitatively evaluated by using a characteristic membrane thickness, $d_{1/2}$, as given by

$$d_{1/2} = \frac{2D_o}{k^0 P^{\alpha-1}}$$

Equation 6.10

A membrane with this thickness gives a half of the limiting permeability, P_m^{lim} (see Equation 6.8). The characteristic membrane thickness calculated using parameters obtained from CVs is larger for a perfluoroalkyl carboxylate than for the alkyl carboxylate with the same chain length (Figure 6-6A), corresponding to different lipophilicities. The calculated thickness strongly depends on the interfacial potential, $\Delta_w^o\phi$, as shown in the range between −171 and +171 mV, which are equal to $\Delta_w^o\phi^{0'}$ for TPB and TPA, respectively. Moreover, Equation 6.10 indicates that an ion with larger k^0 requires a thinner membrane for limiting permeability. The values of k^0 = 0.1−0.01 cm/s as obtained for carboxylates **1** and **2** are relatively large although larger k^0 values of ~1 cm/s[35b, 35c] have been reported for facilitated transfer of alkaline cations at 1,2-dichloroethane/water interfaces. Nevertheless, the characteristic membrane thickness as obtained in the potential range of ±171 mV predicts that a micrometer- or nanometer-thick *n*-octanol membrane is thin enough to give in the limiting permeability to the perfluoroalkyl carboxylates with high lipophilicity.

An important prediction of Equation 6.9 is the weak dependence of limiting permeability on ion lipophilicity. With α = 0.5 in Equation 6.9, the permeability under interfacial transfer control depends only on the square root of a partition coefficient in contrast to the direct proportionality under membrane diffusion control (Equation 6.1). The limiting permeability calculated using Equation 6.9 with experimentally determined parameters confirms the weaker lipophilicity dependence (Figure 6-6B). The limiting permeability at $\Delta_w^o\phi$ = 0 mV varies only

from 0.006 to 0.1 cm/s for all perfluoroalkyl and alkyl carboxylates while their $P^{0'}$ values vary by 4 orders of magnitude. In contrast, diffusion-controlled permeability (Equation 6.1) depends on ion lipophilicity much more strongly and subsequently varies in a wider range by 4 orders of magnitude (Figure 6-S3, Supporting Information).

An application of Equation 6.8 and Equation 6.9 to a BLM implies that permeability of this ultrathin lipophilic membrane to a highly lipophilic perfluoroalkyl oxoanion is limited by its interfacial transfer. In fact, this implication is supported by a classical model that was proposed to explain experimental permeability of a BLM to highly lipophilic ions such as tetraphenyl borate,[36] which is as lipophilic as perfluorodecanoate. Ion diffusion in the membrane interior was not considered in this model, where the transfer of an ion adsorbed just inside the membrane/water interface into the membrane interior limits membrane permeability to the rates given by equations that are equivalent to Equation 6.6 and Equation 6.7 for k_f and k_b.

It should be noted that, in addition to their high lipophilicity, an ionic nature of perfluoroalkyl oxoanions render them advantageous as a probe to investigate whether their membrane transport is controlled by interfacial transfer (Equation 6.9) or membrane diffusion (Equation 6.1). These two mechanisms demonstrate different dependences of ion permeability on the interfacial potential, which can be modulated by externally applying a membrane potential or chemically depolarizing the membrane. Such a discrimination of the two permeation mechanisms based on their potential dependences is not feasible with an electrically neutral probe molecule although the permeability of a BLM to neutral molecules deviate from the solubility-diffusion model as demonstrated experimentally for a homologous series of alkyl carboxylic acids[13b] and also suggested theoretically using partition parameters for various nonelectrolytes between *n*-octanol and water phases.[37]

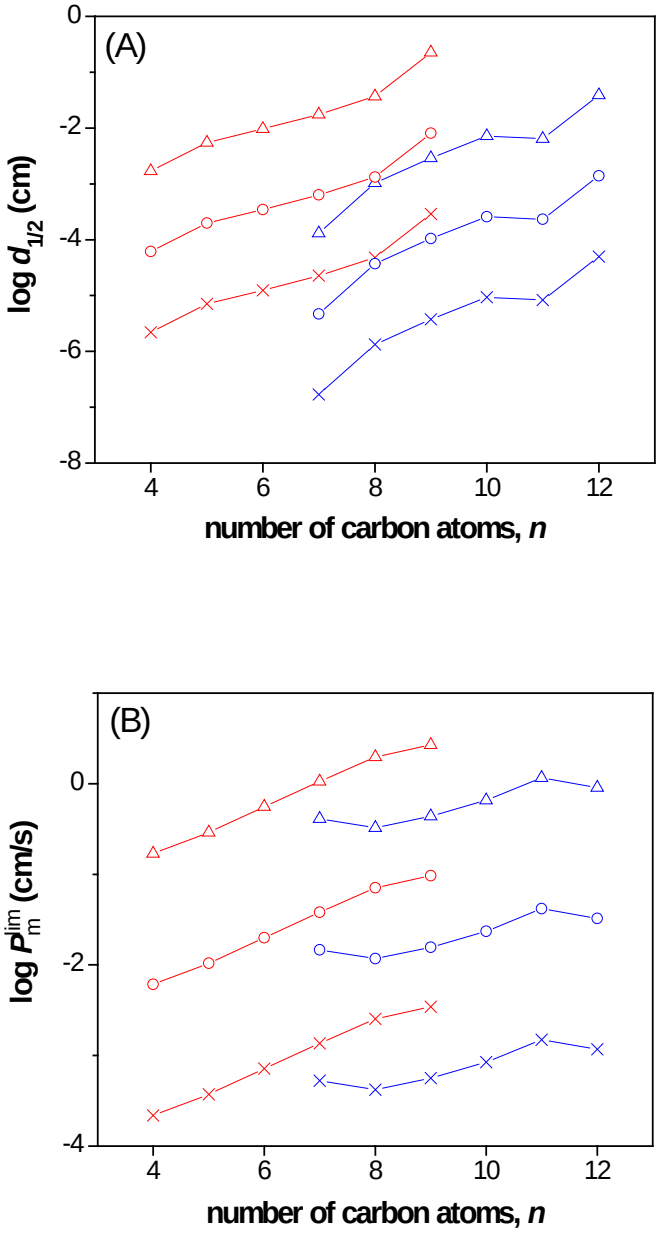

Figure 6-6. (A) The characteristic membrane thickness, $d_{1/2}$, (Equation 6.10) and (B) limiting permeability, P_m^{lim}, (Equation 6.9) as calculated for perfluoroalkyl carboxylates 1 (red symbols and lines) and alkyl carboxylates 2 (blue symbols and lines) at $\Delta_w^o\phi$ = 171, 0, and –171 mV (triangles, circles, and crosses, respectively).

6.5 CONCLUSIONS

Our finding of the remarkably high lipophilicity of perfluoroalkyl carboxylate and sulfonate is significant. This finding quantitatively supports the hypothesis that bioaccumulation and toxicity of these perfluoroalkyl surfactants originate from their lipophilic nature. Interestingly, we found that the high lipophilicity is due not to a perfluoroalkyl group itself but to its electron-withdrawing effect on the adjacent oxoanion group. Understanding of this finding at a molecular level requires more studies about the structure of the oxoanion groups and their interactions with lipophilic and aqueous environments while such studies have been focused on the perfluoroalkyl group.[34]

Ionic nature and high lipophilicity of perfluoroalkyl oxoanions are advantageous to experimentally address the long-standing question: how does permeability of a BLM depend on the lipophilicity of a permeating species? Membrane diffusion versus interfacial transfer control in permeation of a perfluoroalkyl oxoanion across a BLM will be distinguishable by studying potential dependence of its permeability. Such a study will be facilitated by using a highly stable BLM formed at the tip opening of a nanopore electrode, thereby yielding a surprisingly large breakdown voltage of 800 mV.[38] Greater understanding of a lipophilicity–permeability relationship of ions at BLMs will be significant for environmental, pharmaceutical, and biomedical sciences.

This work exemplifies powerfulness of voltammetric approaches that were recently reinforced for the study of ion transfer at liquid/liquid interfaces. Transient cyclic voltammetry at a micropipet electrode provides a more comprehensive set of parameters for ion transfer at

liquid/liquid interfaces in comparison to steady-state voltammetry.[23] Importantly, both thermodynamic and kinetic parameters are necessary to comprehensively model the permeability of a lipophilic liquid membrane as demonstrated in this work and also by Murtomäki et al.[22d] Moreover, the high lipophilicity of perfluoroalkyl oxoanions will enable sensitive and selective detection of these environmentally important analytes by employing ion-transfer stripping voltammetry with a thin lipophilic polymer membrane.[39]

ACKNOWLEDGMENTS

This work was supported by a grant from the National Institutes of Health (GM073439) and a CAREER award from the National Science Foundation (CHE-0645623). Dr. Ping Jing performed the experiments and collected the data in this work. I provided guidance and assistance with the process of fitting and analyzing the cyclic voltammograms by the numerical simulation. We thank Prof. Kohji Maeda, Kyoto Institute of Technology, for his advice on the preparation of $Mg(TPB)_2$, which Dr. Ping Jing prepared.

SUPPORTING INFORMATION

Preparation of Electrolytes

TDDA salts of perfluorobutanoate and perfluorononanoate were prepared as reported previously for the corresponding TFAB salt.[S1] $Mg(TPB)_2$ was prepared as follows: NaTPB was dissolved in deionized water and mixed with a solution of ammonium hydroxide to form precipitates of NH_4TPB. The salt was washed with deionized water several times and then recrystallized from acetone. An equivalent amount of NH_4TPB and magnesium ethoxide were mixed in anhydrous methanol and heated at 50 °C for 24 hours, where NH_3 gas evolved as the reaction proceeded. The solvent was removed by rotary evaporator to obtain $Mg(TPB)_2$. The final product was dried under vacuum for 24 hours.

Numerical Simulation of a CV at a Micropipet Electrode

Transient CVs obtained with oxoanionic surfactants **1**–**5** were fitted with quasi-reversible CVs simulated as reported recently.[S2] A diffusion problem at a liquid/liquid microinterface formed at the tip of a micropipet electrode was defined using dimensionless parameters. A boundary condition at the interface was given by employing heterogeneous rate constants, k_f and k_b, for forward and backward ion transfers in Equation 6.3, respectively (see Equations 6.6 and 6.7). The two-phase diffusion problem was solved numerically by COMSOL Multiphysics version 3.4 (COMSOL, Inc., Burlington, MA), which applies the finite element method. An example of the simulation is attached.

Table S1 lists $\Delta^{o}_{w}\phi^{0'}$ and k^0 values as well as diffusion coefficients in the bulk aqueous and *n*-octanol phases, D_w and D_o, respectively. An α value of 0.5 as obtained for all surfactants is in the normal range of 0.4−0.6,[S3] indicating that CVs of these amphiphilic ions are not complicated by double layer effects.[S4] A k^0 value does not vary with tip diameters, thereby confirming that the CVs are not nernstian. A significantly larger k^0 value of 0.10 ± 0.01 cm/s was obtained for heptanoate so that the deviation of the CVs from a nernstian behavior is not due to an Ohmic potential drop in the resistive *n*-octanol phase. Moreover, a diffusion coefficient of an oxoanionic surfactant in *n*-octanol was found to be ~10 times smaller than that in water. This result agrees with the Walden rule,[S5] where the ratio of the diffusion coefficients is inversely proportional to the ratio of viscosities of the respective solvents (7.498 and 0.8903 mPa·s at 25°C for *n*-octanol and water, respectively).[S6]

It should be noted that our kinetic and thermodynamic data are not only more systematic but also more accurate than the corresponding data obtained only for dodecanoate at *n*-octanol/water interfaces using a nanometer-sized pipet.[S7] In the previous study, both hindered diffusion in the inner water phase and slow diffusion in the outer *n*-octanol phase were neglected in the analysis of steady-state CVs. In our study, the hinder and slow diffusion of ions in the inner *n*-octanol phase was considered in the numerical simulation.

Table S1. Thermodynamic and Kinetic Parameters for Oxoanionic Surfactants 1–5 as Determined by Cyclic Voltammetry[a]

	n	$\Delta^{o}_{w}\phi^{0'}$ mV[b]	k^0 cm/s	$D_w \times 10^{-6}$ cm^2/s	$D_o \times 10^{-6}$ cm^2/s
1	4	39 ± 5	0.026 ± 0.001	11 ± 1	1.7 ± 0.5
	5	−2 ± 5	0.020 ± 0.004	11.1 ± 0.1	1.9 ± 0.5
	6	−41 ± 6	0.018 ± 0.004	12	1.4 ± 0.2
	7	−77 ± 5	0.017 ± 0.004	10.5 ± 0.5	1.2 ± 0.5
	8	−112 ± 6	0.016 ± 0.003	9.3 ± 0.7	1.2 ± 0.4
	9	−152 ± 4	0.0099 ± 0.0008	10.4 ± 0.5	2.1 ± 0.4
2	7	63 ± 6	0.10 ± 0.01	9.9 ± 0.9	0.8 ± 0.2
	8	30 ± 5	0.042 ± 0.004	9 ± 1	1 ± 1
	9	−4 ± 4	0.029 ± 0.007	8.9 ± 0.8	1.4 ± 0.6
	10	−44 ± 5	0.0203 ± 0.0004	10 ± 2	1.1 ± 0.5
	11	−64 ± 5	0.024 ± 0.004	12 ± 2	0.8 ± 0.4
	12	−79 ± 8	0.014 ± 0.003	13	2.2 ± 0.8
3		−145 ± 5	0.010 ± 0.003	9 ± 2	0.7 ± 0.1
4		−34 ± 6	0.057 ± 0.004	10.8 ± 0.9	0.9 ± 0.2
5		3 ± 6	0.039 ± 0.009	12 ± 1	2.4 ± 0.7

[a] A α value of 0.5 was obtained from all CVs. [b] Standardized on the basis of the TPA–TPB assumption.[S9]

Determination of Formal Potentials Based on the TPA–TPB Assumption

A formal ion-transfer potential, $\Delta^{o}_{w}\phi^{0'}$, of an ion was defined on the basis of the nonthermodynamic hypothesis that TPA and TPB have equal molar standard Gibbs energies of transfer.[S9] This assumption is approximated to

$$\Delta^{o}_{w}\phi^{0'}_{TPB} = -\Delta^{o}_{w}\phi^{0'}_{TPA} \quad \text{(S1)}$$

Thus, the interfacial potential is defined as zero at

$$\Delta^{o}_{w}\phi = \frac{\Delta^{o}_{w}\phi^{0'}_{TPA} + \Delta^{o}_{w}\phi^{0'}_{TPB}}{2} = 0 \quad \text{(S2)}$$

A combination of cyclic voltammetric and potentiometric data gives $\Delta^{o}_{w}\phi^{0'}_{TPB} = -\Delta^{o}_{w}\phi^{0'}_{TPA} = -171$ ± 4 mV at *n*-octanol/water interfaces. This value is very close to a value of −160 mV estimated by Scholz and coworkers [S10] while Kihara and co-workers reported a smaller value of −110 mV.[S11]

The values of $\Delta^{o}_{w}\phi^{0'}_{TPA}$ and $\Delta^{o}_{w}\phi^{0'}_{TPB}$ were measured experimentally against $\Delta^{o}_{w}\phi^{0'}$ for perfluorononanoate (PFN). CVs for both TPA and PFN transfers were observed within a potential window to obtain $\Delta^{o}_{w}\phi^{0'}_{TPA} - \Delta^{o}_{w}\phi^{0'}_{PFN} = 323 \pm 2$ mV. On the other hand, TPB is too lipophilic to give a well-defined CV within a potential window in the presence of Mg^{2+} as an aqueous supporting electrolyte. In this case, $Mg(TPB)_2$ is spontaneously extracted into the *n*-octanol phase. Thus, $\Delta^{o}_{w}\phi^{0'}_{TPB} - \Delta^{o}_{w}\phi^{0'}_{PFN} = -19 \pm 8$ mV was obtained by potentiometry (see below), where TPB partitions into the *n*-octanol phase as a counter ion of the lipophilic organic cation, TDDA, to suppress the salt extraction.[S12] A combination of these potential differences with Equation 6.S2 gives $\Delta^{o}_{w}\phi^{0'}_{PFN} = -152 \pm 4$ mV. This value was used to obtain $\Delta^{o}_{w}\phi^{0'}_{TPA}$ and $\Delta^{o}_{w}\phi^{0'}_{TPB}$.

Potentiometric Determination of Formal Potentials for Highly Lipophilic Ions and at Low Ionic Strengths

Potentiometry was employed to determine formal potentials for highly lipophilic ions, i.e., TPB and perfluorodecanoate (PFD), which are too lipophilic to give a well-defined CV within a potential window. As discussed above, $\Delta^{o}_{w}\phi^{0'}_{TPB} - \Delta^{o}_{w}\phi^{0'}_{PFN}$ was determined by potentiometry with the following electrochemical cell

Ag | AgCl | 3 M NaCl || 1 mM $MgSO_4$ in water || 1–30 µM perfluorononanoic acid or 5–150 µM $Mg(TPB)_2$ in water | 0.2 mM TDDAPFN in *n*-octanol | Ag

where a glass micropipet electrode was filled with a *n*-octanol solution and immersed in an aqueous solution. An open circuit potential of this cell was measured using a high impedance potentiometer (EMF-16, Lawson Labs Inc., Malvern, PA). Figure S1 shows nernstian responses to TPB and PFN, where the slope of the plots of the potential versus the logarithm of the ion concentration is –59 mV per log unit. The linear plots were extrapolated to 1 M ion concentration, where the potential difference corresponds to $\Delta^{o}_{w}\phi^{0'}_{TPB} - \Delta^{o}_{w}\phi^{0'}_{PFN}$.

The formal potential of highly lipophilic PFD was also determined by potentiometry with PFN as a reference ion to yield $\Delta^{o}_{w}\phi^{0'}_{PFD} - \Delta^{o}_{w}\phi^{0'}_{PFN} = -22 \pm 7$ mV from their nernstian responses. With knowledge of $\Delta^{o}_{w}\phi^{0'}_{PFN}$, $\Delta^{o}_{w}\phi^{0'}_{PFD} = -174 \pm 8$ mV was obtained from the difference.

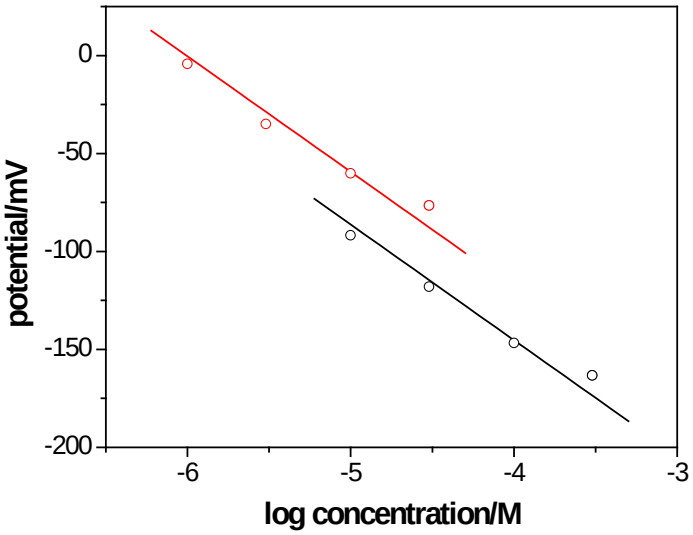

Figure S1. Potentiometric responses to PFN and TPB (red and black circles, respectively). The solid lines represent nernstian responses.

Potentiometric measurements were also carried out to determine the difference in the formal potentials for a perfluoroalkyl and an alkyl carboxylate at a low ionic strength in a *n*-octanol phase. The following electrochemical cell was constructed by using an organic-filled pipet

Ag | AgCl | 3 M NaCl || 1 mM $MgSO_4$ in water || 30–1000 µM perfluorobutanoic acid or 3–100 µM heptanoic acid in water | 0.2 mM tetradodecylammonium perfluorobutanoate in *n*-octanol | Ag

Nernstian responses were obtained for both perfluorobutanoate and heptanoate, thereby yielding a difference between their formal potentials of −29 ± 6 mV (Figure S2). This value is very close to a difference of −24 ± 5 mV determined by cyclic voltammetry in the presence of 40 mM TDDATFAB as an organic supporting electrolyte. Moreover, such consistent differences between the formal potentials at low and high ionic strengths in the *n*-octanol phase were obtained among these two carboxylates and PFN. This result indicates similar stability of ion pairs of the organic cation, TDDA, with perfluoroalkyl and alkyl carboxylates.

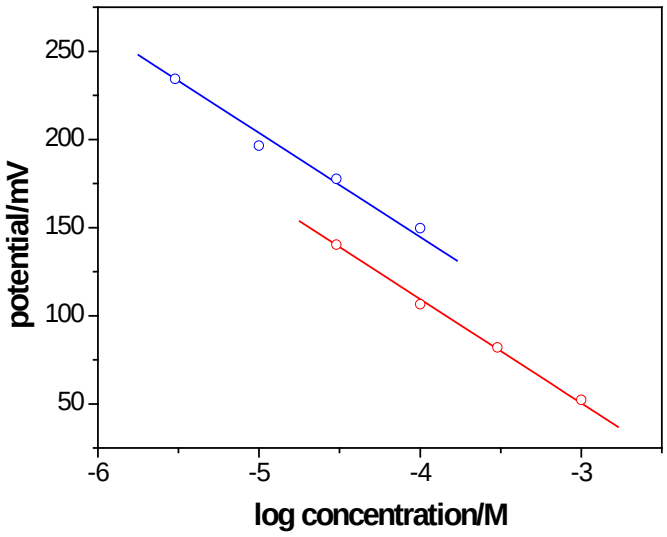

Figure S2. Potentiometric responses to perfluorobutanoate and heptanoate (red and blue circles, respectively). The solid lines represent nernstian responses.

Membrane Permeability

Equation 6.8 was derived as follows. At a steady state, a membrane ion flux, J_i, is driven by the difference of ion concentrations, $c_i^{w_1}$ and $c_i^{w_2}$, at the respective aqueous sides of the interfaces in Figure 5, thereby yielding

$$J_i = P_m(c_i^{w_1} - c_i^{w_2}) \quad \text{(S3)}$$

Electroneutrality in a thick membrane is assumed to be maintained by another ion without affecting the membrane flux of the ion, *i*.[S13] Moreover, the ion permeation across the thin membrane is assumed to be divided into three steps: (1) ion transfer at the interface between the membrane and aqueous solutions, (2) ion diffusion through the interior of the membrane, and (3) interfacial ion transfer at the opposite side of the membrane. Steps 1 and 3 give the ion flux as

$$J_i = k_f c_i^{w_1} - k_b c_i^{m_1} \quad \text{(S4)}$$

$$J_i = k_b c_i^{m_2} - k_f c_i^{w_2} \quad \text{(S5)}$$

where $c_i^{m_1}$ and $c_i^{m_2}$ are the ion concentrations at the respective membrane sides of the interfaces in Figure 5. Step 2 gives the ion flux as

$$J_i = \frac{D_o(c_i^{m_1} - c_i^{m_2})}{d} \quad \text{(S6)}$$

A combination of Equations 6.S4–S6 results in

$$J_i = \frac{k_f}{2 + k_b d / D_o}(c_i^{w_1} - c_i^{w_2}) \quad \text{(S7)}$$

A comparison of Equation 6.S3 with Equation 6.S7 gives Equation 6.8.

Diffusion-Controlled Permeability

Membrane permeability controlled by diffusion of perfluoroalkyl and alkyl carboxylates in the membrane interior was calculated using Equation 6.1 with experimentally determined parameters including D_o instead of D_m (Figure S3). With a nearly constant D_o, the permeability, P_m, is proportional to the formal partition coefficient, $P^{0'}$, which varies by 4 orders of magnitude for all perfluoroalkyl and alkyl carboxylates. The overall range of the permeability is also wide because of the strong dependence of the diffusion-controlled permeability on the interfacial potential.

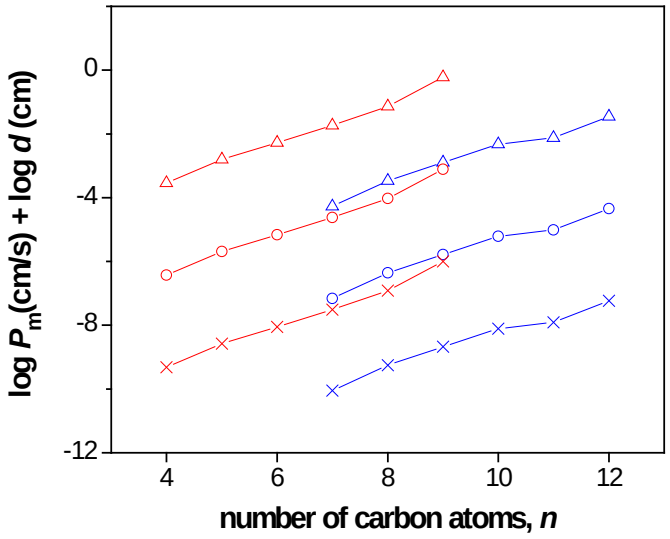

Figure S3. The diffusion-controlled permeability calculated using Equation 6.1 for perfluoroalkyl carboxylates **1** (red symbols and lines) and alkyl carboxylates **2** (blue symbols and lines) at $\Delta^o_w\phi$ = 171, 0, and −171 mV (triangles, circles, and crosses, respectively). The permeability depends on the membrane thickness, *d*.

Supporting Information References

(S1) Guo, J.; Amemiya, S. *Anal. Chem.* **2006**, *78*, 6893–6902.
(S2) (a) Rodgers, P. J.; Amemiya, S. *Anal. Chem.* **2007**, *79*, 9276–9285. (b) Rodgers, P. J.; Jing, P.; Kim, Y.; Amemiya, S. *J. Am. Chem. Soc.* **2008**, *130*, 7436–7442.
(S3) Samec, Z. *Electrochim. Acta* **1998**, *44*, 85–90.
(S4) Marcus, R. A. *J. Chem. Phys.* **2000**, *113*, 1618–1629.
(S5) Samec, Z.; Langmaier, J.; Trojánek, A. *J. Electroanal. Chem.* **1996**, *409*, 1–7.
(S6) (a) Faria, M. A. F.; De Sa, C. F.; Lima, G. R.; Filho, J. I. B. C.; Martins, R. J.; De Cardoso, M. J. E.; Barcia, O. E. *J. Chem. Eng. Data* **2005**, *50*, 1938–1943. (b) Korson, L. D.-H., W.; Millero, F. J. *J. Phys.Chem.* **1996**, *73*, 34–39.
(S7) Jing, P.; Zhang, M. Q.; Hu, H.; Xu, X. D.; Liang, Z. W.; Li, B.; Shen, L.; Xie, S. B.; Pereira, C. M.; Shao, Y. H. *Angew. Chem., Int. Ed. Engl.* **2006**, *45*, 6861–6864.
(S8) Tsujioka, N.; Imakura, S.; Nishi, N.; Kakiuchi, T. *Anal. Sci.* **2006**, *22*, 667–671.
(S9) (a) Samec, Z. *Pure Appl. Chem.* **2004**, *76*, 2147–2180. (b) Zhao, Y. H.; Abraham, M. H. *J. Org. Chem.* **2005**, *70*, 2633–2640.
(S10) Gulaboski, R.; Mirceski, V.; Scholz, F. *Electrochem. Commun.* **2002**, *4*, 277–283.
(S11) Ohde, H.; Uehara, A.; Yoshida, Y.; Maeda, K.; Kihara, S. *J. Electroanal. Chem.* **2001**, *496*, 110–117.
(S12) Amemiya, S. In *Handbook of Electrochemistry*; Zoski, C. G., Ed.; Elsevier: New York, 2007, p 261–294.
(S13) Shirai, O.; Yoshida, Y.; Kihara, S. *Anal. Bioanal. Chem.* **2006**, *386*, 494–505.

COMSOL Model

A copy of the COMSOL model is available free of charge in the Supporting Information via the Internet at http://pubs.acs.org/doi/suppl/10.1021/ja807961s.

REFERENCES

(1) (a) Prevedouros, K.; Cousins, I. T.; Buck, R. C.; Korzeniowski, S. H. *En*V*iron. Sci. Technol.* **2006**, *40*, 32–44. (b) Larsen, B. S.; Kaiser, M. A. *Anal. Chem.* **2007**, *79*, 3966–3973. (c) Conder, J. M.; Hoke, R. A.; De Wolf, W.; Russell, M. H.; Buck, R. C. *En*V*iron. Sci. Technol.***2008**, *42*, 995–1003.

(2) (a) *Fluorinated Surfactants*; Kissa, E., Ed.; Marcel Dekker: New York, 1994; Vol. 50. (b) Kissa, E. *Fluorinated Surfactants and Repellents*; 2nd ed.; Marcel Dekker: New York, 2001.

(3) (a) Lau, C.; Anitole, K.; Hodes, C.; Lai, D.; Pfahles-Hutchens, A.; Seed, J. *Toxicol. Sci.* **2007**, *99*, 366–394. (b) Andersen, M. E.; Butenhoff, J. L.; Chang, S. C.; Farrar, D. G.; Kennedy, G. L.; Lau, C.; Olsen, G. W.; Seed, J.; Wallacekj, K. B. *Toxicol. Sci.* **2008**, *102*, 3–14.

(4) (a) Apelberg, B. J.; Witter, F. R.; Herbstman, J. B.; Calafat, A. M.; Halden, R. U.; Needham, L. L.; Goldman, L. R. *En*V*iron. Health Perspect.* **2007**, *115*, 1670–1676. (b) Austin, M. E.; Kasturi, B. S.; Barber, M.; Kannan, K.; MohanKumar, P. S.; MohanKumar, S. M. J. *En*V*iron. Health Perspect.* **2003**, *111*, 1485–1489.

(5) (a) Freire, P. F.; Martin, J. M. P.; Herrero, O.; Peropadre, A.; de la Pena, E.; Hazen, M. J. *Toxicol. in Vitro* **2008**, *22*, 1228–1233. (b) Slotkin, T. A.; MacKillop, E. A.; Melnick, R. L.; Thayer, K. A.; Seidler, F. J. *En*V*iron. Health Perspect.* **2008**, *116*, 716–722. (c) Harada, K. H.; Ishii, T. M.; Takatsuka, K.; Koizumi, A.; Ohmori, H. *Biochem. Biophys. Res. Commun.* **2006**, *351*, 240–245.

(6) (a) Fan, X. J.; C˘ olic´, M.; Kallay, N.; Matijevic´, E. *Colloid Polym. Sci.* **1988**, *266*, 380–384. (b) Goss, K. U. *En*V*iron. Sci. Technol.* **2008**, *42*, 456–458.

(7) Horva´th, I. T.; Ra´bai, J. *Science* **1994**, *266*, 72–75.

(8) (a) Muller, K.; Faeh, C.; Diederich, F. *Science* **2007**, *317*, 1881–1886. (b) Prakash, G. K. S.; Chacko, S. *Curr. Opin. Drug Disco*V*ery De*V. **2008**, *11*, 793–802.

(9) (a) Krafft, M. P. *Ad*V. *Drug Deli*V*ery Re*V. **2001**, *47*, 209–228. (b) Riess, J. G. *Tetrahedron* **2002**, *58*, 4113–4131.

(10) (a) Curran, D. P. *Science* **2008**, *321*, 1645–1646. (b) Zhang, W.; Cai, C. *Chem. Commun.* **2008**, 5686–5694.

(11) Kelly, B. C.; Ikonomou, M. G.; Blair, J. D.; Morin, A. E.; Gobas, F. *Science* **2007**, *317*, 236–239.

(12) Mannhold, R.; Rekker, R. F. *Perspect. Drug Disco*V*ery Des.* **2000**, *18*, 1–18.

(13) (a) Gennis, R. B. *Biomembranes: Molecular Structure and Function*; Springer-Verlag: New York, 1989. (b) Grime, J. M. A.; Edwards, M. A.; Rudd, N. C.; Unwin, P. R. *Proc. Natl. Acad. Sci. U.S.A.* **2008**, *105*, 14277–14282.

(14) (a) Leo, A.; Hansch, C.; Elkins, D. *Chem. Re*V. **1971**, *71*, 525–616. (b) Caron, G.; Reymond, F.; Carrupt, P. A.; Girault, H. H.; Testa, B. *Pharm. Sci. Technol. Today* **1999**, *2*, 327–335.

(15) Sangster, J. *Octanol-Water Partition Coefficeints: Fundamentals and Physical Chemistry*; John Wiley & Sons: New York, 1997; Vol. 2.
(16) Arp, H. P. H.; Niederer, C.; Goss, K. U. *En*V*iron. Sci. Technol.* **2006**, *40*, 7298–7304.
(17) Hansen, K. J.; Clemen, L. A.; Ellefson, M. E.; Johnson, H. O. *En*V*iron. Sci. Technol.* **2001**, *35*, 766–770.
(18) Boswell, P. G.; Anfang, A. C.; Bu¨hlmann, P. *J. Fluorine Chem.* **2008**, *129*, 961–967.
(19) (a) Kihara, S.; Suzuki, M.; Sugiyama, M.; Matsui, M. *J. Electroanal. Chem.* **1988**, *249*, 109–122. (b) Suzuki, M.; Kihara, S.; Maeda, K.; Ogura, K.; Matsui, M. *J. Electroanal. Chem.* **1990**, *292*, 231–244. (c) Shao, Y.; Weber, S. G. *J. Phys. Chem.* **1996**, *100*, 14714–14720. (d) Reymond, F.; Chopineaux-Courtois, V.; Steyaert, G.; Bouchard, G.; Carrupt, P. A.; Testa, B.; Girault, H. H. *J. Electroanal. Chem.* **1999**, *462*, 235–250. (e) Wilke, S.; Schurz, R.; Wang, H. M. *Anal. Chem.* **2001**, *73*, 1146–1154. (f) Wilke, S.; Zerihun, T. *J. Electroanal. Chem.* **2001**, *515*, 52–60. (g) Kakiuchi, T.; Chiba, M.; Sezaki, N.; Nakagawa, M. *Electrochem. Commun.* **2002**, *4*, 701–704. (h) Komorsky-Lovric, S.; Riedl, K.; Gulaboski, R.; Mirceski, V.; Scholz, F. *Langmuir* **2002**, *18*, 8000–8005. (i) Kakiuchi, T.; Nishi, N.; Kasahara, T.; Chiba, M. *ChemPhysChem* **2003**, *4*, 179–185. (j) Gulaboski, R.; Riedl, K.; Scholz, F. *Phys. Chem. Chem. Phys.* **2003**, *5*, 1284–1289. (k) Jing, P.; Zhang, M. Q.; Hu, H.; Xu, X. D.; Liang, Z. W.; Li, B.; Shen, L.; Xie, S. B.; Pereira, C. M.; Shao, Y. H. *Angew. Chem., Int. Ed.* **2006**, *45*, 6861–6864.
(20) Samec, Z. *Pure Appl. Chem.* **2004**, *76*, 2147–2180.
(21) (a) Shirai, O.; Kihara, S.; Yoshida, Y.; Matsui, M. *J. Electroanal. Chem.* **1995**, *389*, 61–70. (b) Shirai, O.; Yoshida, Y.; Matsui, M.; Maeda, K.; Kihara, S. *Bull. Chem. Soc. Jpn.* **1996**, *69*, 3151–3162. (c) Ichieda, N.; Shirai, O.; Kasuno, M.; Banu, K.; Uehara, A.; Yoshida, Y.; Kihara, S. *J. Electroanal. Chem.* **2003**, *542*, 97–107. (d) Ichieda, N.; Shirai, O.; Yoshida, Y.; Maeda, K.; Torimura, M.; Kihara, S. *Electroanalysis* **2004**, *16*, 779–782. (e) Shirai, O.; Yoshida, Y.; Kihara, S. *Anal. Bioanal. Chem.* **2006**, *386*, 494–505.
(22) (a) Kakiuchi, T. *Electrochim. Acta* **1998**, *44*, 171–179. (b) Beriet, C.; Girault, H. H. *J. Electroanal. Chem.* **1998**, *444*, 219–229. (c) Samec, Z.; Troja´nek, A.; Langmaier, J.; Samcova´, E. *J. Electroanal. Chem.* **2000**, *481*, 1–6. (d) Barker, M. H.; Murtoma¨ki, L.; Kontturi, K. *J. Electroanal. Chem.* **2001**, *497*, 61–68.
(23) (a) Rodgers, P. J.; Amemiya, S. *Anal. Chem.* **2007**, *79*, 9276–9285. (b) Rodgers, P. J.; Jing, P.; Kim, Y.; Amemiya, S. *J. Am. Chem. Soc.* **2008**, *130*, 7436–7442.
(24) Ohde, H.; Uehara, A.; Yoshida, Y.; Maeda, K.; Kihara, S. *J. Electroanal. Chem.* **2001**, *496*, 110–117.
(25) (a) Campbell, J. A.; Girault, H. H. *J. Electroanal. Chem.* **1989**, *266*, 465–469. (b) Shao, Y.; Mirkin, M. V. *Anal. Chem.* **1998**, *70*, 3155–3161.
(26) Zhao, Y. H.; Abraham, M. H. *J. Org. Chem.* **2005**, *70*, 2633–2640.
(27) Kitazumi, Y.; Kakiuchi, T. *J. Phys.: Condens. Matter* **2007**, *19*, 375104.
(28) Reymond, F.; Steyaert, G.; Carrupt, P. A.; Testa, B.; Girault, H. *J. Am. Chem. Soc.* **1996**, *118*, 11951–11957.
(29) (a) Hansch, C.; Leo, A.; Hoekman, D. *Exploring QSAR: Hydrophobic, Electronic, and Steric Constants*; American Chemical Society: Washington, DC, 1995. (b) Scherrer, R. A.; Howard, S. M. The Analysis of Electronic Factors Quantitative Structure-Activity Relationships Using Distribution Coefficients. In *Computer-Assisted Drug Design*; Olson, E. C., Christoffersen, R. E., Eds.; ACS Symposium Series 112; American Chemical Society: Washington, DC, 1979; pp 507–526.

(30) Brace, N. O. *J. Org. Chem.* **1962**, *27*, 4491–4498.
(31) Shinoda, K.; Hato, M.; Hayashi, T. *J. Phys. Chem.* **1972**, *76*, 909–914.
(32) Goss, K. U.; Bronner, G.; Harner, T.; Hertel, M.; Schmidt, T. C. *En*V*iron. Sci. Technol.* **2006**, *40*, 3572–3577.
(33) Smart, B. E. *J. Fluorine Chem.* **2001**, *109*, 3–11.
(34) Ellis, D. A.; Denkenberger, K. A.; Burrow, T. E.; Mabury, S. A. *J. Phys. Chem. A* **2004**, *108*, 10099–10106.
(35) (a) Samec, Z.; Homolka, D.; Marecek, V. *J. Electroanal. Chem.* **1982**, *135*, 265–283. (b) Shao, Y.; Mirkin, M. V. *J. Am. Chem. Soc.* **1997**, *119*, 8103–8104. (c) Yuan, Y.; Shao, Y. H. *J. Phys. Chem. B* **2002**, *106*, 7809–7814.
(36) (a) Ketterer, B.; Neumcke, B.; La¨uger, P. *J. Membr. Biol.* **1971**, *5*, 225–245. (b) Flewelling, R. F.; Hubbell, W. L *Biophys. J.* **1986**, *49*, 54–552.
(37) Miller, D. M. *Biochim. Biophys. Acta* **1991**, *1065*, 75–81.
(38) White, R. J.; Ervin, E. N.; Yang, T.; Chen, X.; Daniel, S.; Cremer, P. S.; White, H. S. *J. Am. Chem. Soc.* **2007**, *129*, 11766–11775.
(39) Kim, Y.; Amemiya, S. *Anal. Chem.* **2008**, *80*, 6056–6065.

7.0 SUBNANOMOLAR ION DETECTION BY STRIPPING VOLTAMMETRY WITH SOLID-SUPPORTED THIN POLYMERIC MEMBRANE

This work has been published as Yushin Kim, Patrick J. Rodgers, Ryoichi Ishimatsu, and Shigeru Amemiya. *Anal. Chem.* **2009**, *81*, 7262–7270.

7.1 ABSTRACT

Subnanomolar limits of detection (LODs) are obtained for stripping voltammetry based on ion transfer at the interface between the aqueous sample and the thin polymeric membrane supported with a solid electrode. It has been predicted theoretically that a lower LOD can be obtained for a more lipophilic analyte ion, which can be preconcentrated at a higher equilibrium concentration in the solid-supported thin polymeric membrane to enhance a stripping current response. This study is the first to experimentally confirm the general theoretical prediction for both cationic and anionic analytes. Proof-of-concept experiments demonstrate that a subnanomolar LOD of (8 ± 4) × 10^{-11} M tetrapropylammonium is significantly lower than a LOD of less lipophilic tetraethylammonium. Importantly, stripping voltammetry of the cationic analytes is enabled by newly introducing an oxidatively doped poly(3,4-ethylenedioxythiophene) film as the intermediate layer between a plasticized poly(vinyl chloride) membrane and a Au electrode. On

the other hand, an undoped poly(3-octylthiophene) film is used as an intermediate layer for voltammetric detection of a lipophilic inorganic anion, hexafluoroarsenate, an arsenical biocide found recently in wastewater. A LOD of $(9 \pm 2) \times 10^{-11}$ M hexafluoroarsenate thus obtained by ion-transfer stripping voltammetry is comparable to a LOD of 80 pM by inductively coupled plasma–mass spectrometry with anion-exchange chromatography. Great sensitivity for a lipophilic ion is potentially useful for environmental analysis because high lipophilicity of an ion is relevant to its bioaccumulation and toxicity.

7.2 INTRODUCTION

Dynamic ion transfer across the interface between two immiscible electrolyte solutions, i.e., ITIES, enables highly sensitive stripping voltammetry.[1] In comparison to traditional stripping voltammetry,[2, 3] ion-transfer stripping voltammetry at the liquid/liquid interface is attractive for trace analysis of redox-inactive ions in environmental, biological, and biomedical samples. High sensitivity of this stripping method originates from preconcentration of an aqueous analyte ion into a water-immiscible organic phase, which is driven by external control of the phase boundary potential at the interface.[1, 4] The preconcentration step is followed voltammetrically by reverse extraction of the ion from the organic phase into the aqueous phase to yield a stripping ionic current with enhanced sensitivity.

During the past decade, a limit of detection (LOD) of ion-transfer stripping voltammetry has been lowered to nanomolar levels while micromolar limits were originally reported for various ions including acetylcholine,[5] tetraethylammonium,[6] alkaline earth cations,[7] and protonated organic amines[8] by employing fluid organic phases. The improved sensitivity is

mainly due to enhanced mass transfer of an analyte ion in the aqueous sample phase, which allows for more efficient preconcentration. Several to tens of nanomolar concentrations of Cd^{2+},[4] Zn^{2+},[4] Pb^{2+},[4, 9] Hg^{2+},[9] and dodecylsulfonate[10] are detectable by rotating a plasticized poly(vinyl chloride) (PVC) membrane as a robust organic phase to hydrodynamically accelerate preconcentration of the analytes. Interestingly, nanomolar LODs were also obtained for electrically neutral surfactants, which were preconcentrated as charged complexes with aqueous cations in the membrane phase.[10-12] A plasticized PVC membrane was also integrated into a flow cell to detect 2 nM Ag^{+} by square-wave stripping voltammetry.[13] Alternatively, radial diffusion of aqueous analyte ions to a micrometer-sized interface[14] or an array of microinterfaces[15] was utilized for preconcentration of nanomolar heparin[16] or β-blocker propranolol,[17] respectively.

Recently, we applied a submicrometer-thick PVC membrane for stripping analysis of nanomolar perchlorate in various drinking waters.[18] The thin PVC membrane was supported by a Au electrode modified with an undoped poly(3-octhylthiophene) (POT) film, which was oxidized to drive anion transfer into the PVC membrane (Figure 7-1a).[18, 19] An analyte ion is not only completely trapped in the solid-supported membrane during a preconcentration step but also exclusively stripped from the thin-layer membrane to maximize a stripping current response. LODs of ~0.5 nM perchlorate thus obtained are much lower than the interim health advisory level of 15 ppb (~150 nM) perchlorate in drinking water set by the U.S. Environmental Protection Agency.[20] These lowest LODs reported so far for ion-transfer stripping voltammetry, however, are an order of magnitude higher than subnanomolar LODs in the range of 10^{-10}–10^{-11} M as obtained by traditional anodic stripping voltammetry with a thin mercury film electrode.[3] Moreover, preconcentration of cationic analytes into the membrane phase requires reduction of

an intermediate conducting-polymer layer while a POT film is not readily reduced or stable in an oxidized form, which is discharged to a reduced form under an open circuit condition.[19]

In this paper, we achieve subnanomolar LODs for both cationic and anionic analytes by ion-transfer stripping voltammetry with solid-supported thin polymeric membranes. These lower LODs represent the first experimental confirmation of a theoretical prediction that a more lipophilic analyte ion gives a lower LOD for stripping voltammetry with a solid-supported thin polymeric membrane.[18] Importantly, lipophilicity of either a cation or an anion is generally quantified by a preconcentration factor, Y,[18] (also known as the apparent ion partition coefficient[21]) to dictate a LOD as demonstrated in proof-of-concept experiments. A subnanomolar LOD of 80 nM tetrapropylammonium (TPA) is compared with a LOD of less lipophilic tetraethylammonium (TEA). Importantly, the voltammetric detection of cationic analytes is enabled by newly introducing an oxidatively doped poly(3,4-ethylenedioxythiophene) (PEDOT) film, which is reduced to preconcentrate cations in the PVC membrane (Figure 7-1b). This conducting polymer has a very high stability in the oxidized form and undergoes a facile redox reaction.[22, 23] A practical significance of the theoretical prediction is demonstrated for trace analysis of a lipophilic inorganic anion, hexafluoroarsenate, which is known as an arsenical biocide[24, 25] and was recently found in wastewater.[26, 27] A LOD of 90 nM hexafluoroarsenate as obtained with a PVC/POT-modified Au electrode is lower than that of less lipophilic perchlorate and compared to a LOD of hexafluoroarsenate by inductively coupled plasma–mass spectrometry with anion-exchange chromatography. Finally, the voltammetric anion- and cation-selective electrodes are characterized by electrochemical impedance spectroscopy (EIS). While both PVC/POT- and PVC/PEDOT-modified electrodes have been used for ion-selective

(a)

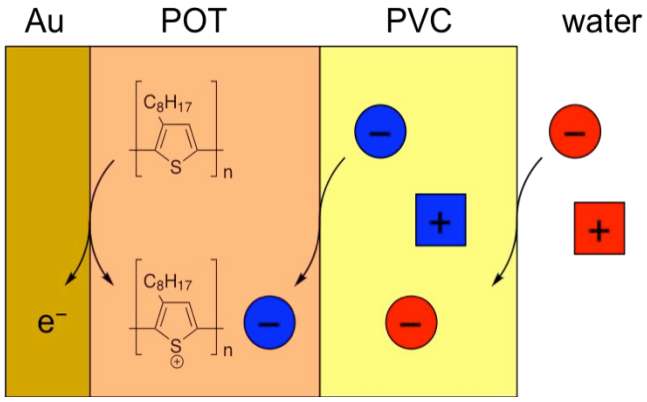

(b)

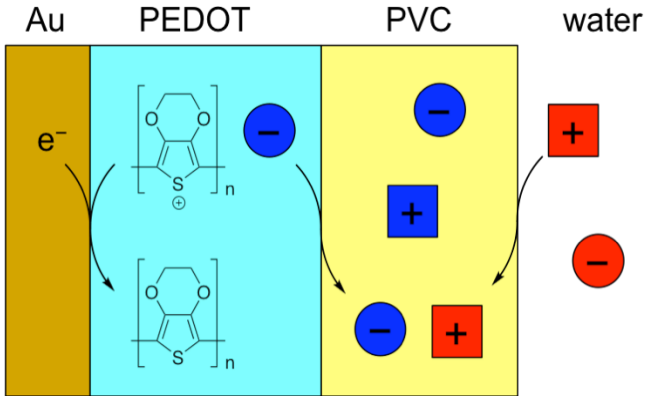

Figure 7-1. Scheme of (a) anion and (b) cation detection by ion-transfer stripping voltammetry with thin PVC membranes coated on POT- and PEDOT-modified Au electrodes, respectively. Red circles and squares represent aqueous anionic and cationic analytes, respectively. Blue circles and squares correspond to organic anion and cation in the membrane phase, respectively.

potentiometry,[28] the solid-supported PVC membranes for ion-transfer stripping voltammetry must be not only thinner for exhaustive ion stripping[18] but also more conductive for avoiding a significant Ohmic potential drop in the membranes,[19] which is confirmed by EIS.

7.3 THEORY

Here we summarize theories of ion-transfer stripping voltammetry with a solid-supported thin polymeric membrane to explain how a more lipophilic ion gives a lower LOD. The proof of the following equations is given in our previous work.[18] Interestingly, the LOD based on dynamic ion transfer at the liquid/liquid interface is ultimately dictated by equilibrium partitioning of an analyte ion with charge z_i, i^{z_i}, between the bulk aqueous and membrane phases

$$i^{z_i}\ (\text{water}) \rightleftharpoons i^{z_i}\ (\text{membrane})$$

Equation 7.1

When an aqueous ion is preconcentrated into the solid-supported thin membrane with a small volume, equilibrium partitioning of the analyte ion is eventually achieved to limit a membrane concentration of the analyte ion. The equilibrium membrane concentration, c_{PVC}, with respect to the sample concentration, c_w, is defined in general for either cation or an anion by a preconcentration factor, Y,[18] (also known as the apparent ion partition coefficient[21]) based on the Nernst equation as

$$Y = \frac{c_{PVC}}{c_w} = \exp\left[-\frac{z_i F(\Delta_w^{PVC}\phi - \Delta_w^{PVC}\phi_i^{0'})}{RT}\right]$$

Equation 7.2

where z_i is the charge of the analyte ion, F is Faraday's constant, $\Delta_w^{PVC}\phi$ is the Galvani potential difference between the aqueous and PVC membrane phases, and $\Delta_w^{PVC}\phi_i^{0'}$ is the formal potential of the analyte ion. Since the amplitude of a stripping current response varies with the membrane concentration, higher sensitivity and, subsequently, a lower LOD are expected for a more lipophilic ion with larger Y. In practice, the same potential near a negative (or positive) side of a potential window at the liquid/liquid interface is applied for cations (or anions) to result in a larger potential difference, $\Delta_w^{PVC}\phi_p - \Delta_w^{PVC}\phi_i^{0'}$, for a more lipophilic cation (or anion) with a more positive (or negative) formal potential,[21] thereby yielding a larger preconcentration factor.

Noticeably, Equation 7.2 is valid not only for simple ion transfer but also for ion transfer facilitated by ionophores, where a formal potential depends on ion lipophilicity and stability of ion–ionophore complexes.[29] Nevertheless, this work is focused on simple ion transfer. Stripping voltammetry based on facilitated ion extraction at a solid-supported thin polymeric membrane requires greater understanding of mass transfers of ionophores and ion–ionophore complexes in the membrane.

A time-dependent preconcentration process was modeled to quantitatively demonstrate that a lower LOD based on equilibrium preconcentration of a more lipophilic ion requires longer preconcentration. The total charge of preconcentrated analyte ions, $Q(t_p)$, depends on preconcentration time, t_p, as given by[18]

$$Q(t_p) = Q_{eq}\left[1 - \exp\left(-\frac{i_l}{Q_{eq}}t_p\right)\right]$$

Equation 7.3

with

$$Q_{eq} = z_i FAlc_{PVC}$$

Equation 7.4

where Q_{eq} is the total charge at an equilibrium, A is an effective area of the PVC membrane/water interface, l is an effective membrane thickness. Since the electrode is rotated during a preconentration step (see Experimental section), the limiting current, i_l, is given by the Levich equation as[30]

$$i_1 = 0.62 z_i FAD_w^{2/3} \omega^{1/2} \nu^{-1/6} c_w$$

Equation 7.5

where D_w is a diffusion coefficient of the ion in the aqueous phase, ω is the angular frequency of electrode rotation, and ν is the kinematic viscosity. The time constant, Q_{eq}/i_l, in Equation 7.3 is given by a combination of Equations 7.4 and 7.5 as

$$\frac{Q_{eq}}{i_l} = \frac{lY}{0.62 D_w^{2/3} w^{1/2} \nu^{-1/6}}$$

Equation 7.6

Equation 7.6 confirms that equilibrium partitioning of a more lipophilic ion with a larger preconcentration factor (see Equation 7.2) requires longer preconcentration.

In the following, the aforementioned theoretical predictions are confirmed experimentally for cationic analytes, TEA and TPA, with different lipophilicities, which result in different time courses toward equilibrium partitioning of the respective ions within a practical preconcentration

time (<1 hr). The theoretical predictions are also tested for hexafluoroarsenate, a lipophilic anion with analytical importance. Overall, a trend of a lower LOD for an ion with larger *Y* is reported for the total of four cations and anions as summarized in Table 7-1.

7.4 EXPERIMENTAL SECTION

7.4.1 Chemicals

Tetradodecylammonium (TDDA) bromide, 3-octylthiophene, 3,4-ethylenedioxythiophene, tetrapropylammonium chloride, lithium sulfate monohydrate, and lithium hexafluoroarsenate (V) were obtained from Aldrich (Milwaukee, WI). Poly(vinyl chloride) (PVC, high molecular weight), tetraethylammonium chloride, and 2-nitrophenyl octyl ether were from Fluka (Milwaukee, WI). Potassium tetrakis(pentafluorophenyl)borate (TFAB) was from Boulder Scientific Company (Mead, CO). All reagents were used as received. The TFAB salt of TDDA was prepared as reported elsewhere.[19]

7.4.2 Electrode Modification

A 5 mm-diameter Au disk attached to a rotating disk electrode tip (Pine Research Instrumentation, Raleigh, NC) was modified with a conducting polymer film and then with a PVC membrane. Preparation of a PVC/POT-modified Au electrode was reported elsewhere.[18] A PVC/PEDOT-modified Au electrode was prepared as follows.

Table 7-1. A Comparison of Lipophilicity, Y, and LOD of Cationic and Anionic Analytes.

	TPA	TEA	hexafluoroarsenate	perchlorate [a]
Y	1.6×10^{5}	1.0×10^{4}	1.7×10^{5}	1.4×10^{4}
LOD / M	8×10^{-11}	4×10^{-10}	9×10^{-11}	5×10^{-10}

[a] Data from ref. 18.

A PEDOT film was deposited on a polished and cleaned Au electrode[18] with 5 mm diameter by cyclic voltammetry using a three-electrode cell with a Ag/Ag^+ reference electrode (CH Instruments) and a Pt-wire counter electrode. The film deposition was conducted in an acetonitrile solution containing 0.01 M 3,4-ethylenedioxythiophene and 0.01 M TDDATFAB by cycling the potential between –1.0 and 1.4 V at 0.1 V/s for 3 times using a computer-controlled CHI 600a electrochemical workstation (CH Instruments). The final potential was set to 0.5 V to oxidatively dope a PEDOT film with TFAB. The modified Au electrode was soaked in acetonitrile for 30 min and washed with THF for 1 min to remove soluble fractions of the PEDOT film. The remaining PEDOT film is not readily soluble in THF and can be spin-coated with a PVC membrane from a THF solution of membrane components.

A PVC membrane was spin-coated on a Au disk modified with a PEDOT film from a membrane cocktail with the composition of 4 mg PVC, 16 mg 2-nitrophenyl octyl ether, and 2.2 mg TDDATFAB in 1 mL THF. A 8 μL THF solution of the membrane cocktail was injected onto the PEDOT-modified Au disk rotating at 300 rpm in a spin-coating device (model SCS-G3-8, Cookson Electronics, Providence, RI). The slow rotation resulted in a relatively thick PVC membrane with ~3 μm thickness, which was required for a good coverage of a PEDOT film. After spinning for 30 s, the modified Au disk was removed from the spin coater and dried in air for >30 min. A membrane cocktail with the same composition was employed to spin-coat a ~0.7 μm-thick PVC membrane on a POT-modified Au electrode rotating at 1500 rpm.[18] An effective thickness of a PVC membrane spin-coated on either PEDOT- or POT-modified Au electrode was determined by ion-transfer cyclic voltammetry as reported elsewhere.[18]

7.4.3 Voltammetric Measurements

Cyclic voltammetry and stripping voltammetry were performed by employing a CHI 900 electrochemical workstation (CH Instruments). A three-electrode arrangement with a Ag/AgCl reference electrode (CH Instruments) and a Pt-wire counter electrode was employed. Electrochemical cells were as follows:

Ag | AgCl | KCl (3 M) || *x* M TEACl or TPACl in 0.01 M $LiSO_4$ (aq) | PVC membrane | PEDOT | Au (cell 1)

Ag | AgCl | KCl (3 M) || *y* M $LiAsF_6$ in 0.01 M $LiSO_4$ (aq) | PVC membrane | POT | Au (cell 2)

The analyte concentrations are given in the Results and Discussion. Aqueous sample solutions were prepared with 18.3 MΩ cm deionized water (Nanopure, Barnstead, Dubuque, IA). The current carried by a positive charge from the aqueous phase to the PVC membrane is defined to be positive. All electrochemical experiments were performed at 22 ± 3 °C.

A piece of Teflon tube[18, 19] was put on a membrane-modified Au electrode tip for cyclic voltammetry to obtain a disk-shaped PVC membrane/water interface with the diameter of 1.5 mm and the interfacial area of 0.0177 cm^2. The tube was not used for stripping voltammetry, where a membrane-modified electrode was rotated by using a modulated speed rotator (Pine Research Instrumentation). A preconcentration potential was set near the limit of the potential window so that a liming current, i_l, was obtained by rotating-electrode voltammetry. A potential sweep rate during a stripping step was slow enough to exhaustively transfer preconcentrated ions from the PVC membrane into the aqueous sample.

7.4.4 Electrochemical Impedance Spectroscopy (EIS)

EIS was carried out by using CHI 660b electrochemical workstation (CH Instruments). In cell 1 or 2 without analyte ions, the center of the membrane surface was vertically directed toward the center of a 2 mm-diameter Pt counter electrode. The distance between the working and counter electrodes was set to 9 mm. A constant dc bias was applied to the membrane-modified electrode such that no ion transfer occurs across the PVC membrane/water interface. The ac component of potential was 20 mV (peak-to-peak) and the ac frequency was swept in the range from 10 Hz to 100 kHz.

7.5 RESULTS AND DISCUSSION

7.5.1 Voltammetric Cation Detection with a Poly(Vinyl Chloride)/Poly(3,4-Ethylenedioxythiophene)-Modified Electrode

An oxidatively doped PEDOT film was newly introduced to enable voltammetric cation detection with a thin PVC membrane supported on a conducting-polymer-modified electrode (Figure 7-1b) while voltammetry of anionic analytes, heparin[19] and perchlorate,[18, 19] has been reported by employing an undoped POT film (Figure 7-1a). A PVC/PEDOT-modified Au electrode was employed to detect tetraalkylammoniums with different alkyl groups, i.e., TPA and TEA, as model cationic analytes with different lipophilicities. Well-defined cyclic voltammograms (CVs) of TPA and TEA were obtained at a PVC/PEDOT-modified electrode (red lines in Figures 2a and b, respectively). More lipophilic TPA is transferred more favorably

from the aqueous phase into the membrane phase, thereby yielding the corresponding CV at less negative potentials. A peak-shaped forward wave based on simple ion transfer from the aqueous phase into the membrane phase is coupled with reduction of the underlying PEDOT film in the oxidized form (Figure 7-1b). Cation transfer during the reverse potential sweep also gives a peak current response, which requires oxidation of the reduced PEDOT film. Noticeably, the shapes of the CVs indicate that the currents are limited by diffusion-controlled ion transfer at the PVC membrane/water interface rather than by electrolysis of the surface-confined PEDOT film, indicating that this conducting polymer has sufficient redox capacity.[19]

Intrinsic lipophilicities of the tetraalkylammoniums were quantitatively assessed as formal ion-transfer potentials, $\Delta_{\mathrm{w}}^{\mathrm{PVC}}\phi^{0'}$, from the corresponding CVs. The experimental CVs at a PVC/PEDOT-modified electrode were fitted with CVs simulated for reversible transfer of a monocation (black circles in Figure 7-2) by the finite element method as reported elsewhere[18] (see also Supporting Information). The relatively good fits confirm that the current is limited by ion transfer rather than by PEDOT electrolysis. The fits show that the difference in lipophilicities of TPA and TEA corresponds to the difference of 70 mV in their formal ion-transfer potentials. In this analysis, the potential applied to the Au electrode, E_{app}, was converted to the potential applied at the PVC membrane/water interface (indicated as $\Delta\phi$ on the top axis of Figure 7-2) by considering polarization of a PVC/PEDOT/Au junction (see Supporting Information).[18, 19] The polarization at the PEDOT-based system, however, does not exactly follow an empirical relationship (see Equation 7.S2), thereby causing the deviation between the experimental and simulated CVs of TEA and TPA transfers. This deviation is not due to an Ohmic potential drop in the membrane, which is sufficiently conductive as demonstrated later by EIS.

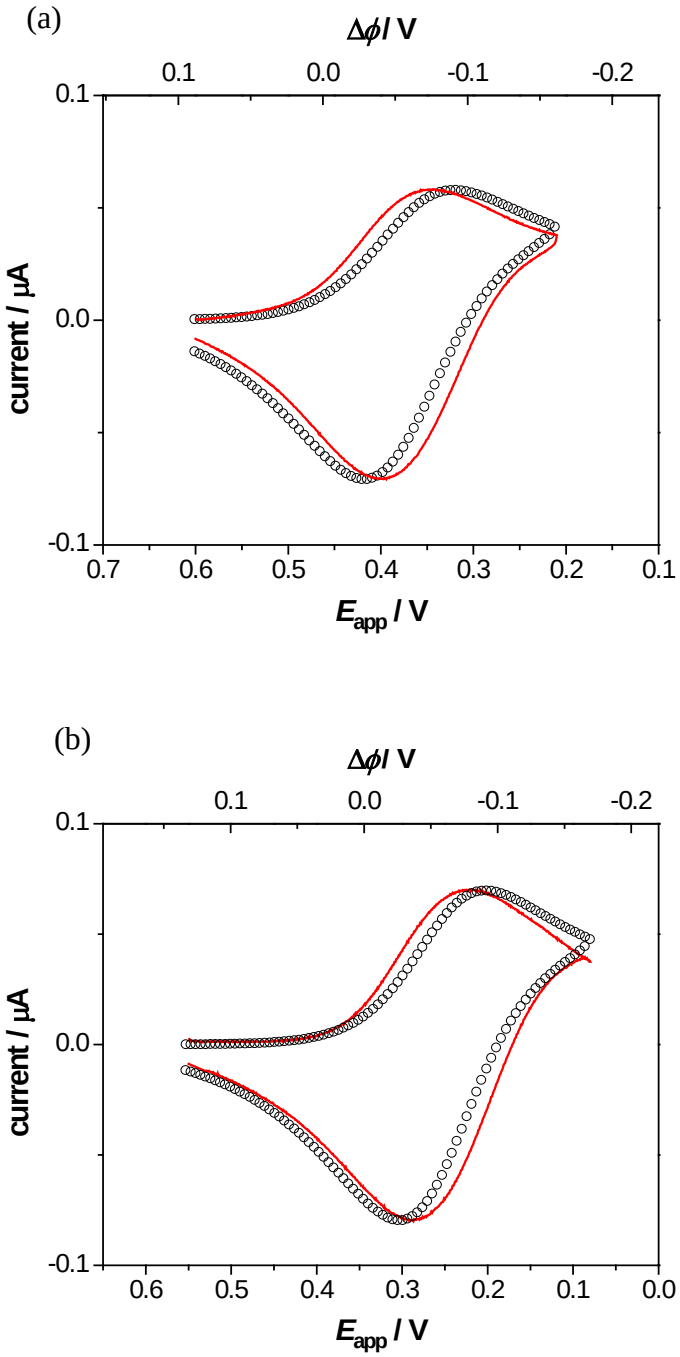

Figure 7-2. Experimental (red line) and simulated (circles) CVs of 20 μM (a) TPA and (b) TEA with a PVC/PEDOT-modified electrode. Scan rate, 0.1 V/s. E_{app} on the bottom axis was converted to $\Delta\phi$ on the top axis by assuming $\partial\Delta_w^{PVC}\phi / \partial E_{app}$ = 0.64 (see Supporting Information).

The CVs of TPA and TEA also demonstrate that the solid-supported membrane is thin enough for these tetraalkylammoniums to be exhaustively stripped from the membrane during the reverse potential sweep at 0.1 V/s. In fact, the total charge under the forward response in the CVs (0.15 and 0.12 μC for TPA and TEA, respectively) is nearly cancelled by the total charge under the reverse response (0.14 and 0.11 μC for the respective ions). Moreover, the resulting reverse peak current is enhanced by efficient ion diffusion in the thin membrane to be larger than the forward peak current, which contrasts to the corresponding peak currents based on semi-infinite ion diffusion in a thick membrane. The modes of membrane ion diffusion are characterized by a dimensionless parameter, σ, as[18]

$$\sigma = \frac{l^2 |z_i| F v}{D_{\mathrm{m}} R T}$$

Equation 7.7

where v is a potential sweep rate, and D_{m} is a diffusion coefficient of the transferred ions in the membrane phase. The numerical analysis of the experimental CVs of TPA and TEA gives σ values of 6.3 and 4.7, respectively, which are much smaller than a σ value of >100 for semi-infinite ion diffusion. These σ values of TPA and TEA, however, are larger than required for an idealistic thin layer behavior (σ < 1), where diffusion of an analyte ion in the membrane is negligible.[18] The intermediate σ values of a PVC/PEDOT-modified electrode are due to a relatively thick PVC membrane, which must be at least as thick as 3 μm to completely cover a PEDOT film.

7.5.2 Membrane Preconcentration of Tetraalkylammoniums with Different Lipophilicities

More lipophilic TPA with a less negative formal potential gives a larger preconcentration factor, *Y* (Equation 7.2), thereby resulting in a larger time constant for preconcentration of TPA. In fact, equilibrium preconcentration of TPA takes longer as proved by measuring stripping voltammograms of TPA and TEA at different preconcentration times. Stripping voltammograms of 25 nM TPA demonstrate that peak current responses vary with preconcentration times even after 1 hour (Figure 7-3a). On the other hand, a stripping response to 250 nM TEA reaches a plateau only after ~2 min preconcentration (data not shown) when equilibrium partitioning of TEA between the membrane and aqueous phases is achieved.

The remarkably different time profiles for preconcentration of TPA and TEA are quantitatively ascribed to their different lipophilicities as represented by a preconcentration factor, *Y*. The integrations of the stripping voltammograms for TPA and TEA give the total charge based on preconcentrated analyte ions, $Q(t_p)$, which is plotted against preconcentration time, t_p (Figure 7-3b). The plots for TPA and TEA fit well with Equation 7.3, thereby yielding equilibrium charges, Q_{eq}, as well as times constants, Q_{eq}/i_l. The good fits confirm that the non-equilibrium preconcentration processes limited by mass transfer of an ion in the aqueous solution is well controlled under the rotating electrode configuration.[18] $Q_{\text{Equation 7.}}$values for the respective ions correspond to applied potentials of $\Delta_w^{PVC}\phi_p - \Delta_w^{PVC}\phi^{0'}$ = 0.31 ± 0.01 and 0.23 ± 0.01 V as obtained by using Equations 7.2 and 7.4 with l = 3 μm. Since the same potential was applied for preconcentration of both TPA and TEA, the different applied potentials correspond to the difference of 0.08 ± 0.01 V in formal potentials of the two ions. This result agrees well with the

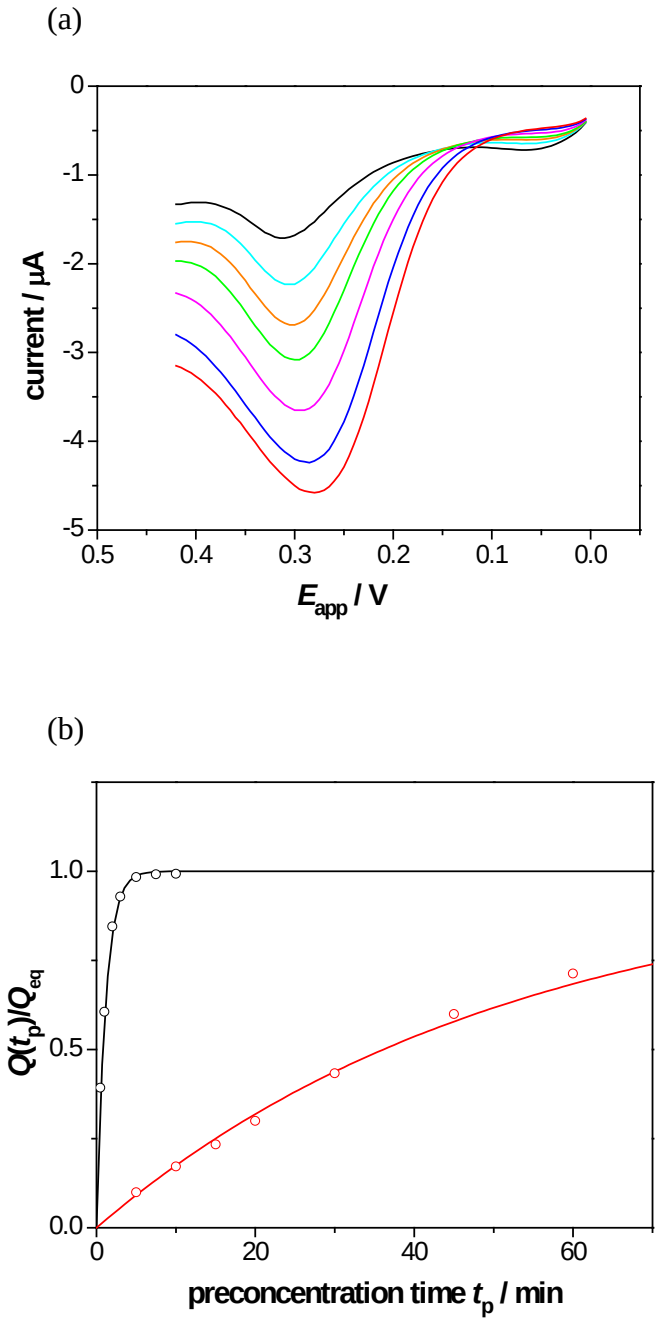

Figure 7-3. (a) Stripping voltammograms of 25 nM TPA at 0.1 V/s after preconcentration for 5 (black), 10 (cyan), 15 (orange), 20 (green), 30 (magenta), 45 (blue), and 60 (red) min. A PVC/PEDOT-modified electrode was rotated at 4000 rpm. (b) Plots of $Q(t_p)/Q_{eq}$ versus t_p for TPA (red) and TEA (black). The circles and solid lines represent experimental and theoretical (Equation 7.3) values, respectively.

difference of the formal potentials determined by cyclic voltammetry (see above). Equation 7.2 with these applied potentials gives $Y = (1.6 \pm 0.7) \times 10^5$ and $(1.0 \pm 0.4) \times 10^4$ for TPA and TEA, respectively, indicating that the PVC membrane has 16 times higher capacity for more lipophilic TPA at the preconcentration potential. It should be noted that the remarkably different time profiles for preconcentration of 25 nM TPA and 250 nM TEA in Figure 7-3b are not due to the different aqueous concentrations, which do not affect a preconcentration time constant, Q_{eq}/i_l, in Equation 7.6 (2.3×10^3 and 7.5×10 s for TPA and TEA, respectively). In fact, a higher concentration was needed for TEA because of lower sensitivity to this less lipophilic analyte (see below).TEA fit well with Equation 7.3, thereby yielding equilibrium charge, Q_{eq}. The Q_{eq} values for the respective ions correspond to $\Delta\phi = 0.31 \pm 0.01$ and 0.23 ± 0.01 V as obtained by using Equations 7.2 and 7.4 with $l = 3$ μm. Since the same potential was applied for preconcentration of both TPA and TEA, the different overpotentials correspond to the difference of 0.08 ± 0.01 V in formal potentials of the two ions. This result agrees well with the difference of the formal potentials determined by cyclic voltammetry (see above). Equation 7.2 with these overpotentials gives $Y = (1.6 \pm 0.7) \times 10^5$ and $(1.0 \pm 0.4) \times 10^4$ for TPA and TEA, respectively, indicating that the PVC membrane has 16 times higher capacity for more lipophilic TPA at the preconcentration potential. It should be noted that the remarkably different time profiles for preconcentration of 25 nM TPA and 250 nM TEA in Figure 7-3b are not due to the different aqueous concentrations, which do not affect a preconcentration time constant, Q_{eq}/i_l, in Equation 7.6. In fact, a higher concentration was needed for TEA because of lower sensitivity to this less lipophilic analyte (see below).

7.5.3 A Subnanomolar LOD for Tetrapropylammonium by Stripping Voltammetry

Stripping voltammetry with a PVC/PEDOT-modified electrode gives a subnanomolar LOD for TPA after 30 min preconcentration. The resulting current responses to TPA vary with its concentrations in the range of 50–1000 pM (Figure 7-4a). The IUPAC's upper limit approach[31] was employed to obtain a LOD of $(8 \pm 4) \times 10^{-11}$ M TPA at a confidence level of 95 % from a linear relationship between the stripping peak current and TPA concentration (Figure 7-4b). This LOD is the lowest value reported so far for ion-transfer stripping voltammetry. The LOD for TPA is not significantly lowered by increasing the preconcentration time from 30 min, at which the concentration of TPA in the membrane reaches 43 % of the equilibrium concentration (Figure 7-3b). A much higher LOD of 0.44 nM TPA was obtained by reducing preconcentration time to 3 min (Figure 7-4b). On the other hand, a stripping peak current varies linearly with TEA concentrations only at >0.5 nM after either 3 or 30 min preconcentration, thereby yielding LODs of 0.37 and 0.42 nM, respectively. A PVC membrane is saturated with TEA after ~2 min preconcentration (Figure 7-3b) so that longer preconcentration does not increase the membrane concentration of TEA or, subsequently, lower the LOD. Overall, the lower LOD for TPA in comparison to the LODs for TEA is consistent with higher lipophilicity of TPA as expected from its larger *Y* value (Table 7-1). The LOD for TPA, however, is only ~5 times lower while the preconcentration factor, *Y*, for TPA is 16 times larger. The apparently moderate LOD for TPA is due to increasing background current in this potential range (inset of Figure 7-4a).

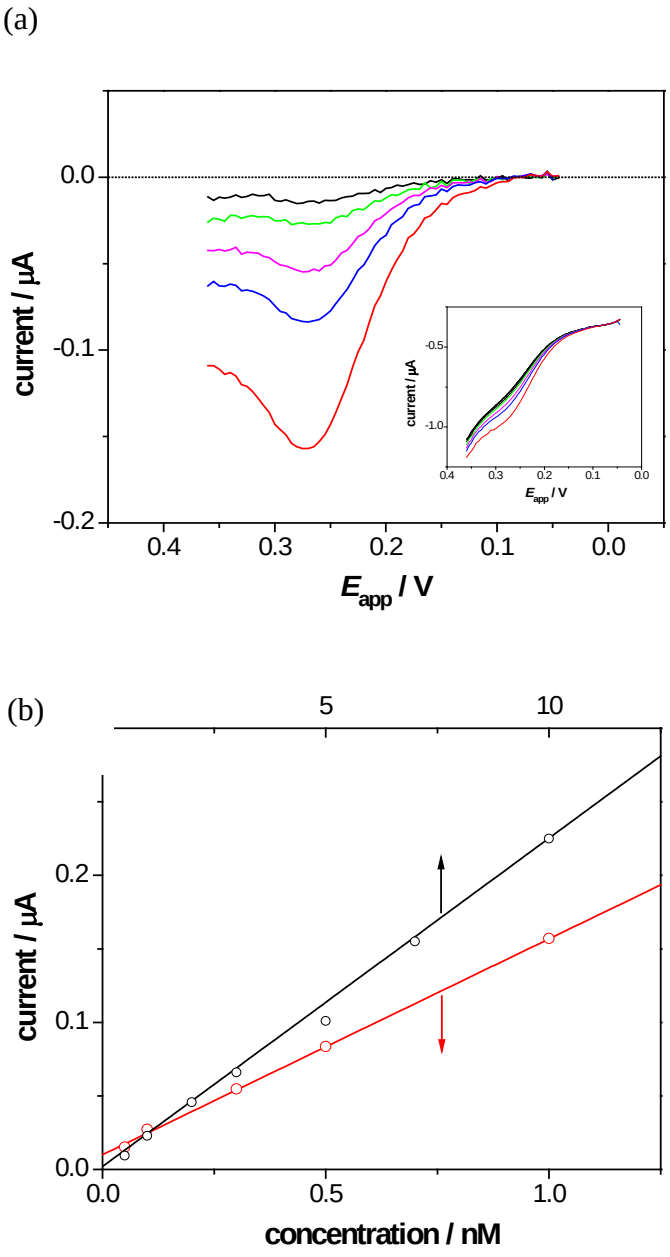

Figure 7-4. Background-subtracted stripping voltammograms of 50 (black), 100 (green), 300 (magenta), 500 (blue), 1000 (red) pM TPA in deionized water at 0.1 V/s after 30 min preconcentration. The inset shows original stripping voltammograms including a background stripping voltammogram. A PVC/PEDOT-modified electrode was rotated at 4000 rpm. (b) Plots of background-subtracted peak current versus TPA concentrations after 3 (black circles) and 30 min (red circles) preconcentration. The solid lines represent the best fits used for determination of LODs.

It should be noted that a lower LOD for TPA at a long preconcentration time of 30 minutes is also advantageous for its detection in the presence of TEA. A stripping voltammogram with a mixed solution of TEA and TPA at the identical concentration is dominated by a response to TPA around ~0.3 V after 30 minutes preconcentration (Figure 7-5a). This apparently high selectivity for TPA over TEA is due to immediate saturation of a PVC membrane with less lipophilic TEA at the early stage of a preconcentration step while TPA is steadily preconcentrated into the membrane for 30 minutes to give a much larger stripping current response. On the other hand, a significant stripping response to TEA is observed around ~ 0.19 V after 30 seconds preconcentration (Figure 7-5b), which is resolved from the response to TPA, because of their different formal potentials.

7.5.4 Hexafluoroarsenate as a Lipophilic Anionic Contaminant

Hexafluoroarsenate was investigated as one of the most lipophilic inorganic anions in the so-called Hofmeister series[32] to demonstrate that a subnanomolar LOD is obtained also for a lipophilic anion. Hexafluoroarsenate is an arsenical biocide[24] used as a pesticide, Hexaflurate.[23] Hexafluoroarsenate was recently found in wastewater from a crystal glass factory containing high concentrations of arsenic and fluoride.[25, 26]

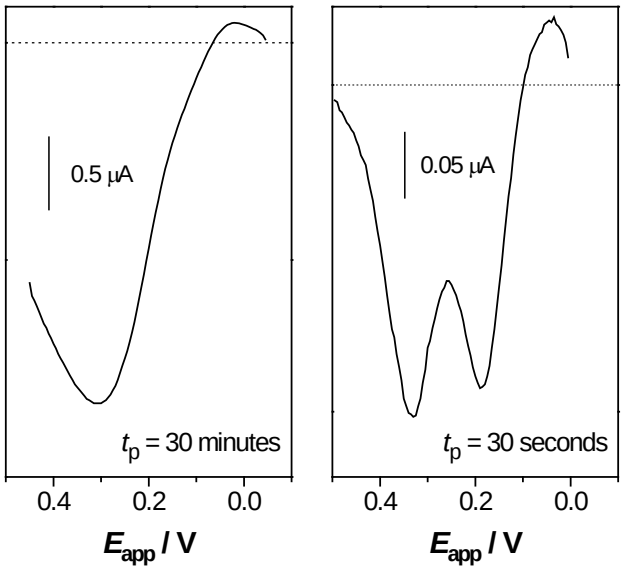

Figure 7-5. Background-subtracted stripping voltammograms of TEA and TPA in a mixed solution at the identical concentration after preconcentration for 30 minutes (left) and 30 seconds (right). The ion concentrations are 24 and 50 nM, respectively. The dotted lines represent zero current.

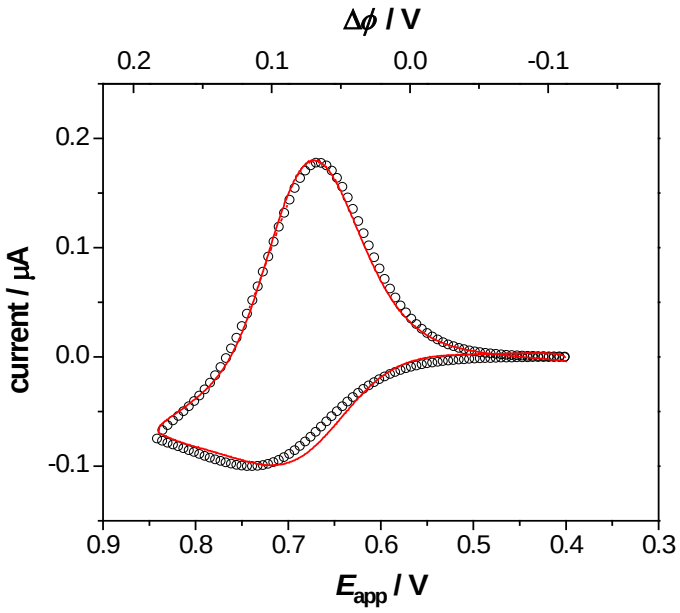

Figure 7-6. Experimental (red line) and simulated (circles) CVs of 20.4 μM hexafluoroarsenate at a PVC/POT-modified electrode. Scan rate, 0.1 V/s. E_{app} on the bottom axis was converted to $\Delta\phi$ on the top axis by assuming $\partial\Delta_w^{PVC}\phi / \partial E_{app}$ = 0.67 (see Supporting Information).

A well-defined CV of lipophilic hexafluoroarsenate was obtained favorably with a PVC/POT-modified electrode (Figure 7-6). The CV fits very well with a CV simulated for reversible anion transfer, which controls measured currents. A σ value of < 1 as obtained from the fit indicates that the solid-supported membrane serves as a thin-layer cell.[18] This σ value for hexafluoroarsenate with a PVC/POT-modified electrode is smaller than σ values obtained for TEA and TPA with a PVC/PEDOT modified electrode, because a PVC membrane of the former electrode is thinner than that of the latter (l = 0.7[18] and 3 μm in Equation 7.7, respectively). The numerical analysis also gives a formal potential of hexafluoroarsenate, which is by 61 mV less positive than that of less lipophilic perchlorate.[18]

The higher lipophilicity of hexafluoroarsenate is confirmed by stripping voltammetry of 25 nM hexafluoroarsenate at various preconcentration times (Figure 7-7a). The stripping current response increases monotonically at a longer preconcentration time to reach a plateau value within 20 min preconcentration when equilibrium partitioning of hexafluoroarsenate between the membrane and aqueous phases is achieved. The preconcentration time required for equilibration is ~10 times longer than that for prechlorate,[18] which is due to higher lipophilicity of hexafluoroarsenate (Equation 7.6). A plot of $Q(t_p)/Q_{eq}$ versus t_p for hexafluoroarsenate fits well with Equation 7.3 (Figure 7-7b) to give a Q_{eq} value, which corresponds to an applied potential of 0.31 V with respect to a formal potential as given by using Equations 7.2 and 7.4 with l = 0.7 μm. This applied potential is more positive than the corresponding applied potential of 0.25 V for perchlorate by 60 mV, which is consistent with the difference in formal potentials of hexafluoroarsenate and perchlorate as determined by cyclic voltammetry. Consequently, the corresponding Y value of hexafluoroarsenate is 12 times larger than that of perchlorate (Table 7-1).

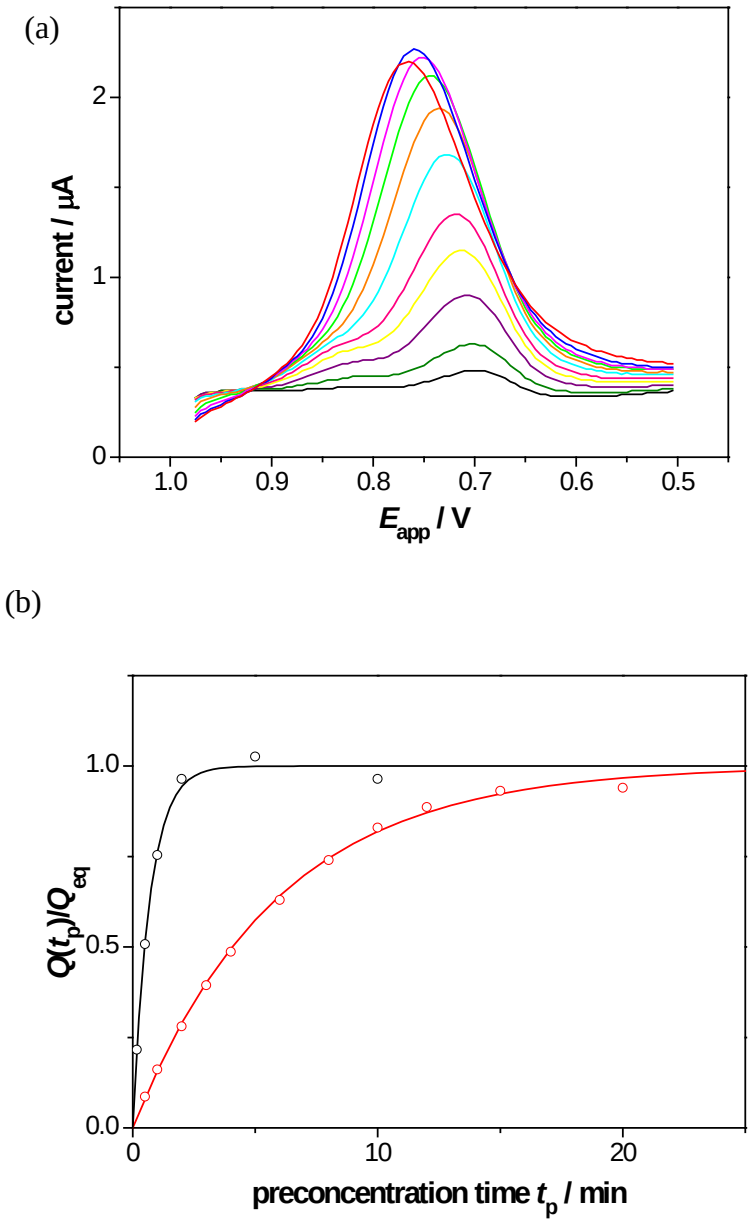

Figure 7-7. (a) Stripping voltammograms of 25 nM hexafluoroarsenate at 0.1 V/s after a preconcentration step of 0.5 (black), 1 (olive), 2 (purple), 3 (yellow), 4 (pink), 6 (cyan), 8 (orange), 10 (green), 12 (magenta), 15 (blue), and 20 (red) min. A PVC/POT electrode was rotated at 4000 rpm. (b) Plots of $Q(t_p)/Q_{eq}$ versus t_p for hexafluoroarsenate (red) and perchlorate (black). The circles and solid lines represent experimental and theoretical (Equation 7.3) values, respectively.

It should be noted that, despite similar applied potentials and, subsequently, preconcentration factors for TPA and hexafluoroarsenate, a thinner PVC membrane covered on a POT-modified electrode is more quickly saturated with hexafluoroarsenate than a PVC/PEDOT membrane with TPA (Figures 3b and 6b, respectively) as expected from the dependence of preconcentration time constant on the membrane thickness (Equation 7.6).

7.5.5 A Subnanomolar Limit of Detection for Hexafluoroarsenate by Stripping Voltammetry

A subnanomolar LOD for hexafluoroarsenate was obtained by stripping voltammetry with a PVC/POT-modified electrode in deionized water containing 0.01 M Li_2SO_4. Stripping current responses after 8 min preconcentration vary with 0.25–1.25 nM hexafluoroarsenate (Figure 7-7). The background-subtracted peak current is linear to the sample ion concentration (inset of Figure 7-7). A LOD of $(9 \pm 2) \times 10^{-11}$ M was obtained by using the IUPAC's upper limit approach at a confidence level of 95 %.[31] This LOD is comparable to the LOD of 80 pM hexafluoroarsenate (6 ng/L as arsenic) in waters by inductively coupled plasma–mass spectrometry with anion-exchange chromatography.[33] Moreover, the LOD for hexafluoroarsenate with a PVC/POT-modified electrode in 0.01 M Li_2SO_4 is significantly lower than the corresponding LOD of 0.5 ± 0.1 nM perchlorate, to which stripping current responses vary with its concentrations only at ≥1 nM. [18] The lower limit of detection for more lipophilic hexafluoroarsenate is expected from its larger *Y* value (Table 7-1). In fact, the higher lipophilicity of hexafluoroarsenate is shown also in the stripping voltammograms (Figure 7-7), where the background peak current responses around ~0.87 V are due to perchlorate contaminated in the membrane during electrochemical deposition of a POT film in 0.5 M

$LiClO_4$.[18] Overall, LODs of both cations and anions examined in this study are mainly dictated by their lipophilicities as quantified by their *Y* values (see Table 7-1).

7.5.6 EIS of Membrane-Modified Electrodes

Ac impedance responses of PVC/PEDOT- and PVC/POT-modified electrodes confirm that these thin double-polymer membranes are conductive enough to avoid a significant Ohmic potential drop in the membranes. A membrane-modified electrode was immersed in 0.01 M Li_2SO_4 and biased with a dc potential such that no ion transfer occurs across the PVC membrane/water interface. For the blocking electrode, the impedance, *Z*, can be expressed by use of a resistor and a constant phase element as[34]

$$Z = Z_{\mathrm{Re}} - jZ_{\mathrm{Im}} = R + \frac{1}{(j\omega)^{\alpha} Q}$$

Equation 7.8

where *R*, α, and *Q* are real values and independent of the ac frequency, ω, of potential. Equation 7.8 fits well with impedance responses in low frequency regions ($R < Z_{\mathrm{Re}}$ in Figure 7-8), thereby yielding the corresponding parameters listed in Table 7-2. The following discussion is focused on the resistance, *R*, which represents the sum of resistances in the bulk membrane and aqueous phases. Interpretation of the constant phase element can be hardly made because of the presence of multiple interfaces in the membrane-modified electrodes.

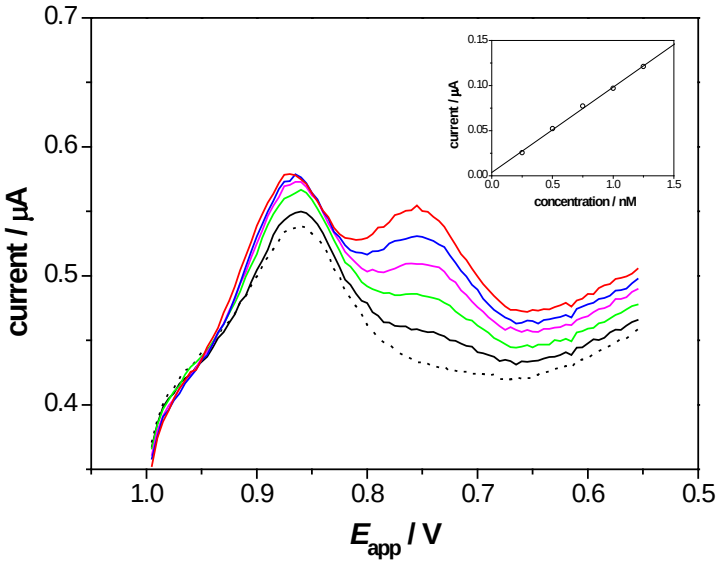

Figure 7-8. Stripping voltammograms of 0 (black dotted), 0.25 (black solid), 0.5 (green), 0.75 (magenta), 1 (blue), and 1.25 (red) nM hexafluoroarsenate at 0.1 V/s. The inset shows a plot of background-subtracted peak current versus analyte concentration. The solid line represents the best fit used for determination of LODs. Preconcentration time was 8 min. A PVC/POT-modified electrode was rotated at 4000 rpm.

The R values with the membrane-modified electrodes are similar to the R value with a bare Au electrode (Table 7-2), indicating that the R values mainly reflect the solution resistance between the working and counter electrodes. The R value with the PVC/PEDOT-modified electrode is larger than that with the bare Au electrode only by 0.06 kΩ, which corresponds to the resistance of the PVC/PEDOT membrane. Despite a thinner PVC membrane, the R value with the PVC/POT-modified electrode is larger than that with the PVC-PEDOT-modified electrode by 0.08 kΩ. This result indicates that the undoped POT film is more resistive than the oxidatively doped PEDOT film. Both membrane resistances of <0.15 kΩ and total resistances of ≤0.60 kΩ are small enough to cause a negligible Ohmic potential drop of < 1 mV in the membranes when stripping current of <1.5 μA flows across the membranes under the experimental conditions employed in this study.

It should also be noted that impedance responses of membrane-modified and bare Au electrodes in lower frequency regions ($R << Z_{\mathrm{Re}}$) depend on the dc component of potential such that α values are affected (data not shown). Impedance responses in higher frequency regions ($Z_{\mathrm{Re}} \approx R$ or lower) are rather independent of the dc bias, thereby yielding similar R values as listed in Table 7-2. We were not able to find a good equivalent circuit for the impedance responses in the higher frequency regions, where data points are limited by the available frequency range of our instrument (Figure 7-9b).

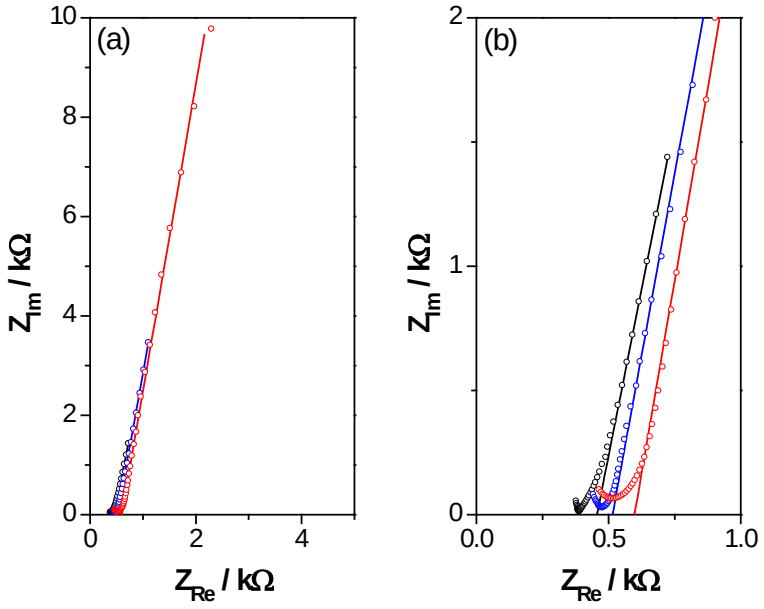

Figure 7-9. Nyquist plots of experimental (circles) and simulated (solid lines) impedance responses in the (a) whole and (b) higher frequency regions as obtained with PVC/POT-modified (red), PVC/PEDOT-modified (blue), and bare (black) Au electrodes in 0.01 M Li_2SO_4. The dc biases applied to the respective electrodes were 0.15, 0, and 0 V against a Ag/AgCl reference electrode. An equivalent circuit based on a constant phase element was used for the simulations.

Table 7-2. Parameters Determined from Impedance Responses of Membrane-Modified and Bare Au Electrodes in 0.01 M Li_2SO_4.

electrode	R / kΩ	α	Q^a
PVC/PEDOT[b]	0.52	0.89	1.6×10^5
PVC/POT[b]	0.60	0.90	4.8×10^5
bare	0.46	0.88	6.7×10^4

[a] The unit depends on α.[34] [b] A PVC membrane was spin-coated on a conducting polymer-modified Au electrode with 5 mm diameter as described in the Experimental section.

7.6 CONCLUSION

The subnanomolar LODs that were obtained for both cationic and anionic analytes by employing PVC/PEDOT- and PVC/POT-modified electrodes, respectively, are the lowest LODs reported so far for ion-transfer stripping voltammetry. The subnanomolar LODs were obtained for lipophilic ions as predicted by Equation 7.2. The great sensitivity for lipophilic ions is potentially useful for environmental analysis because high lipophilicity of an ion is relevant to its bioaccumulation and toxicity. Hexafluoroarsenate[32] and perchlorate[35] are two of the most lipophilic inorganic anions in the Hofmeister series. Moreover, we have recently employed ion-transfer voltammetry to demonstrate that perfluoroalkyl carboxylate and sulfonate, which are an emerging class of organic contaminants,[36] are much more lipophilic than their alkyl counterparts.[37] Other lipophilic ions that potentially possess adverse health effects include ionizable pharmaceuticals[38] and ionic liquids.[39] These ions are detectable also by ion-transfer voltammetry.[40-42]

The subnanomolar LODs represent practical limits for monovalent ions. An even lower LOD as expected for a more lipophilic monovalent ion requires extremely long preconcentration (>>1 hr). On the other hand, an ion with a larger charge will give a lower LOD without prolonged preconcentration, because stripping currents based on a thin-layer behavior vary with the square of the charge number.[43] Picomolar LODs are expected for ion-transfer stripping voltammetry based on facilitated extraction of polyions, e.g., polypeptide protamine (~+20)[44-46] and pentasaccharide Arixtra (~–10).[47] The extremely high sensitivity may be useful for detection of these biological polyions in complicated biological and biomedical samples such as whole blood, where a liquid/liquid interface is fouled to lower voltammetric sensitivity.[16]

Voltammetric cation detection with a thin polymeric membrane supported on a conducting-polymer-modified electrode was demonstrated for the first time by employing a PEDOT film. In contrast to anionic analytes, many ionophores with excellent selectivity among cations were developed for potentiometry.[48] These highly selective ionophores will significantly widen the range of applications of PVC/PEDOT-modified electrodes. On the other hand, a LOD for either cation or anion as obtained with a PVC/PEDOT- or PVC/POT-modified electrode, respectively, is ultimately dictated by the Nernst equation (Equation 7.2). In this regard, our voltammetric approach contrasts to a recent potentiometric approach with a PVC/PEDOT-modified electrode.[49] In the latter approach, both cationic analytes and their co-ions are galvanostatically extracted into a PVC membrane to inevitably obtain a non-equilibrium super-Nernstian response. A LOD of such a non-selective potentiometric response is compromised in comparison to a LOD of an equilibrium, selective Nernstian response.[50]

ACKNOWLEDGEMENTS

This work was supported by a CAREER award from the National Science Foundation (CHE-0645623). In this body of work, I fabricated the electrodes and collected and analyzed the data for hexafluoroarsenate (Figures 7-6, 7-7 and 7-8). Yushin Kim expanded the ISE to detect cationic species using the PEDOT conducting polymer. He collected and analyzed all of the data related to the cationic species (Figures 7-1 through 7-6). Yushin Kim, Ryoichi Ishimatsu and I contributed to the design and fine-tuning of the EIS experiment to characterize the resistance of the ISE, however, Yushin Kim collected the data (Figure 7-9).

SUPPORTING INFORMATION

Finite Element Simulation of CVs

CVs at PVC/POT- and PVC/PEDOT-modified electrodes were numerically analyzed by employing the finite element method as reported elsewhere.[S1] Specifically, CVs were simulated by using COMSOL Multiphysics version 3.5a (COMSOL, Inc., Burlington, MA. An example of the finite element simulation is attached.

A current response was simulated as a function of the potential drop at the PVC membrane/water interface, $\Delta_{\mathrm{w}}^{\mathrm{PVC}}\phi$. An experimental CV, however, is obtained against the potential applied to the underlying gold electrode, E_{app}, which is also used for a redox reaction of a conducting-polymer film as given by

$$E_{\mathrm{app}} = \Delta_{\mathrm{PVC}}^{\mathrm{Au}}\phi + \Delta_{\mathrm{w}}^{\mathrm{PVC}}\phi - E_{\mathrm{ref}} \qquad \text{(S1)}$$

where $\Delta_{\mathrm{PVC}}^{\mathrm{Au}}\phi$ is the potential drop across the PVC/conducting polymer/gold junction, and E_{ref} is the reference electrode potential. In our previous work,[S1,S2] a linear relationship between $\Delta_{\mathrm{w}}^{\mathrm{PVC}}\phi$ and E_{app} was observed empirically for PVC/POT-modified gold electrodes. With this empirical relationship of a constant value of $\partial\Delta_{\mathrm{w}}^{\mathrm{PVC}}\phi / \partial E_{\mathrm{app}}$, Equation 7.S1 is equivalent to

$$\Delta\phi = \Delta_{\mathrm{w}}^{\mathrm{PVC}}\phi - \Delta_{\mathrm{w}}^{\mathrm{PVC}}\phi_{\mathrm{i}}^{0'} = (E_{\mathrm{app}} - E_{\mathrm{i}}^{0'})\frac{\partial\Delta_{\mathrm{w}}^{\mathrm{PVC}}\phi}{\partial E_{\mathrm{app}}} \quad \text{(S2)}$$

where $E_{\mathrm{i}}^{0'}$ is the applied potential at $\Delta_{\mathrm{w}}^{\mathrm{PVC}}\phi = \Delta_{\mathrm{w}}^{\mathrm{PVC}}\phi_{\mathrm{i}}^{0'}$. In the analysis of CVs in Figures 2 and 5, $\partial\Delta_{\mathrm{w}}^{\mathrm{PVC}}\phi / \partial E_{\mathrm{app}}$ was assumed to be same for two ions i and j so that the difference of their formal potentials is given by

$$\Delta_{\mathrm{w}}^{\mathrm{PVC}}\phi_{\mathrm{j}}^{0'} - \Delta_{\mathrm{w}}^{\mathrm{PVC}}\phi_{\mathrm{i}}^{0'} = (E_{\mathrm{j}}^{0'} - E_{\mathrm{i}}^{0'})\frac{\partial\Delta_{\mathrm{w}}^{\mathrm{PVC}}\phi}{\partial E_{\mathrm{app}}} \quad \text{(S3)}$$

It should also be noted that this assumption may be an origin of the deviation between experimental and simulated CVs for a PVC/PEDOT-modified electrode in Figure 7-2. In contrast, a good fit is obtained for a PVC/POT-modified electrode by using this assumption (Figure 7-5).[S1,S2]

Supporting Information References

(S1) Kim, Y.; Amemiya, S. *Anal. Chem.* **2008**, *80*, 6056–6065.
(S2) Guo, J.; Amemiya, S. *Anal. Chem.* **2006**, *78*, 6893–6902.

COMSOL Model

A copy of the COMSOL model is available free of charge in the Supporting Information via the Internet at http://pubs.acs.org/doi/suppl/10.1021/ac900995a.

REFERENCES

(1) Samec, Z.; Samcová, E.; Girault, H. H. *Talanta* **2004**, *63*, 21–32.
(2) Wang, J. *Stripping Analysis: Principles, Instrumentation, and Applications*; VCH: Deerfield Beach, FL, 1985.
(3) Wang, J. In *Laboratory Techniques in Electroanalytical Chemistry*, 2nd ed.; Kissinger, P. T., Heineman, W. R., Eds.; Marcel Dekker: New York, 1996, pp 719–737.
(4) Senda, M.; Katano, H.; Kubota, Y. *Collect. Czech. Chem. Commun.* **2001**, *66*, 445–455.
(5) Marecek, V.; Samec, Z. *Anal. Lett.* **1981**, *14*, 1241–1253.
(6) Marecek, V.; Samec, Z. *Anal. Chim. Acta* **1982**, *141*, 65–72.
(7) Marecek, V.; Samec, Z. *Anal. Chim. Acta* **1983**, *151*, 265–269.
(8) Homolka, D.; Marecek, V.; Samec, Z.; Base, K.; Wendt, H. *J. Electroanal. Chem.* **1984**, *163*, 159–170.
(9) Katano, H.; Senda, M. *Anal. Sci.* **1998**, *14*, 63–65.
(10) Katano, H.; Senda, M. *Anal. Sci.* **2001**, *17*, i337–i340.
(11) Senda, M.; Katano, H.; Yamada, M. *J. Electroanal. Chem.* **1999**, *468*, 34–41.
(12) Katano, H.; Senda, M. *J. Electroanal. Chem.* **2001**, *496*, 103–109.
(13) Sherburn, A.; Arrigan, D. W. M.; Dryfe, R. A. W.; Boag, N. M. *Electroanalysis* **2004**, *16*, 1227–1231.
(14) Ohkouchi, T.; Kakutani, T.; Osakai, T.; Senda, M. *Anal. Sci.* **1991**, *7*, 371–376.
(15) Lee, H. J.; Beriet, C.; Girault, H. H. *Anal. Sci.* **1998**, *14*, 71–77.
(16) Guo, J.; Yuan, Y.; Amemiya, S. *Anal. Chem.* **2005**, *77*, 5711–5719.
(17) Collins, C. J.; Arrigan, D. W. M. *Anal. Chem.* **2009**, *81*, 2344–2349.
(18) Kim, Y.; Amemiya, S. *Anal. Chem.* **2008**, *80*, 6056–6065.
(19) Guo, J.; Amemiya, S. *Anal. Chem.* **2006**, *78*, 6893–6902.
(20) *Interim Drinking Water Health Advisory for Perchlorate*; EPA 822-R-08-025; Health and Ecological Criteria Division, Office of Science and Technology, Office of Water, U.S. Environmental Protection Agency: Washington, DC, 2008.
(21) Groenendaal, B. L.; Jonas, F.; Freitag, D.; Pielartzik, H.; Reynolds, J. R. *Adv. Mater. (Weinheim, Ger.)* **2000**, *12*, 481–494.
(22) Groenendaal, L.; Zotti, G.; Aubert, P. H.; Waybright, S. M.; Reynolds, J. R. *Adv. Mater. (Weinheim Ger.)* **2003**, *15*, 855–879.
(23) Hamilton, D. J.; Ambrus, A.; Dieterle, R. M.; Felsot, A. S.; Harris, C. A.; Holland, P. T.; Katayama, A.; Kurihara, N.; Linders, J.; Unsworth, J.; Wong, S. S. *Pure Appl. Chem.* **2003**, *75*, 1123–1155.
(24) Reisinger, H. J.; Burris, D. R.; Hering, J. G. *Environ. Sci. Technol.* **2005**, *39*, 458A–464A.
(25) Daus, B.; von Tumpling, W.; Wennrich, R.; Weiss, H. *Chemosphere* **2007**, *68*, 253–258.
(26) Daus, B.; Weiss, H.; Bernhard, K.; Hoffmann, P.; Neu, T. R.; von Tumpling, W.; Wennrich, R. *Eng. Life Sci.* **2008**, *8*, 598–602.
(27) Bobacka, J.; Ivaska, A.; Lewenstam, A. *Chem. Rev.* **2008**, *108*, 329–351.

(28) Samec, Z. *Pure Appl. Chem.* **2004**, *76*, 2147–2180.
(29) Homolka, D.; Hung, L. Q.; Hofmanova, A.; Khalil, M. W.; Koryta, J.; Marecek, V.; Samec, Z.; Sen, S. K.; Vanysek, P. *Anal. Chem.* **1980**, *52*, 1606–1610.
(30) Bard, A. J.; Faulkner, L. R. *Electrochemical Methods: Fundamentals and Applications*, 2nd ed.; John Wiley and Sons: New York, 2001; p 339.
(31) Mocak, J.; Bond, A. M.; Mitchell, S.; Scollary, G. *Pure Appl. Chem.* **1997**, *69*, 297–328.
(32) Zhang, G.-X.; Imato, T.; Ishibashi, N. *Bunseki Kagaku* **1989**, *38*, 283–285.
(33) Wallschlager, D.; London, J. *J. Anal. At. Spectrom.* **2005**, *20*, 993–995.
(34) Orazem, M. E.; Tribollet, B. *ELectrochemical Impedance Spectroscopy*; John Wiley & Sons: Hobeken, NJ, 2008, pp 233.
(35) Wegmann, D.; Weiss, H.; Ammann, D.; Morf, W. E.; Pretsch, E.; Sugahara, K.; Simon, W. *Mikrochim. Acta* **1984**, *3*, 1–16.
(36) Larsen, B. S.; Kaiser, M. A. *Anal. Chem.* **2007**, *79*, 3966–3973.
(37) Jing, P.; Rodgers, P. R.; Amemiya, S. *J. Am. Chem. Soc.* **2009**, *131*, 2290–2296.
(38) Ternes, T. A. *Trac Trends Anal. Chem.* **2001**, *20*, 419–434.
(39) Jastorff, B.; Stormann, R.; Ranke, J.; Molter, K.; Stock, F.; Oberheitmann, B.; Hoffmann, W.; Hoffmann, J.; Nuchter, M.; Ondruschka, B.; Filser, J. *Green Chem.* **2003**, *5*, 136–142.
(40) Caron, G.; Reymond, F.; Carrupt, P. A.; Girault, H. H.; Testa, B. *Pharm. Sci. Technol. Today* **1999**, *2*, 327–335.
(41) Quinn, B. M.; Ding, Z. F.; Moulton, R.; Bard, A. J. *Langmuir* **2002**, *18*, 1734–1742.
(42) Kakiuchi, T. *Anal. Chem.* **2007**, *79*, 6442–6449.
(43) Bard, A. J.; Faulkner, L. R., 2nd ed.; John Wiley & Sons: New York, 2001, pp 458–464.
(44) Amemiya, S.; Yang, X.; Wazenegger, T. L. *J. Am. Chem. Soc.* **2003**, *125*, 11832–11833.
(45) Yuan, Y.; Amemiya, S. *Anal. Chem.* **2004**, *76*, 6877–6886.
(46) Rodgers, P. J.; Amemiya, S. *Anal. Chem.* **2007**, *79*, 9276–9285.
(47) Rodgers, P. J.; Jing, P.; Kim, Y.; Amemiya, S. *J. Am. Chem. Soc.* **2008**, *130*, 7436–7442.
(48) Umezawa, Y.; Bühlmann, P.; Umezawa, K.; Tohda, K.; Amemiya, S. *Pure Appl. Chem.* **2000**, *72*, 1851–2082
(49) Perera, H.; Fordyce, K.; Shvarev, A. *Anal. Chem.* **2007**, *79*, 4564–4573.
(50) Ceresa, A.; Radu, A.; Peper, S.; Bakker, E.; Pretsch, E. *Anal. Chem.* **2002**, *74*, 4027–4036.